Title
Characterization of Jumonji demethylase activity on peptides and nucleosomes

Permalink
https://escholarship.org/uc/item/8kd530js

Author
Shiau, Carrie

Publication Date
2012

Peer reviewed|Thesis/dissertation

Characterization of Jumonji demethylase activity on peptides and nucleosomes

by

Carrie Shiau

DISSERTATION

Submitted in partial satisfaction of the requirements for the degree of

DOCTOR OF PHILOSOPHY

in

Chemistry and Chemical Biology

in the

GRADUATE DIVISION

of the

UNIVERSITY OF CALIFORNIA, SAN FRANCISCO

Copyright 2012

By

Carrie Shiau

To my family with love and gratitude.

ACKNOWLEDGEMENTS

Additionally, it was during my time here at UCSF that I met Jonathan Gable. I must thank him for his care and support. Thanks for sticking with me through tough times and smiling with me through happy times.

Lastly, and most importantly, I would like to thank my mother Lynn Sing, sister Celia, and family friend Shi Gong. Achieving this doctorate and everything else in my life could not have been possible without their unwavering support, optimism, love, care, and confidence in me. Thank you for being my constant pillar in life.

Characterization of Jumonji demethylase activity on peptides and nucleosomes

by

Carrie Shiau

ABSTRACT

Jumonji histone demethylases catalyze removal of methyl marks from lysine residues in histone proteins within nucleosomes. Misregulation of demethylation has been correlated with diseases including various forms of cancer, obesity, and x-linked mental retardation. Our study of these enzymes is described in this dissertation. In Chapter 1, we described the preparation of histone H3 lysine 9 (H3K9) demethylases and the optimization of demethylase assay conditions. In Chapter 2, we described our work on the demethylation of homogeneously methylated nucleosomes and the investigation of the intrinsic processivity of the catalytic domains of a H3K9 Jumonji demethylase, JMJD2A. By developing a method to assess demethylation of homogeneous, site-specifically methylated nucleosomes, we determined that the kinetic parameters for demethylation of nucleosomes by cJMJD2A are comparable to those of peptide substrates, suggesting that the catalytic domain does not recognize additional features of the nucleosome. These findings imply that other domains of the demethylase or its protein partners may contribute to nucleosome recognition *in vivo*, and in this way, may regulate demethylation activity and processivity. Importantly, our work demonstrates that quantitative assessment of nucleosome

demethylation is feasible and provides a platform for future work with complex chromatin substrates and full-length demethylases. In Chapter 3, we described our studies on the possible oligomerization of JMJD2A. Lastly, in Chapter 4, we presented our work on the synthesis and evaluation of candidate mechanism-based inhibitors of JMJD2A. Together, our work provides a better understanding of the intrinsic properties of JMJD2A mediated demethylation and serves as foundations for future studies in demethylase activity regulation.

TABLE OF CONTENTS

LIST OF TABLES

LIST OF FIGURES

INTRODUCTION

Though all cells of an organism contain the same genomic DNA, epigenetics is responsible for the differential expression and phenotype of different cells types and tissues. As proposed by a recent paper, "an epigenetic trait is a stably heritable phenotype resulting from changes in a chromosome without alterations in the DNA sequence" (Berger et al., 2009). This heritable phenotype can be passed on through mitosis or meiosis. Proper epigenetic regulation is vital for an array of cellular processes including stem cell self-renewal and differentiation (Juliandi et al., 2010; Wu and Sun, 2006), and its improper regulation can result in cancer (Dawson and Kouzarides, 2012).

Epigenetic regulations include post-translational modifications of histones, proteins that along with its surrounding 146 bp DNA make up the basic chromatin repeating unit called the nucleosome. Nucleosomes allow for the condensation and spatial organization of DNA in the nucleus. Among the modifications that can occur on histone proteins are acetylation, phosphorylation, sumoylation, methylation, and ubiquitination (Latham and Dent, 2007). Several of these marks alter the packing of the chromatin and thus the accessibility of DNA to transcriptional machinery.

Unlike other histone tail post-translational modifications, histone methylation had long been thought to be a static modification due to the stability of the $N\text{-}CH_3$ bond. This irreversibility of methylation was further supported by comparable turnover rates of bulk histones and methylated lysines and arginines (Byvoet et al., 1972; Thomas et al., 1972). Interestingly, another group found low

1

methylation turnovers of approximately 2% per hour (Borun et al., 1972), and witnessed what appeared to be demethylation in a rat kidney extract (Paik and Kim, 1967); however, the molecular machinery responsible for this was not identified. It was not until 2004 that the very first histone demethylase, Lysine Specific Demethylase (LSD1), was discovered (Shi et al., 2004). This finding revolutionized the field of epigenetics. LSD1 is a flavin-dependent demethylase whereby the FAD cofactor oxidizes the methylated Lys into its iminium intermediate. Subsequent addition of water and elimination of formaldehyde result in lysine demethylation (Figure I-1A) (Culhane and Cole, 2007). Thus, due to the necessity of the iminium intermediate formation, LSD1 cannot demethylate trimethylated Lys. Currently, LSD1 and LSD2 reside as the two member of this class of histone demethylases (Karytinos et al., 2009; Shi et al., 2004).

The limited substrate specificity of LSD1 and its inability to remove methyl marks from trimethylated lysine suggested that the inventory of demethylases was incomplete. In 2006, the first Jumonji histone demethylase was discovered and consequently established the second class of histone demethylases (Figure I-1B) (Tsukada et al., 2006). As a member of the Fe(II) and α-ketoglutarate-dependent dioxygenase superfamily, these enzymes demethylate via a radical mechanism, involving the intermediacy of a highly oxidative iron-oxo ($Fe^{IV}=O$) intermediate. In the starting complex, the active site iron in these enzymes is hexa-coordinated by two His, an Asp, a water and an α-ketoglutarate. Binding of substrate displaces the axially coordinated water residue and initiates oxygen activation and iron-oxo intermediate formation. The resultant highly potent iron-

oxo species initiates hydrogen abstraction from the substrate to form a ferric-hydroxy species and a carbon-centered radical. Subsequent oxygen rebound yields an unstable hemiaminal intermediate that spontaneously collapses to afford the demethylated product and formaldehyde (Figure I-2). Members of this class of enzymes were shown to catalyze demethylation of mono-, di-, or tri-methylated Lys. Bioinformatic search of the human genome identified 27 members of the Jumonji histone demethylase class, making Jumonji demethylases the largest class of histone demethylases.

Methylated H3K9s have been shown to play important biological roles. Di- and tri-methylated H3K9 (H3K9Me2/3) play crucial roles in heterochromatin formation (Lachner et al., 2001; Rea et al., 2000). Differentiation of embryonic stem cells is accompanied by an increase in H3K9 methylation (Loh et al., 2007). JMJD1A, a H3K9(Me2/1) demethylase, has been found to control metabolic gene expression and obesity in mice (Tateishi et al., 2009). Additionally, demethylases of H3K9 have been linked to acute myeloid leukemia (Hu et al., 2001), prostate (Wissmann et al., 2007) and esophageal cancer (Yang et al., 2000). Though expression levels of JHDMs were shown to correlate with the presence of these diseases, JHDM activity levels of H3K9 in healthy and disease states are yet to be established.

Of the 27 predicted JHDM members, the most well characterized constituent thus far is JMJD2A with determined crystal structures and kinetic properties (Chen et al., 2006; Couture et al., 2007; Hillringhaus et al., 2011; Krishnan et al., 2012; Ng et al., 2007). JMJD2A demethylates methylated H3K9

and H3K36. H3K9(Me3) is largely found in pericentric heterochromatin, whereas H3K36(Me3/2) are largely found in actively transcribed genes. As such, JMJD2A can act as a transcriptional repressor or an activator and the regulation of JMJD2A in these roles is not known. *In vitro* studies of JMJD2A catalytic domains have shown preference for H3K9(Me3) over H3K36(Me3) (Couture et al., 2007; Hillringhaus et al., 2011; Ng et al., 2007), however, it is unclear how JMJD2A is regulated for each of the substrates *in vivo*. Auxiliary Tudor and PHD domains and protein complex partners are thought to play roles in recruitment of the demethylase to specific sites, and thus may regulate specificity of JMJD2A.

Here, we describe the preparation and optimization of H3K9 demethylases. Subsequently, we characterize the intrinsic demethylation properties of the catalytic domains of a H3K9 demethylase, JMJD2A (1-350 aa, cJMJD2A), and its demethylation on the more physiological nucleosome substrate. Until our work, kinetics of demethylation of nucleosomes has not been characterized for any demethylase. By using our quantitative western blot approach along with homogenously methylated nucleosomes, we unveil intrinsic properties of the catalytic domains of JMJD2A (1-350 aa, cJMJD2A) and establish a method that can be used for future work on other demethylases and more complex substrates. We also demonstrate the distributive mechanism of cJMJD2A in its demethylation of multiple methyl marks. Together, these findings raise the possibility that the Tudor and PHD domains of full length JMJD2A may contribute to the recognition of the nucleosome scaffold and the regulation of demethylase processivity.

Additionally, our work on the possible oligomerization of JMJD2A may have important implications for the biological function of these enzymes, such as the oligomeric state playing a role in enzymatic efficiency. Lastly, our development of mechanism-based inhibitors lays a foundation for the development of chemical tools to probe Jumonji demethylase activity. Having a mechanism-based inhibitor that mimics the substrate is uniquely suited to studying substrate regulation in ways that have not been previously accomplished for Jumonji demethylases.
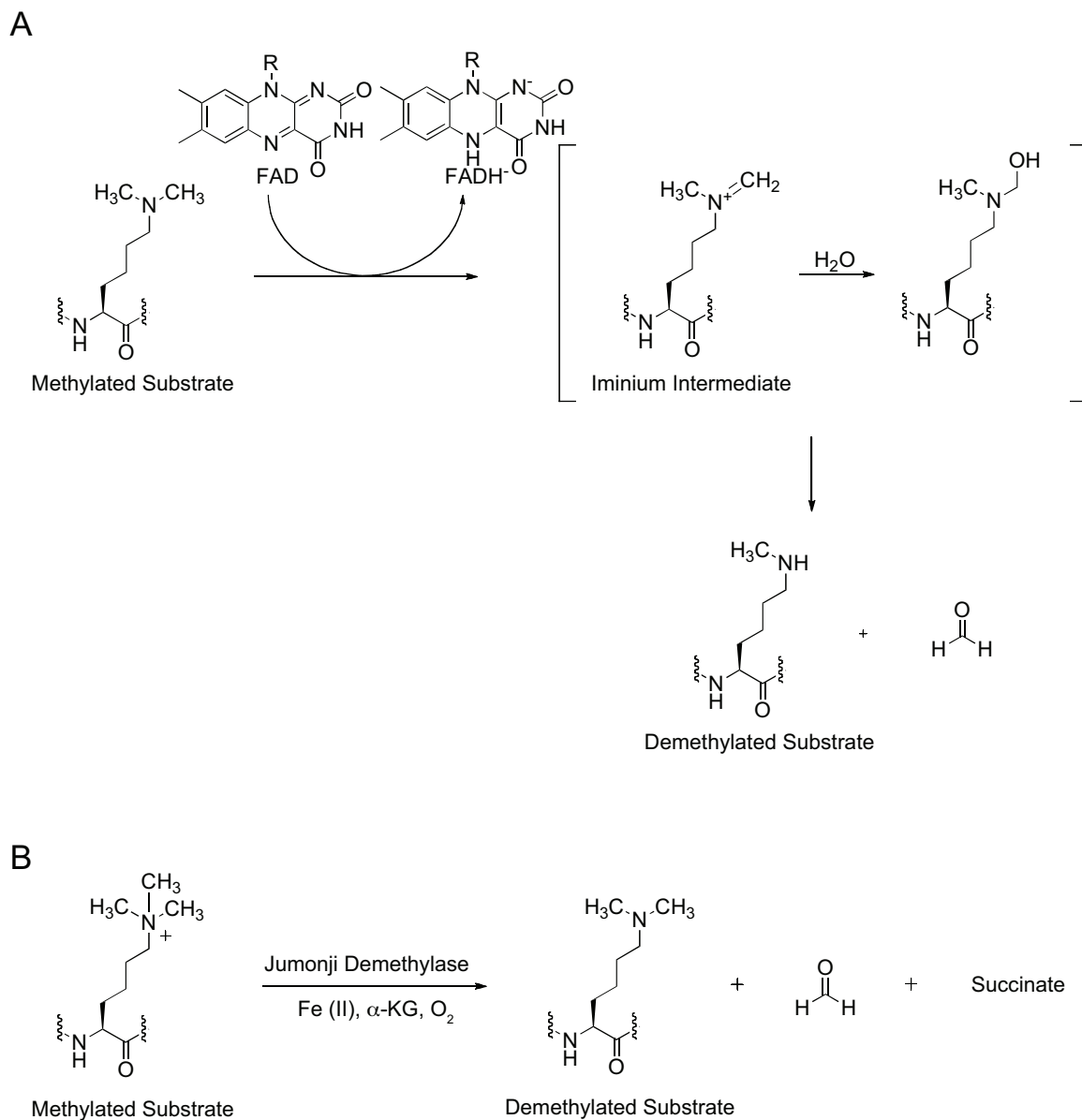
Figure I-1. Histone demethylase reactions. (A) Mechanism of LSD1 and LSD2. (B) Overall reaction of Jumonji demethylase.
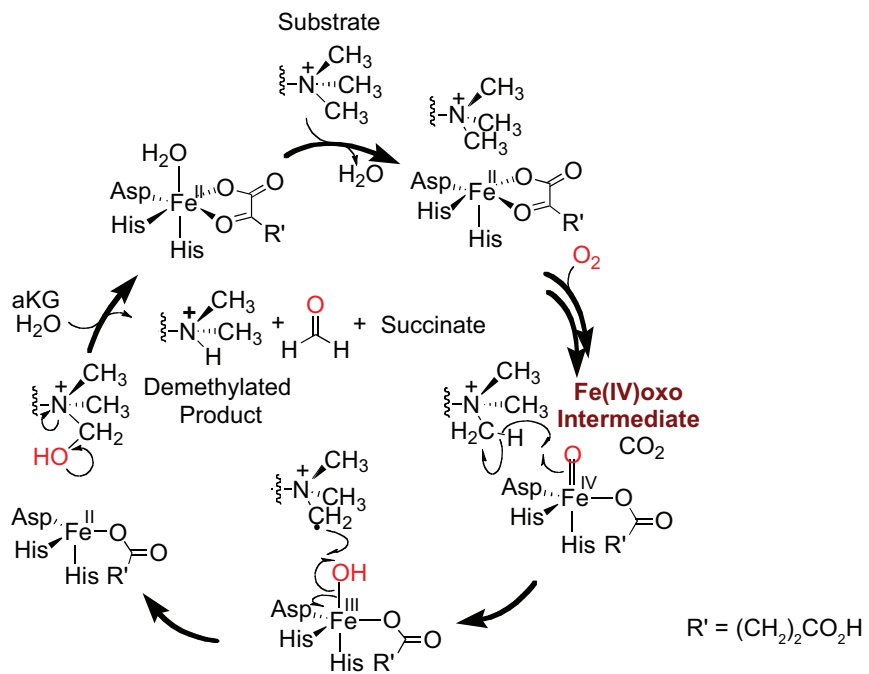
Figure I-2. Jumonji demethylase mechanism.

REFERENCES

Berger, S.L., Kouzarides, T., Shiekhattar, R., and Shilatifard, A. (2009). An operational definition of epigenetics. Genes Dev *23*, 781-783.

Borun, T.W., Pearson, D., and Paik, W.K. (1972). Studies of histone methylation during the HeLa S-3 cell cycle. J Biol Chem *247*, 4288-4298.

Byvoet, P., Shepherd, G.R., Hardin, J.M., and Noland, B.J. (1972). The distribution and turnover of labeled methyl groups in histone fractions of cultured mammalian cells. Arch Biochem Biophys *148*, 558-567.

Chen, Z., Zang, J., Whetstine, J., Hong, X., Davrazou, F., Kutateladze, T.G., Simpson, M., Mao, Q., Pan, C.-H., Dai, S.*, et al.* (2006). Structural insights into histone demethylation by JMJD2 family members. Cell *125*, 691-702.

Couture, J.-F., Collazo, E., Ortiz-Tello, P.A., Brunzelle, J.S., and Trievel, R.C. (2007). Specificity and mechanism of JMJD2A, a trimethyllysine-specific histone demethylase. Nat Struct Mol Biol *14*, 689-695.

Culhane, J.C., and Cole, P.A. (2007). LSD1 and the chemistry of histone demethylation. Curr Opin Chem Biol *11*, 561-568.

Dawson, M.A., and Kouzarides, T. (2012). Cancer epigenetics: from mechanism to therapy. Cell *150*, 12-27.

Hillringhaus, L., Yue, W.W., Rose, N.R., Ng, S.S., Gileadi, C., Loenarz, C., Bello, S.H., Bray, J.E., Schofield, C.J., and Oppermann, U. (2011). Structural and evolutionary basis for the dual substrate selectivity of human KDM4 histone demethylase family. J Biol Chem *286*, 41616-41625.

Hu, Z., Gomes, I., Horrigan, S.K., Kravarusic, J., Mar, B., Arbieva, Z., Chyna, B., Fulton, N., Edassery, S., Raza, A.*, et al.* (2001). A novel nuclear protein, 5qNCA (LOC51780) is a candidate for the myeloid leukemia tumor suppressor gene on chromosome 5 band q31. Oncogene *20*, 6946-6954.

Juliandi, B., Abematsu, M., and Nakashima, K. (2010). Epigenetic regulation in neural stem cell differentiation. Dev Growth Differ *52*, 493-504.

Karytinos, A., Forneris, F., Profumo, A., Ciossani, G., Battaglioli, E., Binda, C., and Mattevi, A. (2009). A novel mammalian flavin-dependent histone demethylase. J Biol Chem *284*, 17775-17782.

Krishnan, S., Collazo, E., Ortiz-Tello, P.A., and Trievel, R.C. (2012). Purification and assay protocols for obtaining highly active Jumonji C demethylases. Anal Biochem *420*, 48-53.

Lachner, M., O'Carroll, D., Rea, S., Mechtler, K., and Jenuwein, T. (2001). Methylation of histone H3 lysine 9 creates a binding site for HP1 proteins. Nature *410*, 116-120.

Latham, J.A., and Dent, S.Y. (2007). Cross-regulation of histone modifications. Nat Struct Mol Biol *14*, 1017-1024.

Loh, Y.-H., Zhang, W., Chen, X., George, J., and Ng, H.-H. (2007). Jmjd1a and Jmjd2c histone H3 Lys 9 demethylases regulate self-renewal in embryonic stem cells. Genes Dev *21*, 2545-2557.

Ng, S.S., Kavanagh, K.L., McDonough, M.A., Butler, D., Pilka, E.S., Lienard, B.M.R., Bray, J.E., Savitsky, P., Gileadi, O., von Delft, F.*, et al.* (2007). Crystal

structures of histone demethylase JMJD2A reveal basis for substrate specificity. Nature *448*, 87-91.

Paik, W.K., and Kim, S. (1967). Enzymatic methylation of protein fractions from calf thymus nuclei. Biochem Biophys Res Commun *29*, 14-20.

Rea, S., Eisenhaber, F., O'Carroll, D., Strahl, B.D., Sun, Z.W., Schmid, M., Opravil, S., Mechtler, K., Ponting, C.P., Allis, C.D.*, et al.* (2000). Regulation of chromatin structure by site-specific histone H3 methyltransferases. Nature *406*, 593-599.

Shi, Y., Lan, F., Matson, C., Mulligan, P., Whetstine, J.R., Cole, P.A., Casero, R.A., and Shi, Y. (2004). Histone demethylation mediated by the nuclear amine oxidase homolog LSD1. Cell *119*, 941-953.

Tateishi, K., Okada, Y., Kallin, E.M., and Zhang, Y. (2009). Role of Jhdm2a in regulating metabolic gene expression and obesity resistance. Nature *458*, 757-761.

Thomas, G., Lange, H.W., and Hempel, K. (1972). [Relative stability of lysine-bound methyl groups in arginie-rich histones and their subfrations in Ehrlich ascites tumor cells in vitro]. Hoppe Seylers Z Physiol Chem *353*, 1423-1428.

Tsukada, Y.-i., Fang, J., Erdjument-Bromage, H., Warren, M.E., Borchers, C.H., Tempst, P., and Zhang, Y. (2006). Histone demethylation by a family of JmjC domain-containing proteins. Nature *439*, 811-816.

Wissmann, M., Yin, N., Müller, J.M., Greschik, H., Fodor, B.D., Jenuwein, T., Vogler, C., Schneider, R., Günther, T., Buettner, R.*, et al.* (2007). Cooperative demethylation by JMJD2C and LSD1 promotes androgen receptor-dependent gene expression. Nat Cell Biol *9*, 347-353.

Wu, H., and Sun, Y.E. (2006). Epigenetic regulation of stem cell differentiation. Pediatr Res *59*, 21R-25R.

Yang, Z.Q., Imoto, I., Fukuda, Y., Pimkhaokham, A., Shimada, Y., Imamura, M., Sugano, S., Nakamura, Y., and Inazawa, J. (2000). Identification of a novel gene, GASC1, within an amplicon at 9p23-24 frequently detected in esophageal cancer cell lines. Cancer Res *60*, 4735-4739.

Chapter 1: Preparation of H3K9 demethylases and optimization of demethylase assays

Methylation of lysine 9 of histone H3 (H3K9) is an important histone modification due to its role in heterochromatin formation. Like other lysine residues, H3K9 can be mono-, di-, or trimethylated, and different methylation states can result in different functional outputs by recruiting specific readers and consequently specific protein complexes (Yun, et al., 2011). For example, heterochromatin protein 1 (HP1), a critical protein involved in heterochromatin spread (Grewal and Jia, 2007) is known to preferentially bind dimethyl and trimethyl H3K9 over monomethyl and nonmethyl H3K9 through its chromodomain (Bannister, et al., 2001; Canzio, et al., 2011; Lachner, et al., 2001; Nakayama, et al., 2001). In addition to chromodomains, effector modules that bind methylated H3K9 include PHD, Tudor, WD40, and ankyrin repeat domains (Yun, et al., 2011). As a number of these domains can be found in demethylases (eg. PHD and Tudor domains in JMJD2A (Klose, et al., 2006; Vermeulen, et al., 2010)) and methyltransferases (eg. ankyrin repeats in G9a), these domains are postulated to play roles in regulating demethylases and methyltransferases through recruitment of the enzymes to the site of interest.

In addition to histone turnover, the regulation of H3K9 methylation is controlled by enzymes that append and remove methyl marks (methyltransferases and demethylases, respectively). The H3K9 methyltransferases are comprised of the SET-domain-containing SUV39 family and the PRDI-BF1-RIZ1 (PR)-type SET-domain protein RIZ1/KMT8. The SET-domain-containing SUV39 family is composed of a number of enzymes including G9a and ESET (Kim, et al., 2003; Shilatifard, 2006; Shinkai, 2007). *In vivo*

studies of G9a and ESET deficient mouse embryos showed severe growth abnormalities and lethality, which indicate the importance and lack of redundancy of these enzymes (Dodge, et al., 2004; Tachibana, et al., 2002).

H3K9 demethylation is mediated by a flavoprotein demethylase LSD1 (when associated with androgen receptor and JMJD2C (Wissmann, et al., 2007)) and Jumonji demethylases (Cloos, et al., 2008). H3K9 Jumonji demethylases make up the majority of the H3K9 demethylases and are comprised of three families, JMJD1 (KDM3), JMJD2 (KDM4) and PHF (Table 1-1). Jumonji demethylases are Fe(II) and α-ketoglutarate (α-KG) dependent enzymes.

The JMJD1 family consists of two members, JMJD1A and JMJD1B, both of which demethylate H3K9(Me2/Me1) (Klose, et al., 2006; Yamane, et al., 2006). These demethylases contain a zinc-finger-like domain and a JmjC domain. JMJD1A contains a nuclear receptor interaction motif (LXXLL, amino acids 885 - 889) and has been implicated in H3K9(Me2) demethylation of AR target genes (Yamane, et al., 2006). *In vivo*, JMJD1A has been found to partake in spermiogenesis through transcriptional regulation of transition nuclear protein and protamine 1, proteins required for the final stages of sperm chromatin maturation (Okada, et al., 2007). The infertile phenotype of JMJD1A knockout mice demonstrates JMJD1A as a crucial regulator of male fertility (Okada, et al., 2010). JMJD1B is located at 5q31, a chromosomal region that is often found to be lost in myeloid leukemias and myelodysplasias. Overexpression of JMJD1B in a 5q deleted myelodysplasia cell line resulted in suppression of clonogenic

colony formation, suggestive of tumor suppressive properties of JMJD1B (Hu, et al., 2001).

JMJD2 family is comprised of JMJD2A, JMJD2B, JMJD2C, JMJD2D, and two annotated pseudogenes JMJD2E and JMJD2F (Katoh and Katoh, 2004). The majority of these enzymes can demethylate both H3K9 and H3K36 and are comprised of a JmjN, JmjC, double PhD domain and a tandem Tudor domain. Overexpression of several members of the JMJD2 family has been observed in various diseases. Higher levels of JMJD2C have been found in esophageal squamous carcinomas, medulloblastomas, breast cancer, and prostate cancer (Ehrbrecht, et al., 2006; Katoh and Katoh, 2004; Liu, et al., 2009; Northcott, et al., 2009; Yang, et al., 2000). Additionally, JMJD2C has been identified as an oncogene in primary mediastinal B cell lymphomas and Hodgkins lymphomas, where it promotes proliferation and survival of cancer (Rui, et al., 2010). Similarly, elevated levels of JMJD2A and JMJD2B have been found in prostate and breast cancer tissue (Berry, et al., 2012; Cloos, et al., 2006; Kawazu, et al., 2011), further implicating an oncogenic role for these enzymes.

The PHF family has a broad substrate specificity, including H3K9 methylation and consists of PHF2, PHF8, and KIAA1718 (KDM7) (Baba, et al., 2011; Horton, et al., 2010; Huang, et al., 2010; Loenarz, et al., 2010; Suganuma and Workman, 2010; Tsukada, et al., 2010; Yokoyama, et al., 2010). PHF2 is located on the chromosomal region of 9q22, which has been associated with hereditary neuropathy I (Blair, et al., 1997; Nicholson, et al., 1996), suggesting that PHF2 may play a role in the development of neuropathy. Interestingly, PHF2

has been found to be inactive until phosphorylation by protein kinase A. Phosphorylated PHF2 demethylates methylated ARID5B and forms the PHF2-ARID5B complex. Subsequently, ARID5B recruits PHF2 to the chromatin site to demethylate H3K9(Me2) (Baba, et al., 2011). This is one of the first reports demonstrating post-translational regulation of demethylases. KIAA1718 is predominantly expressed in the brain and morpholino knockdown of the demethylase in zebrafish showed diminished tectum and loss of neurons, while ectopic overexpression lead to phenotypic abnormalities of the embryo (Tsukada, et al., 2010). Taken together, these findings indicate a critical role of KIAA1718 in brain development. X-linked mental retardation and cleft lip/palate have been associated with mutations of PHF8 (Abidi, et al., 2007; Koivisto, et al., 2007; Laumonnier, et al., 2005; Loenarz, et al., 2010; Siderius, et al., 1999). Most mutations found in patients are truncating mutations of early stop and nonsense mutations (Abidi, et al., 2007; Laumonnier, et al., 2005). Interestingly, another study of patient populations identified a F279S point mutation (Koivisto, et al., 2007), one that has been found to abolish demethylase activity (Yu, et al., 2010). Recent kinetic studies have shown the presence of a secondary mark, H3K4(Me3), to enhance PHF8 demethylation activity on H3K9(Me2) (Feng, et al., 2010; Horton, et al., 2010), marking the regulatory action of surrounding chromatin marks on these demethylases.

Cloning of H3K9 Jumonji demethylases

Constructs of members from the three subfamilies were made. From the KDM4 family, the catalytic domains of JMJD2A (1-350 aa, His-cJMJD2A) and JMJD2D (1-354 aa, His-cJMJD2D) were cloned into N-terminally and C-terminally His-tagged constructs respectively. JMJD2A was cloned into pET47b plasmid (Novagen) using *SmaI* and *BamHI* sites. JMJD2D was cloned into pET24 vector plasmid (Novagen) using *NdeI* and *XhoI*. For the PHF family, the PHD and catalytic domains of PHF8 (1-447 aa, His-cPHF8) was cloned into N-terminally His-tagged pET47b construct (Novagen) using *KpnI* and *SacI*. Full-length JMJD1B (His-JMJD1B) was cloned into pET47b construct (Novagen) using *BamHI* and *NotI* sites. Additionally, the catalytically inactive constructs His-cJMJD2A H188A, His-cJMJD2D H192A, His-cPHF8 H247A, and His-JMJD1B H558A were made.

Expressions and purifications of His-cPHF8, His-cJMJD2D, His-cJMJD2A, and His-JMJD1B

His-cPHF8, His-cJMJD2D, His-cJMJD2A, and His-JMJD1B constructs were transformed into BL-21(DE3) (New England Biolabs), Rosetta2(DE3) (EMD Millipore), and BL-21 CodonPlus (Stratagene) cells and tested for optimal expression. His-JMJD1B was found to be optimally expressed in BL-21 CodonPlus cells, while the remainder of the demethylases were found to be optimally expressed in BL-21(DE3) cells. All cells were grown at 37 °C to OD_{600} 0.6 and induced with a final concentration of 0.4 mM isopropyl β-D-

thiogalactoside at 18 °C overnight in the presence of kanamycin. Cells were harvested and lysed in 50 mM Hepes (pH 7.5), 500 mM NaCl, 20 mM imidazole, 0.5 mM TCEP, 1 mM $MgCl_2$, 1 mM $CaCl_2$, and 0.1 mg/mL DNaseI (Sigma). Cell debris was removed by centrifugation and the supernatant was incubated with Ni-NTA beads (Qiagen) at 4 °C for 1 hr. Beads were washed with 50 mM Hepes (pH 7.5), 500 mM NaCl, 40 mM imidazole and 0.5 mM TCEP, and the protein eluted with 50 mM Hepes (pH 7.5), 500 mM NaCl, 250 mM imidazole, and 0.5 mM TCEP. Eluted enzyme fractions were pooled, concentrated using Amicon Ultra 30 kDa MWCO (Millipore), and ran on HiLoad 26/60 Superdex200 (GE Healthcare) in 10 mM Hepes (pH 7.9) and 500 mM NaCl for His-cPHF8, His-cJMJD2D, and His-JMJD1B and on HiLoad 26/60 Superdex75 (GE Healthcare) in 50 mM Hepes (pH 7.5) and 500 mM NaCl for His-cJMJD2A at 4 °C. His-cJMJD2D eluted at ~ 220 mL (Figure 1-1), His-cPHF8 at ~ 210 mL (Figure 1-2), His-cJMJD2A at ~ 180 mL (Figure 1-3), and His-JMJD1B at ~ 144 mL (Figure 1-4).

Activities of His-cPHF8, His-cJMJD2D, His-cJMJD2A, and His-JMJD1B

Activities of His-cPHF8, His-cJMJD2D, and His-cJMJD2A were assessed via MALDI-TOF mass spectrometry using histone H3 tail peptide ARK(Me3)STGGK or ARK(Me2)STGGK (7 – 14 amino acids) as substrates (Figure 1-5). His-cPHF8 (1 μM) was incubated with α-ketoglutarate (1 mM), ascorbate (1 mM) and $Fe(NH_4)_2(SO_4)_2$ (50 μM). Assays were started upon addition of ARK(Me2)STGGK (300 μM) and proceeded for 2 hr at room

temperature. His-cJMJD2D (10 μM) was incubated with α-ketoglutarate (1 mM), ascorbate (1 mM), and Fe(NH$_4$)$_2$(SO$_4$)$_2$ (50 μM). Reactions were started by addition of ARK(Me3)STGGK (300 μM) and allowed to proceed for 1 hr at room temperature. His-cJMJD2A (3 μM), was incubated with α-ketoglutarate (500 μM), ascorbate (500 μM), and Fe(NH$_4$)$_2$(SO$_4$)$_2$ (50 μM). Reactions were started by addition of ARK(Me3)STGGK (300 μM) and allowed to proceed for 20 min at room temperature. Time points were taken and quenched with equal volume of 0.5 M EDTA (pH 8.0) and desalted through C$_{18}$ ZipTips (Millipore). The extent of peptide demethylation was analyzed by MALDI-TOF mass spectrometry.

Demethylation products of His-cJMJD2A and His-cJMJD2D were clearly observed, while the demethylation product of His-cPHF8 was minimal. This may be due to the lack of H3K4(Me3) on the peptide substrate. Recent studies from Horton et al. showed a 12-fold difference in the half-lives of H3K9(Me2) peptides in the presence and absence of H3K4(Me3) (Horton, et al., 2010). The difference in activity is likely due to the binding of trimethylated H3K4 to the PHD domain of PHF8 (Horton, et al., 2010).

His-JMJD1B activity was confirmed via an enzyme-coupled fluorescence assay, where demethylation was measured by following formation of byproduct formaldehyde formation. Concomitant oxidation of formaldehyde to formate and reduction of NAD$^+$ to NADH by formaldehyde dehydrogenase (FDH) allowed for measurement of demethylation through NADH fluorescence at 350 nm excitation and 460 nm emission wavelengths (Figure 1-6) (Couture, et al., 2007). His-JMJD1B exhibits activity on ARK(Me2)STGGK using this assay (Figure 1-7).

Optimization of His-cJMJD2A activity

Activity of His-cJMJD2A was optimized through analysis of various buffer pH (Figure 1-8), temperature (Figure 1-9), salt (Figure 1-10), iron (Figure 1-11), α-ketoglutarate (Figure 1-12), and ascorbate (Figure 1-13) concentrations. Optimal His-cJMJD2A activity was achieved in 50 mM Hepes (pH 7.5) at 25 °C. When testing iron concentrations, comparable activities were observed between 0 to 100 μM Fe(NH$_4$)$_2$(SO$_4$)$_2$ indicating saturation of iron at concentrations 12.5 μM – 100 μM. Observation of demethylation in the no iron addition sample suggests retention of iron from the enzyme preparation. Relatively comparable activities were seen for the range of tested α-ketoglutarate concentrations (0.25 mM – 2 mM) indicating that α-ketoglutarate was at saturating concentrations between 500 μM – 2 mM. Comparable activities in the tested concentrations of ascorbate suggest saturation of ascorbate in the tested conditions. Given that activity was seen in the no ascorbate addition, it is possible that ascorbate is not necessary for multiple turnovers of the substrate.

Using the optimized conditions, kinetic parameters for His-cJMJD2A demethylation of peptides were determined (Figure 1-14) by the enzyme-coupled assay that monitors the production of formaldehyde (Couture, et al., 2007). In these experiments, His-cJMJD2A (1 μM), NAD$^+$ (2 mM), formaldehyde dehydrogenase (FDH, 0.05 U, Sigma), α-ketoglutarate (1 mM), ascorbate (1 mM), and Fe(NH$_4$)$_2$(SO$_4$)$_2$ (50 μM) were incubated with varying concentrations of ARK(Me3)STGGK (Genscript) in 50 mM Hepes (pH 7.5). Reactions were started

by addition of substrate and followed at 15 sec intervals at room temperature on a SpectraMax M5e (Molecular Devices) using 350 nm excitation and 460 nm emission wavelengths. An NADH standard curve was used to convert fluorescence into concentration of product formed. The initial 2.5 min were used to calculate initial velocities, which were graphed against substrate concentration. Michaelis-Menten values were determined by non-linear least squares fitting using Kaleidagraph.

While early studies indicated low turnover numbers for this enzyme family (0.015 min^{-1} for demethylation of H3K9(Me3) peptides by JMJD2A) (Couture, et al., 2007), more recent investigations identified improved catalytic properties, with turnover numbers ranging from 0.6 to 1.9 min^{-1} for JMJD2A catalyzed demethylation of H3K9(Me3) peptides (Hillringhaus, et al., 2011; Krishnan, et al., 2012), with overall catalytic efficiency of 1.3 – 1.9 x 10^{-2} $\mu M^{-1} min^{-1}$.

Our obtained parameters of a K_M of 54 μM and a k_{cat} of 2.5 min^{-1} are comparable to those from recent reports of K_M = 96 μM and k_{cat} = 1.9 min^{-1} (Krishnan, et al., 2012) and K_M = 45 μM and k_{cat} = 0.6 min^{-1} (Hillringhaus, et al., 2011).

Cloning, expression, purification, and activity of streptavidin-tagged JMJD2A

Jumonji histone demethylases are known to bind nickel. To determine if potential binding of nickel during Ni-NTA purification might affect demethylase acivity, we produced streptavidin-tagged cJMJD2A. To test whether a

streptavidin-tagged JMJD2A (Strep-cJMJD2A) may provide a more active enzyme, JMJD2A (1-350 aa) was cloned into a streptavidin and TEV protease cleavage site containing pBH4 plasmid using *BamHI* and *NotI*. The cloned plasmid was transformed into Rosetta 2(DE3)pLysS (EMD Millipore) cells. Cells were grown at 37 °C in the presence of ampicillin to OD_{600} 0.6 and induced with a final concentration of 0.4 mM isopropyl β-D-thiogalactoside at 18 °C overnight.

Cells were harvested and lysed in 50 mM Hepes (pH 7.5), 500 mM NaCl, 0.5 mM TCEP, 1 mM $MgCl_2$, 1 mM $CaCl_2$, Complete EDTA-free protease inhibitor cocktail tablets (Roche) and 0.1 mg/mL DNaseI (Sigma). Cell debris was removed by centrifugation and the supernatant passed through Strep-Tactin resin (IBA) at 4 °C and washed with 5 mL of 50 mM Hepes (pH 7.5) and 500 mM NaCl (for 2 L pellet of cells) twice. Using 50 mM Hepes (pH 7.5), 500 mM NaCl and 2.5 mM desthiobiotin (Sigma), 5 mL fractions were eluted. Fractions 1-3 were collected, concentrated using 30 kDa MWCO Amicon concentrators (Millipore), and injected onto a pre-equilibriated Superdex 200 10/300 GL (GE Healthcare). The column was ran at 4 °C and protein eluted in 50 mM Hepes (pH 7.5) and 500 mM NaCl at ~16 min (Figure 1-15).

Activity of Strep-cJMJD2A was assessed using the fluorescent assay. Strep-JMJD2A has a higher K_M and a lower k_{cat} than His-cJMJD2A (Figure 1-16), demonstrating lower efficiency.

Cloning, expression, purification, and activity of de-tagged cJMJD2A

JMJD2A (1- 350 aa) was cloned into a hexahistidine tag and TEV protease cleavage site containing pBH4 plasmid using *BamHI* and *NotI*. Cloned plasmid was transformed into Rosetta 2(DE3)pLysS (EMD Millipore) cells. Cells were grown at 37 °C in the presence of ampicillin to OD_{600} 0.6 and induced with a final concentration of 0.4 mM isopropyl β-D-thiogalactoside at 18 °C overnight.

Cells were harvested and lysed in 50 mM Hepes (pH 7.5), 500 mM NaCl, 0.5 mM TCEP, 1 mM $MgCl_2$, 1 mM $CaCl_2$, Complete EDTA-free protease inhibitor cocktail tablets (Roche) and 0.1 mg/mL DNaseI (Sigma). Cell debris was removed by centrifugation and the supernatant was incubated with Ni-NTA beads (Qiagen) at 4 °C for 1 hr. Beads were washed with 50 mM Hepes (pH 7.5), 500 mM NaCl, 40 mM imidazole and 0.5 mM TCEP, and the protein eluted with 50 mM Hepes (pH 7.5), 500 mM NaCl, 250 mM imidazole, and 0.5 mM TCEP. Eluted JMJD2A fractions were pooled and incubated with recombinantly expressed His-tagged TEV protease (1:10 by weight) at 4 °C for 3 hr while dialyzing in 50 mM Hepes (pH 7.5), 500 mM NaCl, 20 mM imidazole, and 0.5 mM TCEP. To separate TEV protease and the cleaved His tag, the sample was incubated with Ni-NTA beads (Qiagen) for 30 min at 4 °C. The flow-through was collected, concentrated, and purified on HiLoad 26/60 Superdex75 (GE Healthcare) in 50 mM Hepes (pH 7.5) and 500 mM NaCl at 4 °C (Figure 1-17).

cJMJD2A activity on ARK(Me3)STGGK and ARK(Me2)STGGK were analyzed using the fluorescent assay (Figure 1-18). Consistent with other reports where His-tagged JMJD2A was used, trimethylated substrate was found to be a

better substrate than the dimethylated substrate (Couture, et al., 2007; Hillringhaus, et al., 2011). We observed a two-fold increase in turnover and a six-fold decrease in K_M from dimethyl to trimethyl substrates.

Metal analysis of JMJD2A constructs

Nickel replacement of the demethylase active site iron renders the enzyme inactive. A report showed that once the Jumonji demethylase JMJD1A was inhibited by nickel, replacement of nickel with iron was not achieved even at 2 mM concentrations of iron (Chen, et al., 2010). Given the use of nickel during the purification process of histadine-tagged demethylases, we wanted to assess the extent to which our demethylases were acquiring nickel.

To determine the amount of nickel present in our purified protein samples, we utilized ICP mass spectrometry (ActLabs, Ancaster, Ontario). The percentage of nickel present was calculated by dividing the concentration of nickel in the sample by the concentration of JMJD2A. This provided an indication of the percentage of demethylases that was occupied by nickel. In addition to His-cJMJD2A, EDTA and EDTA and DTT treated His-cJMJD2A were tested (Table 1-2). We found that EDTA treatment (both with and without DTT) lowered the percentage of nickel occupation but not by an appreciable amount. Activities of the treated His-cJMJD2A were tested and no appreciable difference was seen among the treatments. His-cleaved demethylase had comparable amounts of nickel with non-cleaved constructs indicating that the protocols used for the two purifications offered comparable nickel retention. The C-terminally histadine-

tagged enzyme MetK, a protein that lacked an iron active site, was used as negative control as it was also nickel-affinity purified. As expected, the results indicated little to no nickel presence in the control sample providing confidence in the metal analysis (Table 1-2). Given the higher activity of His-cJMJD2A compared to Strep-cJMJD2A, we decided to utilize His-cJMJD2A and cJMJD2A for our experiments.

Name	Synonym	Specificity	Domains
JMJD1A	KDM3A JHDM2A TSGA	H3K9(Me2/Me1)	
JMJD1B	KDM3B JHDM2B TRIP8 5qCNA	H3K9(Me2/Me1)	
JMJD2A	KDM4A JHDM3A	H3K9(Me3/Me2) H3K36(Me3/Me2)	
JMJD2B	KDM4B	H3K9(Me3/Me2) H3K36(Me3/Me2)	
JMJD2C	KDM4C GASC1	H3K9(Me3/Me2) H3K36(Me3/Me2)	
JMJD2D	KDM4D	H3K9(Me3/Me2/Me1) H3K36(Me3/Me2)	
PHF8	PHD8	H3K9(Me2/Me1) H3K27(Me2) H4K20(Me1)	
PHF2	PHD2	H3K9Me2	
KIAA1718	KDM7	H3K9(Me2) H3K27(Me2)	

JmjN JmjC PHD Tudor ZF-like

Table 1-1. H3K9 Jumonji demethylase domain architectures and substrate specificity.
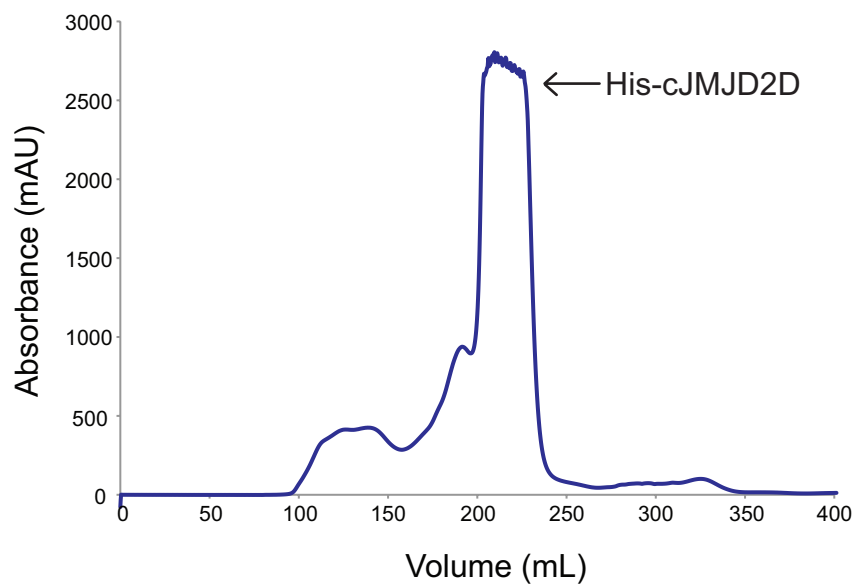
Figure 1-1. His-cJMJD2D gel filtration trace.
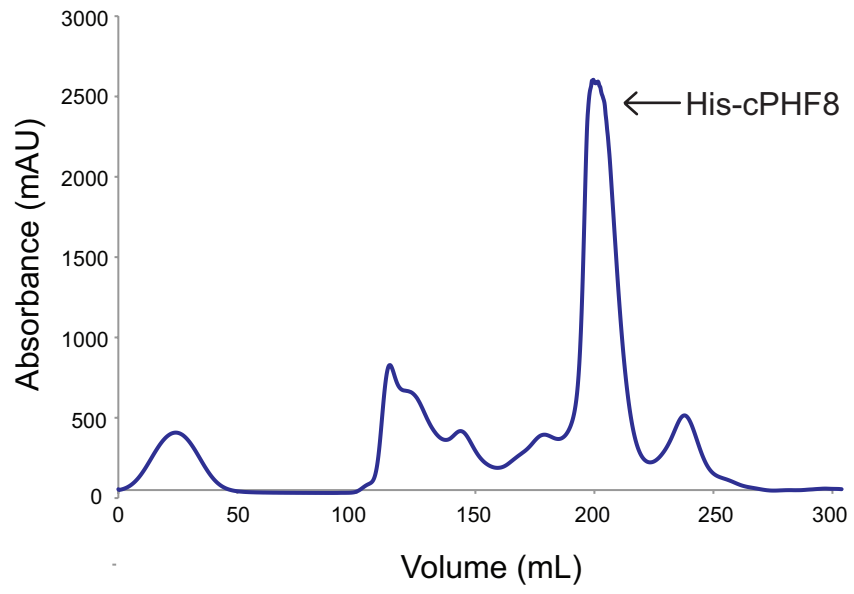
Figure 1-2. His-cPHF8 gel filtration trace.
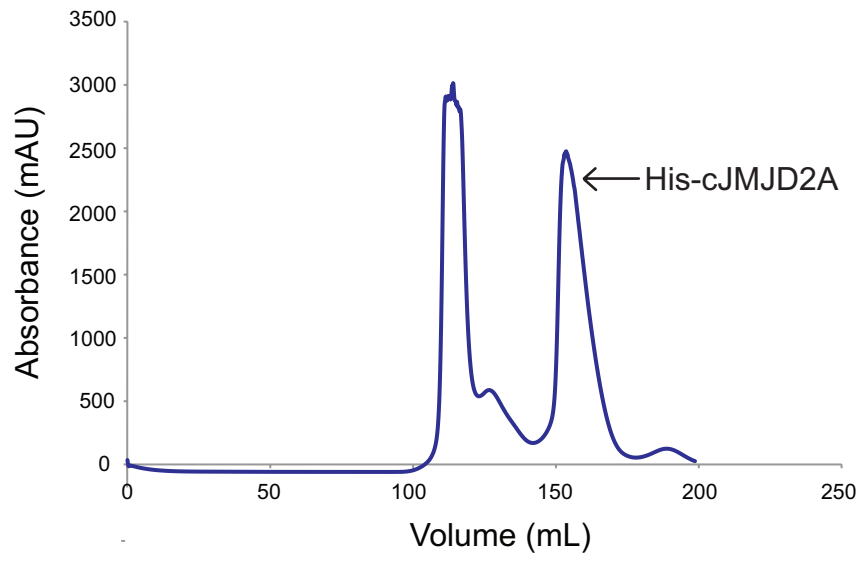
Figure 1-3. His-cJMJD2A gel filtration trace.
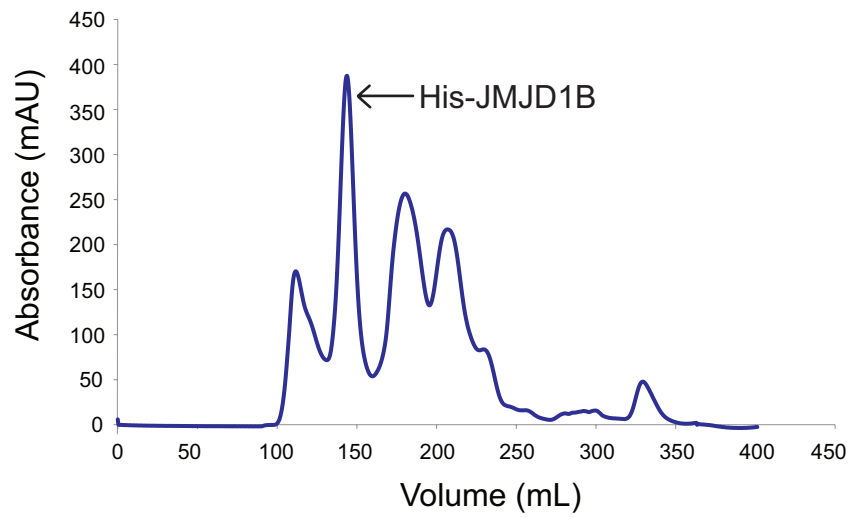
Figure 1-4. His-JMJD1B gel filtration trace.

His-cPHF8 - ARK(Me2)STGGK
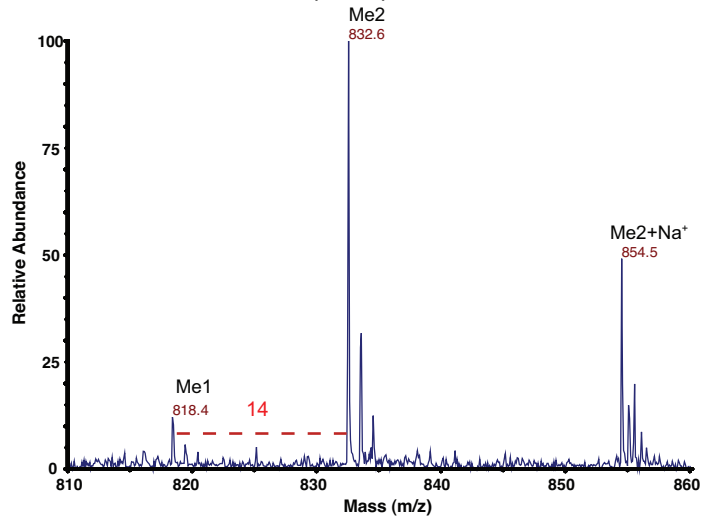
His-cJMJD2D - ARK(Me3)STGGK
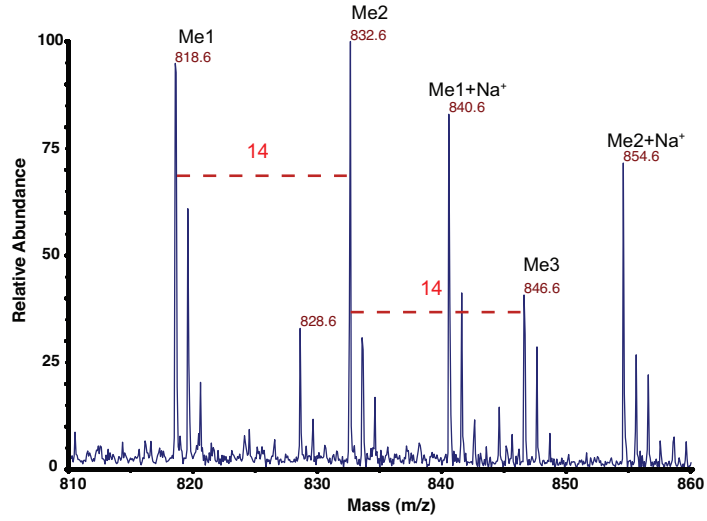
His-cJMJD2A - ARK(Me3)STGGK

29
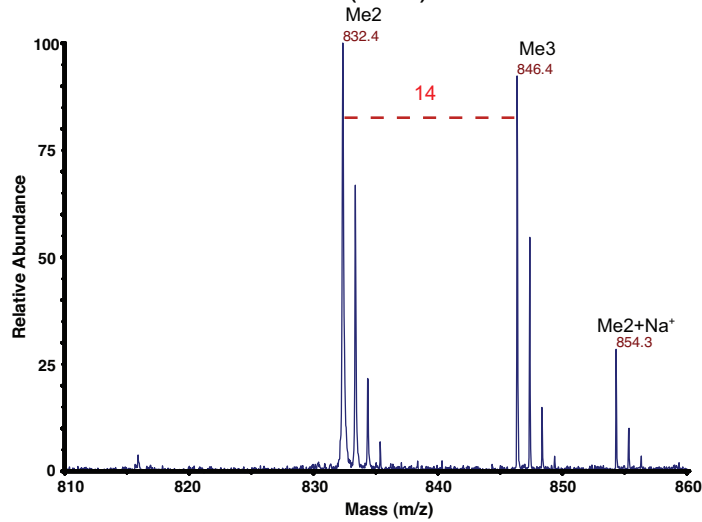
Figure 1-5. Demethylation activities of His-cPHF8, His-cJMJD2D, and His-cJMJD2A.
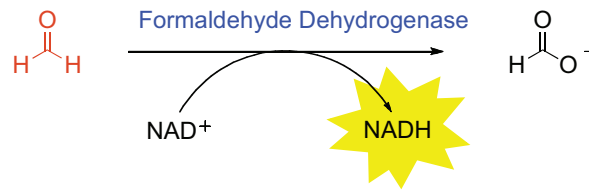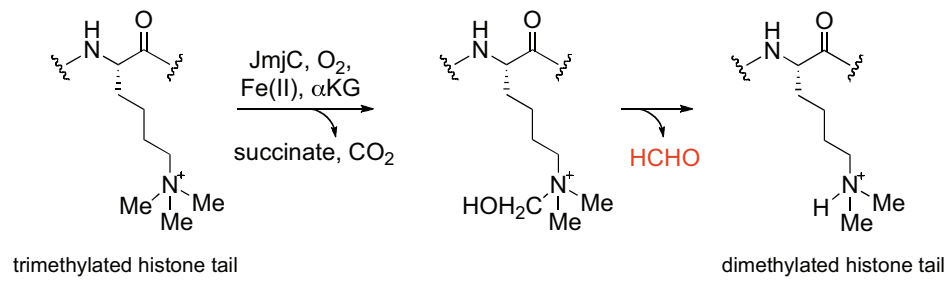
Figure 1-6. Enzyme-coupled fluorescence assay used for monitoring demethylase activity (Couture et al., 2007).
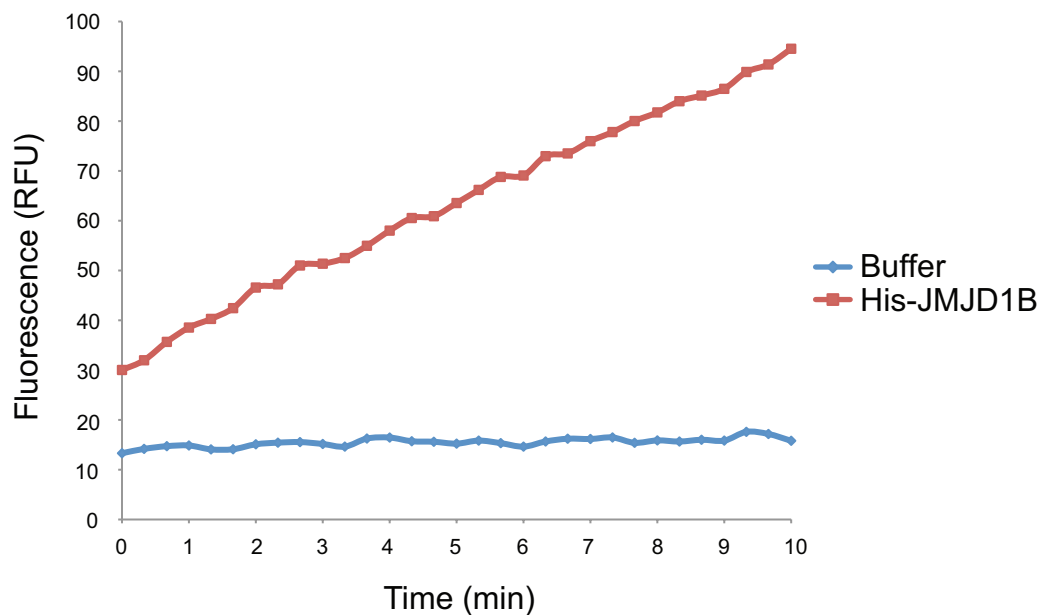
Figure 1-7. Measurement of demethylation activity of His-JMJD1B with ARK(Me2)STGGK peptide. His-JMJD1B (6 μM) or gel filtration buffer of an equivalent volume was incubated with α-ketoglutarate (500 μM), ascorbate (500 μM), Fe(NH$_4$)$_2$(SO$_4$)$_2$ (50 μM), NAD$^+$ (2 mM), FDH (0.076 U), and ARK(Me2)STGGK (300 μM). Reactions were initiated by addition of substrate and allowed to proceed at room temperature.
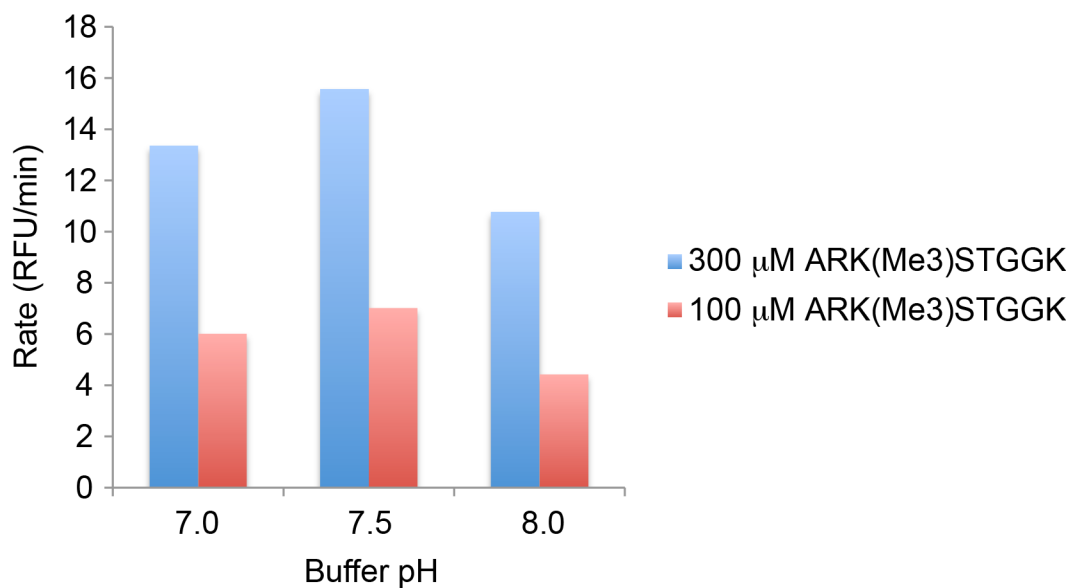
Figure 1-8. His-cJMJD2A activity as a function of pH. His-cJMJD2A (1 μM) was incubated with α-ketoglutarate (500 μM), ascorbate (500 μM), Fe(NH$_4$)$_2$(SO$_4$)$_2$ (50 μM), NAD$^+$ (2 mM), and formaldehyde dehydrogenase (0.05 U) in 50 mM Hepes (pH 7.0 – 8.0). Reactions were started by addition of ARK(Me3)STGGK (300 μM or 100 μM) and allowed to proceed at room temperature.
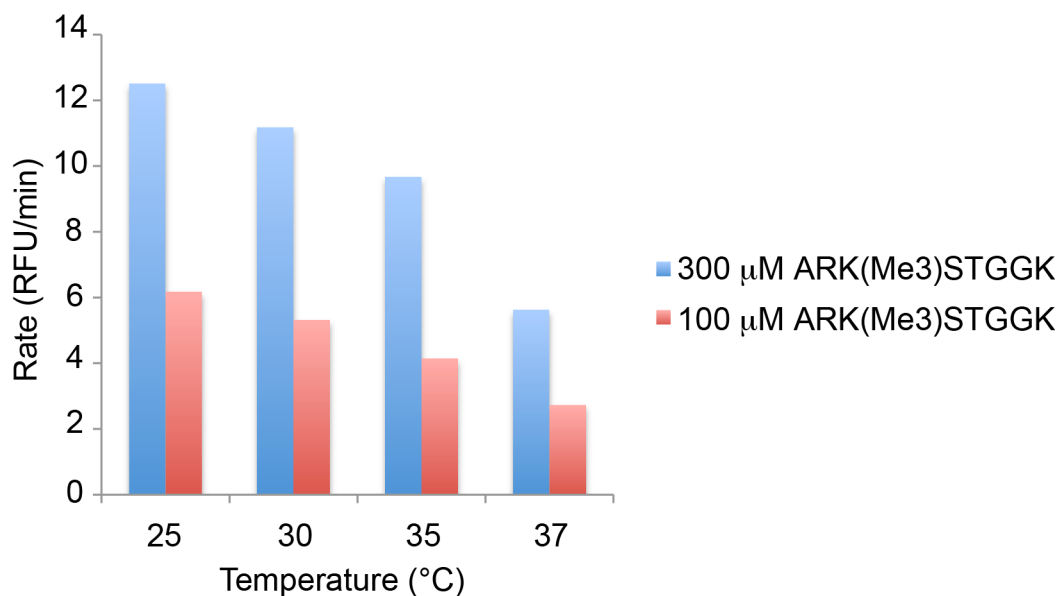
Figure 1-9. His-cJMJD2A activity as a function of temperature. His-cJMJD2A (1 μM) was incubated with α-ketoglutarate (500 μM), ascorbate (500 μM), Fe(NH$_4$)$_2$(SO$_4$)$_2$ (50 μM), NAD$^+$ (2 mM), and formaldehyde dehydrogenase (0.05 U) in 50 mM Hepes (pH 7.5). Reactions were started by addition of ARK(Me3)STGGK (300 μM or 100 μM) and allowed to proceed at various temperatures.
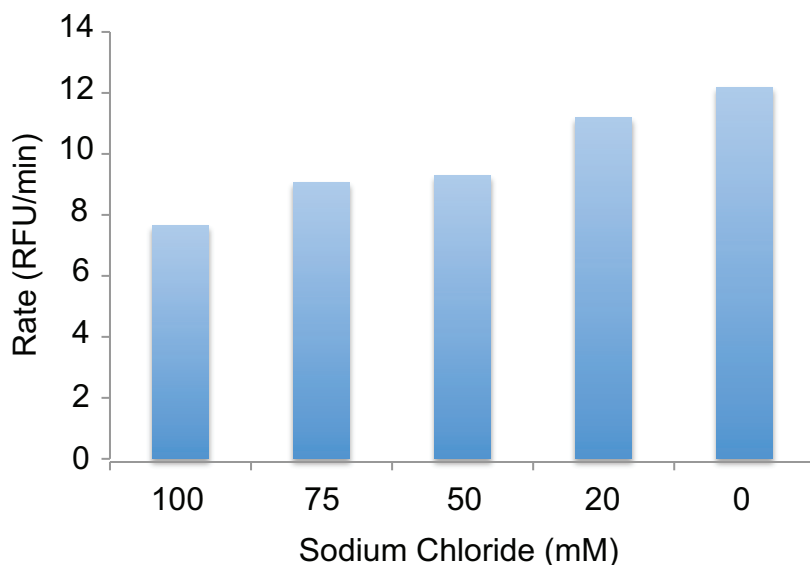
Figure 1-10. His-cJMJD2A activity as a function of sodium chloride concentration. His-cJMJD2A (1 μM) was incubated with α-ketoglutarate (500 μM), ascorbate (500 μM), Fe(NH$_4$)$_2$(SO$_4$)$_2$ (50 μM), NAD$^+$ (2 mM), and formaldehyde dehydrogenase (0.05 U) in 50 mM Hepes (pH 7.5) and various NaCl concentrations (0 – 100 mM). Reactions were started by addition of ARK(Me3)STGGK (300 μM) and allowed to proceed at room temperature.
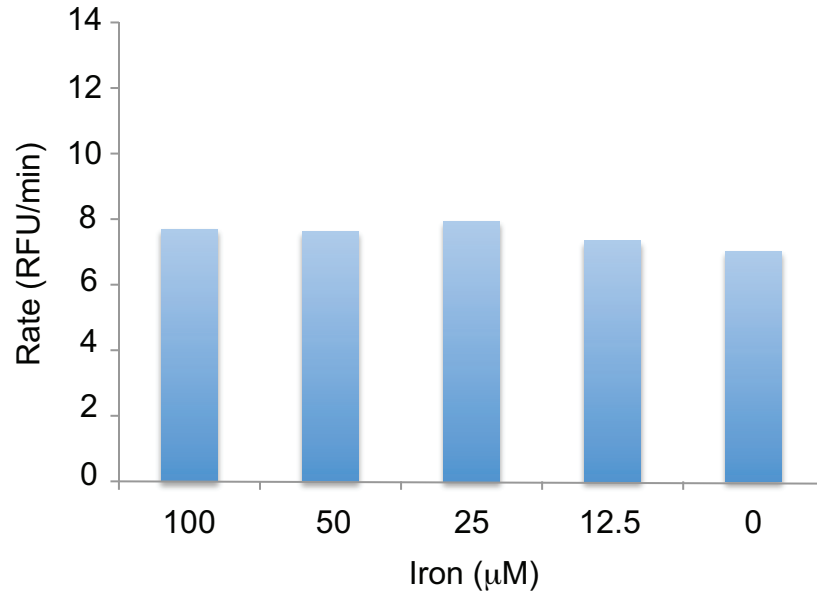
Figure 1-11. His-cJMJD2A activity as a function of iron concentration. His-cJMJD2A (1 μM) was incubated with α-ketoglutarate (500 μM), ascorbate (500 μM), $Fe(NH_4)_2(SO_4)_2$ (0 – 100 μM), NAD^+ (2 mM), and formaldehyde dehydrogenase (0.05 U) in 50 mM Hepes (pH 7.5). Reactions were started by addition of ARK(Me3)STGGK (300 μM) and allowed to proceed at room temperature.
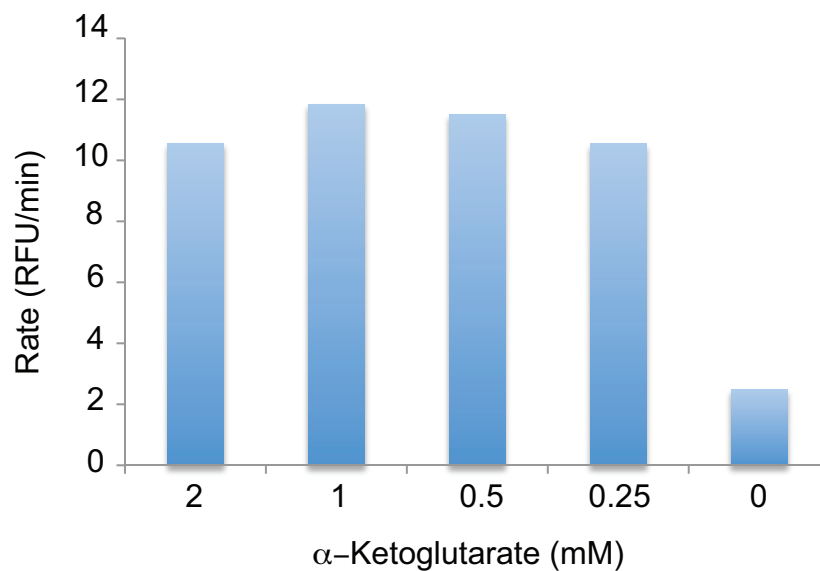
Figure 1-12. His-cJMJD2A activity as a function of α-ketoglutarate concentration. His-cJMJD2A (1 μM) was incubated with α-ketoglutarate (0 – 2 mM), ascorbate (500 μM), $Fe(NH_4)_2(SO_4)_2$ (50 μM), NAD^+ (2 mM), and formaldehyde dehydrogenase (0.05 U) in 50 mM Hepes (pH 7.5). Reactions were started by addition of ARK(Me3)STGGK (300 μM) and allowed to proceed at room temperature.
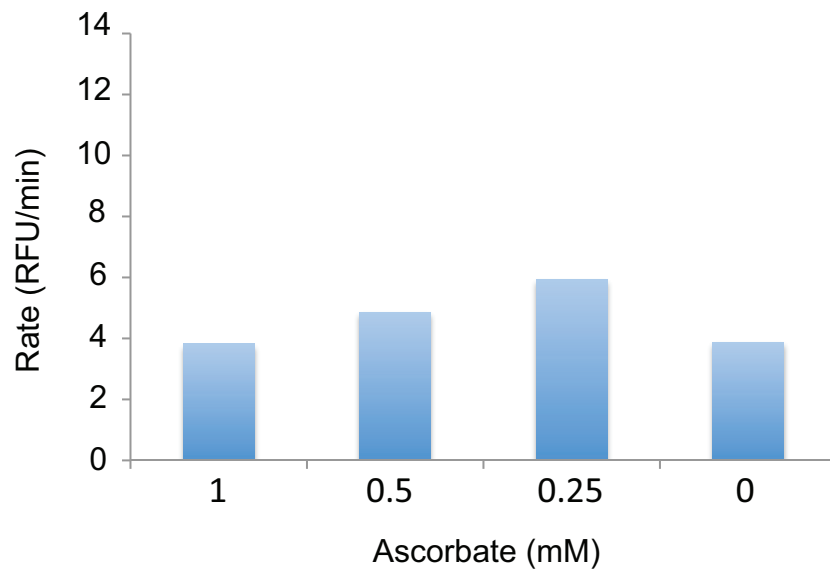
Figure 1-13. His-cJMJD2A activity as a function of ascorbate concentration. His-cJMJD2A (1 μM) was incubated with α-ketoglutarate (500 μM), ascorbate (0 - 1 mM), Fe(NH$_4$)$_2$(SO$_4$)$_2$ (50 μM), NAD$^+$ (2 mM), and formaldehyde dehydrogenase (0.05 U) in 50 mM Hepes (pH 7.5). Reactions were started by addition of ARK(Me3)STGGK (300 μM) and allowed to proceed at room temperature.

$k_{cat} = 2.5 \pm 0.09$ min^{-1}
$K_M = 54 \pm 5$ μM
$k_{cat}/K_M = (4.6 \pm 0.5) \times 10^{-2}$ min^{-1} μM^{-1}
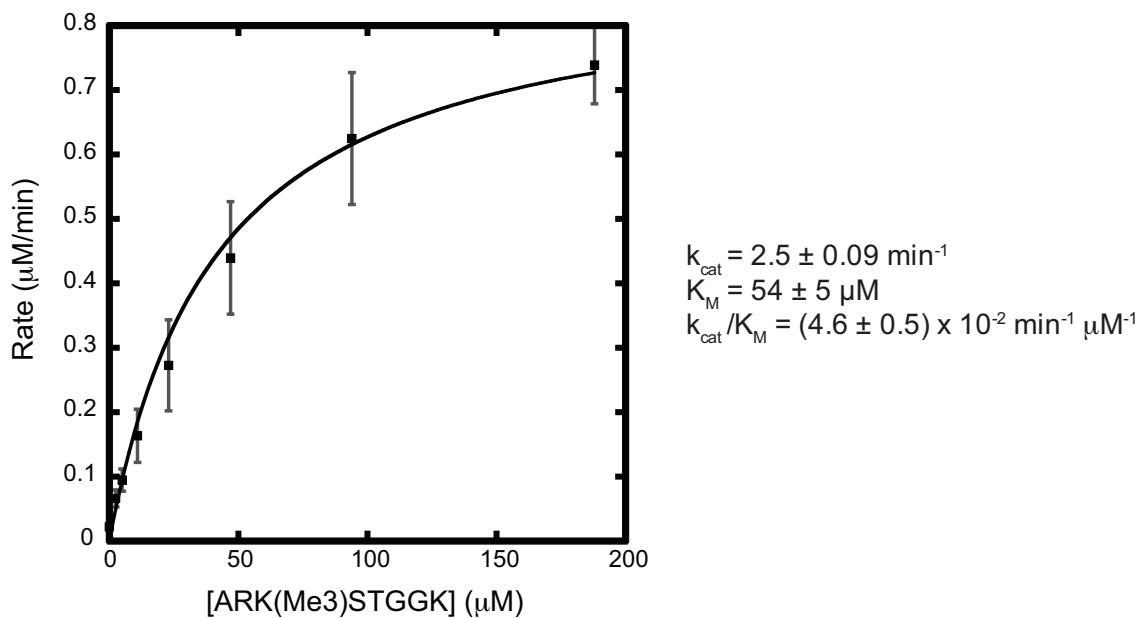
Figure 1-14. Kinetic analysis of His-cJMJD2A demethylation of ARK(Me3)STGGK peptide. His-cJMJD2A (0.385 μM) was incubated with α-ketoglutarate (1 mM), ascorbate (1 mM), $Fe(NH_4)_2(SO_4)_2$ (50 μM), NAD$^+$ (2 mM), and formaldehyde dehydrogenase (0.05 U) in 50 mM Hepes (pH 7.5). Reactions were started by addition of ARK(Me3)STGGK (300 μM) and allowed to proceed at room temperature. Experiments were done in triplicate.
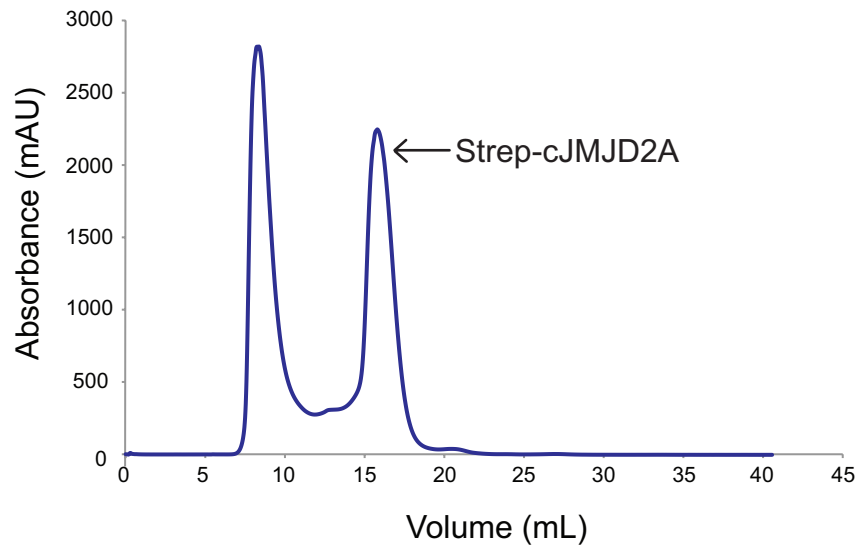
Figure 1-15. Strep-cJMJD2A gel filtration trace.

$k_{cat} = 1.8 \pm 0.2$ min^{-1}
$K_M = 370 \pm 100$ μM
$k_{cat}/K_M = (4.9 \pm 1) \times 10^{-3}$ min^{-1} μM^{-1}
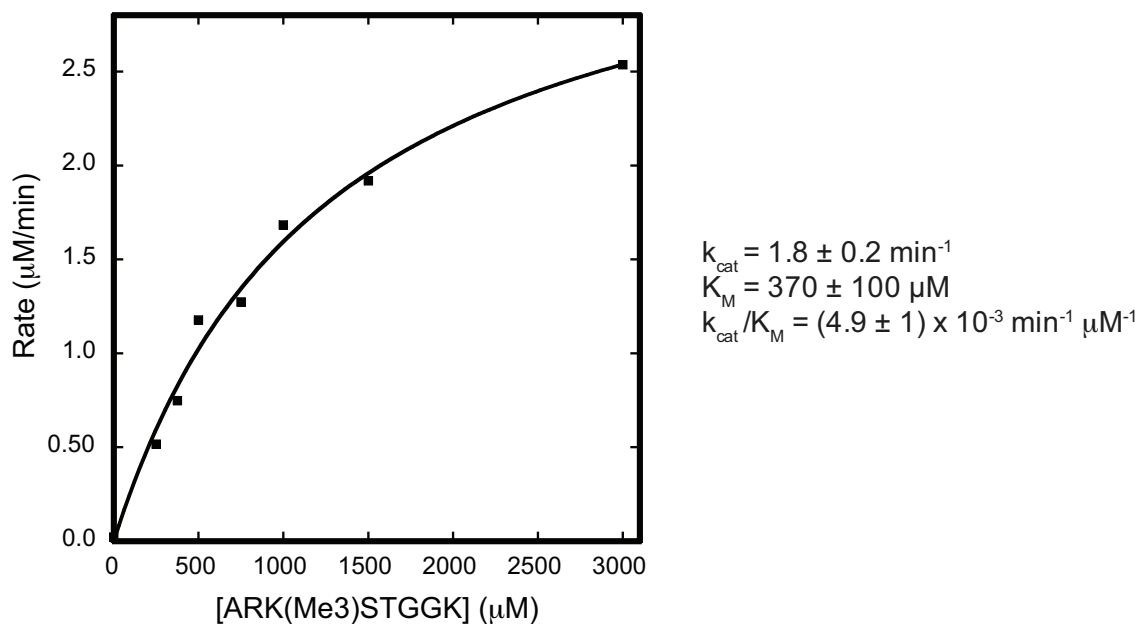
Figure 1-16. Strep-JMJD2A activity on ARK(Me3)STGGK peptide. Strep-

cJMJD2A (3 μM) was incubated with α-ketoglutarate (1 mM), ascorbate (1 mM),

Fe(NH$_4$)$_2$(SO$_4$)$_2$ (50 μM), NAD$^+$ (2 mM), and formaldehyde dehydrogenase (0.1

U) in 50 mM Hepes (pH 7.5). Reactions were started by addition of varying

ARK(Me3)STGGK (0 – 3 mM) and allowed to proceed at room temperature.
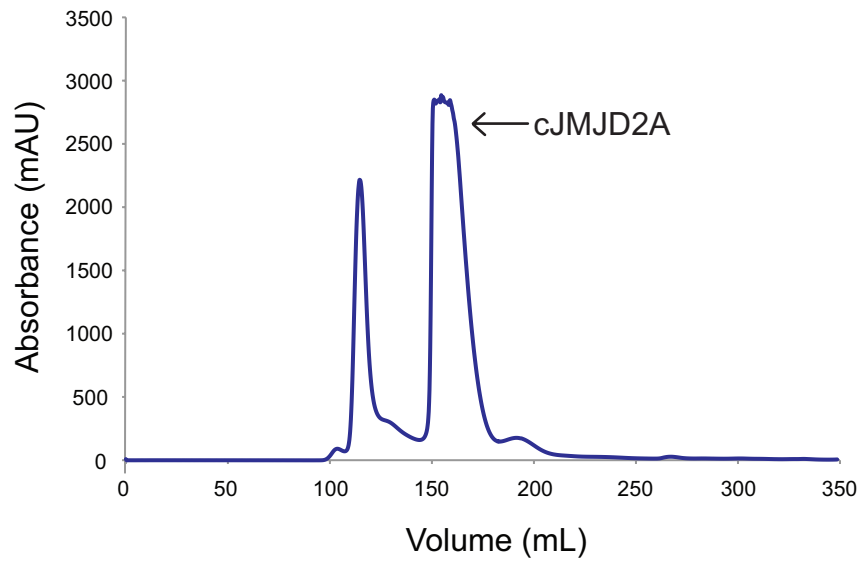
Figure 1-17. cJMJD2A gel filtration trace.

A
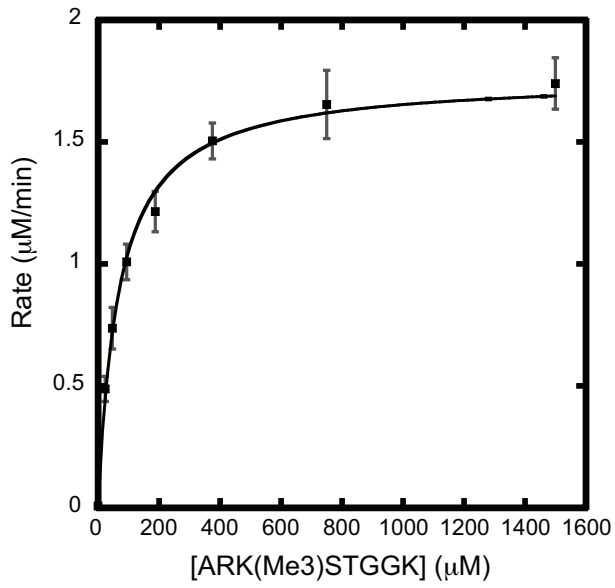
k_{cat} (Me3) = 1.8 ± 0.08 min^{-1}
K_M (Me3) = 67 ± 9 µM
k_{cat}/K_M (Me3) = (2.7 ± 0.4) x 10^{-2} min^{-1} µM^{-1}

B
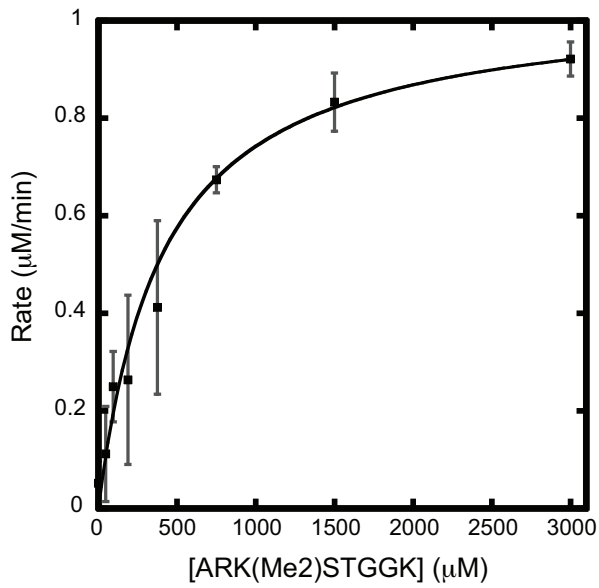
k_{cat} (Me2) = 1.0 ± 0.06 min^{-1}
K_M (Me2) = 410 ± 90 µM
k_{cat}/K_M (Me2) = (2.4 ± 0.6) x 10^{-3} min^{-1} µM^{-1}

43

Figure 1-18. Kinetic analysis of peptide demethylation by cJMJD2A. (A-B) Michaelis-Menten plots of initial velocity as a function of the concentration of ARK(Me$_3$)STGGK (A) and ARK(Me$_2$)STGGK (B). Experiments were done in triplicate and are represented as mean ± SEM.

Table 1-2. Metal analysis of JMJD2A protein preparations for nickel retention

assessment.

REFERENCES

Abidi, F.E., Miano, M.G., Murray, J.C., and Schwartz, C.E. (2007). A novel mutation in the PHF8 gene is associated with X-linked mental retardation with cleft lip/cleft palate. Clin Genet 72, 19-22.

Baba, A., Ohtake, F., Okuno, Y., Yokota, K., Okada, M., Imai, Y., Ni, M., Meyer, C.A., Igarashi, K., Kanno, J., et al. (2011). PKA-dependent regulation of the histone lysine demethylase complex PHF2-ARID5B. Nat Cell Biol 13, 668-675.

Bannister, A.J., Zegerman, P., Partridge, J.F., Miska, E.A., Thomas, J.O., Allshire, R.C., and Kouzarides, T. (2001). Selective recognition of methylated lysine 9 on histone H3 by the HP1 chromo domain. Nature 410, 120-124.

Berry, W.L., Shin, S., Lightfoot, S.A., and Janknecht, R. (2012). Oncogenic features of the JMJD2A histone demethylase in breast cancer. Int J Oncol 41, 1701-1706.

Blair, I.P., Dawkins, J.L., and Nicholson, G.A. (1997). Fine mapping of the hereditary sensory neuropathy type I locus on chromosome 9q22.1-->q22.3: exclusion of GAS1 and XPA. Cytogenet Cell Genet 78, 140-144.

Canzio, D., Chang, E.Y., Shankar, S., Kuchenbecker, K.M., Simon, M.D., Madhani, H.D., Narlikar, G.J., and Al-Sady, B. (2011). Chromodomain-Mediated Oligomerization of HP1 Suggests a Nucleosome-Bridging Mechanism for Heterochromatin Assembly. Mol Cell 41, 67-81.

Chen, H., Giri, N.C., Zhang, R., Yamane, K., Zhang, Y., Maroney, M., and Costa, M. (2010). Nickel ions inhibit histone demethylase JMJD1A and DNA repair enzyme ABH2 by replacing the ferrous iron in the catalytic centers. J Biol Chem 285, 7374-7383.

Cloos, P.A.C., Christensen, J., Agger, K., and Helin, K. (2008). Erasing the methyl mark: histone demethylases at the center of cellular differentiation and disease. Genes Dev 22, 1115-1140.

Cloos, P.A.C., Christensen, J., Agger, K., Maiolica, A., Rappsilber, J., Antal, T., Hansen, K.H., and Helin, K. (2006). The putative oncogene GASC1 demethylates tri- and dimethylated lysine 9 on histone H3. Nature 442, 307-311.

Couture, J.-F., Collazo, E., Ortiz-Tello, P.A., Brunzelle, J.S., and Trievel, R.C. (2007). Specificity and mechanism of JMJD2A, a trimethyllysine-specific histone demethylase. Nat Struct Mol Biol 14, 689-695.

Dodge, J.E., Kang, Y.K., Beppu, H., Lei, H., and Li, E. (2004). Histone H3-K9 methyltransferase ESET is essential for early development. Mol Cell Biol 24, 2478-2486.

Ehrbrecht, A., Muller, U., Wolter, M., Hoischen, A., Koch, A., Radlwimmer, B., Actor, B., Mincheva, A., Pietsch, T., Lichter, P., et al. (2006). Comprehensive genomic analysis of desmoplastic medulloblastomas: identification of novel amplified genes and separate evaluation of the different histological components. J Pathol 208, 554-563.

Feng, W., Yonezawa, M., Ye, J., Jenuwein, T., and Grummt, I. (2010). PHF8 activates transcription of rRNA genes through H3K4me3 binding and H3K9me1/2 demethylation. Nat Struct Mol Biol 17, 445-450.

Grewal, S.I., and Jia, S. (2007). Heterochromatin revisited. Nat Rev Genet 8, 35-46.

Hillringhaus, L., Yue, W.W., Rose, N.R., Ng, S.S., Gileadi, C., Loenarz, C., Bello, S.H., Bray, J.E., Schofield, C.J., and Oppermann, U. (2011). Structural and evolutionary basis for the dual substrate selectivity of human KDM4 histone demethylase family. J Biol Chem 286, 41616-41625.

Horton, J.R., Upadhyay, A.K., Qi, H.H., Zhang, X., Shi, Y., and Cheng, X. (2010). Enzymatic and structural insights for substrate specificity of a family of jumonji histone lysine demethylases. Nat Struct Mol Biol 17, 38-43.

Hu, Z., Gomes, I., Horrigan, S.K., Kravarusic, J., Mar, B., Arbieva, Z., Chyna, B., Fulton, N., Edassery, S., Raza, A., et al. (2001). A novel nuclear protein, 5qNCA (LOC51780) is a candidate for the myeloid leukemia tumor suppressor gene on chromosome 5 band q31. Oncogene 20, 6946-6954.

Huang, C., Xiang, Y., Wang, Y., Li, X., Xu, L., Zhu, Z., Zhang, T., Zhu, Q., Zhang, K., Jing, N., et al. (2010). Dual-specificity histone demethylase KIAA1718 (KDM7A) regulates neural differentiation through FGF4. Cell Res 20, 154-165.

Katoh, M., and Katoh, M. (2004). Identification and characterization of JMJD2 family genes in silico. Int J Oncol 24, 1623-1628.

Kawazu, M., Saso, K., Tong, K.I., McQuire, T., Goto, K., Son, D.O., Wakeham, A., Miyagishi, M., Mak, T.W., and Okada, H. (2011). Histone demethylase JMJD2B functions as a co-factor of estrogen receptor in breast cancer proliferation and mammary gland development. PLoS ONE 6, e17830.

Kim, K.C., Geng, L.Q., and Huang, S. (2003). Inactivation of a histone methyltransferase by mutations in human cancers. Cancer Research 63, 7619-7623.

Klose, R.J., Kallin, E.M., and Zhang, Y. (2006). JmjC-domain-containing proteins and histone demethylation. Nat Rev Genet 7, 715-727.

Klose, R.J., Yamane, K., Bae, Y., Zhang, D., Erdjument-Bromage, H., Tempst, P., Wong, J., and Zhang, Y. (2006). The transcriptional repressor JHDM3A demethylates trimethyl histone H3 lysine 9 and lysine 36. Nature 442, 312-316.

Koivisto, A.M., Ala-Mello, S., Lemmela, S., Komu, H.A., Rautio, J., and Jarvela, I. (2007). Screening of mutations in the PHF8 gene and identification of a novel mutation in a Finnish family with XLMR and cleft lip/cleft palate. Clin Genet 72, 145-149.

Koivisto, A.M., Ala-Mello, S., Lemmelä, S., Komu, H.A., Rautio, J., and Järvelä, I. (2007). Screening of mutations in the PHF8 gene and identification of a novel mutation in a Finnish family with XLMR and cleft lip/cleft palate. Clin Genet 72, 145-149.

Krishnan, S., Collazo, E., Ortiz-Tello, P.A., and Trievel, R.C. (2012). Purification and assay protocols for obtaining highly active Jumonji C demethylases. Anal Biochem 420, 48-53.

Lachner, M., O'Carroll, D., Rea, S., Mechtler, K., and Jenuwein, T. (2001). Methylation of histone H3 lysine 9 creates a binding site for HP1 proteins. Nature 410, 116-120.

Laumonnier, F., Holbert, S., Ronce, N., Faravelli, F., Lenzner, S., Schwartz, C.E., Lespinasse, J., Van Esch, H., Lacombe, D., Goizet, C., et al. (2005). Mutations in

PHF8 are associated with X linked mental retardation and cleft lip/cleft palate. J Med Genet 42, 780-786.

Laumonnier, F., Holbert, S., Ronce, N., Faravelli, F., Lenzner, S., Schwartz, C.E., Lespinasse, J., Van Esch, H., Lacombe, D., Goizet, C., et al. (2005). Mutations in PHF8 are associated with X linked mental retardation and cleft lip/cleft palate. J Med Genet 42, 780-786.

Liu, G., Bollig-Fischer, A., Kreike, B., van de Vijver, M.J., Abrams, J., Ethier, S.P., and Yang, Z.Q. (2009). Genomic amplification and oncogenic properties of the GASC1 histone demethylase gene in breast cancer. Oncogene 28, 4491-4500.

Loenarz, C., Ge, W., Coleman, M.L., Rose, N.R., Cooper, C.D.O., Klose, R.J., Ratcliffe, P.J., and Schofield, C.J. (2010). PHF8, a gene associated with cleft lip/palate and mental retardation, encodes for an Nepsilon-dimethyl lysine demethylase. Hum Mol Genet 19, 217-222.

Nakayama, J., Rice, J.C., Strahl, B.D., Allis, C.D., and Grewal, S.I. (2001). Role of histone H3 lysine 9 methylation in epigenetic control of heterochromatin assembly. Science 292, 110-113.

Nicholson, G.A., Dawkins, J.L., Blair, I.P., Kennerson, M.L., Gordon, M.J., Cherryson, A.K., Nash, J., and Bananis, T. (1996). The gene for hereditary sensory neuropathy type I (HSN-I) maps to chromosome 9q22.1-q22.3. Nat Genet 13, 101-104.

Northcott, P.A., Nakahara, Y., Wu, X., Feuk, L., Ellison, D.W., Croul, S., Mack, S., Kongkham, P.N., Peacock, J., Dubuc, A., et al. (2009). Multiple recurrent genetic events converge on control of histone lysine methylation in medulloblastoma. Nat Genet 41, 465-472.

Okada, Y., Scott, G., Ray, M.K., Mishina, Y., and Zhang, Y. (2007). Histone demethylase JHDM2A is critical for Tnp1 and Prm1 transcription and spermatogenesis. Nature 450, 119-123.

Okada, Y., Tateishi, K., and Zhang, Y. (2010). Histone demethylase JHDM2A is involved in male infertility and obesity. J Androl 31, 75-78.

Rui, L., Emre, N.C.T., Kruhlak, M.J., Chung, H.-J., Steidl, C., Slack, G., Wright, G.W., Lenz, G., Ngo, V.N., Shaffer, A.L., et al. (2010). Cooperative epigenetic modulation by cancer amplicon genes. Cancer Cell 18, 590-605.

Shilatifard, A. (2006). Chromatin modifications by methylation and ubiquitination: implications in the regulation of gene expression. Annu Rev Biochem 75, 243-269.

Shinkai, Y. (2007). Regulation and function of H3K9 methylation. Subcell Biochem 41, 337-350.

Siderius, L.E., Hamel, B.C., van Bokhoven, H., de Jager, F., van den Helm, B., Kremer, H., Heineman-de Boer, J.A., Ropers, H.H., and Mariman, E.C. (1999). X-linked mental retardation associated with cleft lip/palate maps to Xp11.3-q21.3. Am J Med Genet 85, 216-220.

Suganuma, T., and Workman, J.L. (2010). Features of the PHF8/KIAA1718 histone demethylase. Cell Res 20, 861-862.

Tachibana, M., Sugimoto, K., Nozaki, M., Ueda, J., Ohta, T., Ohki, M., Fukuda, M., Takeda, N., Niida, H., Kato, H., et al. (2002). G9a histone methyltransferase

plays a dominant role in euchromatic histone H3 lysine 9 methylation and is essential for early embryogenesis. Genes Dev 16, 1779-1791.

Tsukada, Y.-i., Ishitani, T., and Nakayama, K.I. (2010). KDM7 is a dual demethylase for histone H3 Lys 9 and Lys 27 and functions in brain development. Genes Dev 24, 432-437.

Vermeulen, M., Eberl, H.C., Matarese, F., Marks, H., Denissov, S., Butter, F., Lee, K.K., Olsen, J.V., Hyman, A.A., Stunnenberg, H.G., et al. (2010). Quantitative interaction proteomics and genome-wide profiling of epigenetic histone marks and their readers. Cell 142, 967-980.

Wissmann, M., Yin, N., Müller, J.M., Greschik, H., Fodor, B.D., Jenuwein, T., Vogler, C., Schneider, R., Günther, T., Buettner, R., et al. (2007). Cooperative demethylation by JMJD2C and LSD1 promotes androgen receptor-dependent gene expression. Nat Cell Biol 9, 347-353.

Yamane, K., Toumazou, C., Tsukada, Y., Erdjument-Bromage, H., Tempst, P., Wong, J., and Zhang, Y. (2006). JHDM2A, a JmjC-containing H3K9 demethylase, facilitates transcription activation by androgen receptor. Cell 125, 483-495.

Yamane, K., Toumazou, C., Tsukada, Y.-i., Erdjument-Bromage, H., Tempst, P., Wong, J., and Zhang, Y. (2006). JHDM2A, a JmjC-containing H3K9 demethylase, facilitates transcription activation by androgen receptor. Cell 125, 483-495.

Yang, Z.Q., Imoto, I., Fukuda, Y., Pimkhaokham, A., Shimada, Y., Imamura, M., Sugano, S., Nakamura, Y., and Inazawa, J. (2000). Identification of a novel gene, GASC1, within an amplicon at 9p23-24 frequently detected in esophageal cancer cell lines. Cancer Res 60, 4735-4739.

Yokoyama, A., Okuno, Y., Chikanishi, T., Hashiba, W., Sekine, H., Fujiki, R., and Kato, S. (2010). KIAA1718 is a histone demethylase that erases repressive histone methyl marks. Genes Cells 15, 867-873.

Yu, L., Wang, Y., Huang, S., Wang, J., Deng, Z., Zhang, Q., Wu, W., Zhang, X., Liu, Z., Gong, W., et al. (2010). Structural insights into a novel histone demethylase PHF8. Cell Res 20, 166-173.

Yun, M.Y., Wu, J., Workman, J.L., and Li, B. (2011). Readers of histone modifications. Cell Research 21, 564-578.

Chapter 2: Reconstitution of nucleosome demethylation and catalytic properties of a Jumonji histone demethylase

Authors: Carrie Shiau, Michael J. Trnka, Alen Bozicevic, Idelisse Ortiz Torres, Bassem Al-Sady, Alma L. Burlingame, Geeta J. Narlikar, and Danica Galonić Fujimori

This work has been submitted.

INTRODUCTION

Nucleosomes are comprised of histone proteins that are subject to diverse post-translational modifications. These modifications are predominantly found in the N-terminal tails of histones and have a profound impact on the regulation of transcription. Methylation of lysine 9 in histone H3 (H3K9) is a conserved eukaryotic modification that demarcates heterochromatin, a transcriptionally silent chromatin state. Trimethylated H3K9 (H3K9(Me$_3$)) is required for heritable gene silencing, formation of centromeres, and maintenance of telomere stability (Grewal and Jia, 2007). H3K9 methylation has also been observed at genes that are transcriptionally silenced in cancer (Kondo et al., 2004). The extent (mono-, di- or tri-) and the half-life of methylation are controlled by opposing actions of histone methyltransferases and demethylases, as well as histone turnover.

Removal of methyl groups from lysine residues in histones is carried out by two classes of demethylases: the flavin-dependent lysine specific demethylase family consisting of LSD1 and LSD2 (Karytinos et al., 2009; Shi et al., 2004) as well as the iron- and α-ketoglutarate dependent Jumonji C domain-containing demethylases (Klose et al., 2006a; Kooistra and Helin, 2012). The Jumonji family proteins catalyze a wide set of demethylation reactions on histone substrates, including removal of methyl marks from H3K4, H3K9, H3K27, H3K36 and H4K20. Common to these proteins is their ability to oxidize methyl groups of methylated lysine substrates to form hemiaminal intermediates. Subsequent release of formaldehyde yields demethylated product (Figure 2-1A) (Cloos, Nature 2006; Tsukada, Nature 2006; Ng Nature 2007).

The removal of transcriptionally repressive H3K9(Me$_3$) marks is carried out by the JMJD2 (also known as the KDM4) family of demethylases (Cloos et al., 2006; Fodor et al., 2006; Klose et al., 2006b; Whetstine et al., 2006). Overexpression of several members of the JMJD2 family have been implicated in various diseases (Berry et al., 2012; Cloos et al., 2006; Kawazu et al., 2011; Rui et al., 2010), underscoring the importance of precise regulation of demethylation. Members of the JMJD2 family contain JmjN, JmjC, two PHD domains, and a tandem Tudor domain (Figure 2-1B). While JmjN and JmjC domains form a composite active site (Couture et al., 2007; Ng et al., 2007), the double Tudor domain is thought to allow recruitment of demethylases to their target sites by binding H3K4(Me$_3$) and H4K20(Me3) marks (Lee et al., 2008). The function of PHD domains in JMJD2 family is yet to be determined.

The biological significance of this demethylase family has prompted an investigation into its kinetic and structural features (Couture et al., 2007; Hillringhaus et al., 2011; Hopkinson et al., 2010; Krishnan et al., 2012; Ng et al., 2007). In all of these studies, a catalytic construct consisting of JmjN and JmjC domain was used (cJMJD2A). To date, there is no published kinetic data on the full-length enzyme. Additionally, no kinetic studies have evaluated the ability of any demethylase to remove methyl marks from intact and homogenously modified nucleosomes, a necessary first step in the analysis of the demethylation of chromatin substrates.

Herein, we analyzed the intrinsic processivity and nucleosome demethylation ability of cJMJD2A. Our study reveals that the cJMJD2A uses a

distributive mechanism to affect multiple demethylations. Successful reconstitution of the demethylation of homogeneous site-specifically methylated nucleosomes has allowed us to compare the kinetic parameters for demethylation of nucleosomes and histone tail peptides. Our findings suggest that nucleosome recognition is not intrinsic to cJMJD2A and may be mediated by other domains in JMJD2A or its interacting partners. These domains and protein partners could provide a regulatory mechanism for demethylase activity and processivity *in vivo*. To our knowledge, this is the first report of the demethylation kinetics of nucleosomes by any demethylase. Accomplishing this task sets the stage for analysis of the demethylation of more complex chromatin substrates by JMJD2A and other jumonji demethylases.

RESULTS

Kinetic analysis of peptide demethylation by cJMJD2A

To eliminate possible artifacts due to the presence of an affinity tag, we used a tag-less catalytic domain construct where the hexahistidine tag had been removed from cJMJD2A (amino acids 1-350 of JMJD2A) after purification (see Supporting Information). Using a fluorescent assay that follows the formation of the demethylation byproduct formaldehyde (Couture et al., 2007), demethylation of tri- and dimethylated H3K9 peptides corresponding to amino acids 7-14 of the histone H3 tail (ARK(Me$_3$)STGGK and ARK(Me$_2$)STGGK) by cJMJD2A was analyzed (Figure 2-2A and Figure 2-2B). In these assays, ARK(Me$_3$)STGGK is demethylated more efficiently than ARK(Me$_2$)STGGK. The dimethylated peptide exhibited a six-fold increase in K_M and a two-fold decrease in turnover numbers compared to the trimethylated peptide (K_M = 410 μM, k_{cat} = 1.0 min^{-1} for ARK(Me$_2$)STGGK and K_M = 67 μM, k_{cat} = 1.8 min^{-1} for ARK(Me$_3$)STGGK).

We used mass spectrometry (MS) to measure the extent of demethylation of the trimethylated substrate as a function of time (Figure 2-2C). The rapid disappearance of trimethylated species and accumulation of dimethylated intermediates further support the observation that cJMJD2A demethylates ARK(Me$_3$)STGGK more efficiently than ARK(Me$_2$)STGGK. A slow decay of the dimethyl species and concomitant increase in monomethyl species past the initial four hours of incubation suggest that the enzyme is mostly inactive by this time.

Distributive demethylation by cJMJD2A

Two consecutive demethylations are required for the formation of monomethylated product from the starting trimethylated peptide. The serial demethylation events can proceed by a processive or distributive mechanism. In a processive demethylation mechanism, the intermediate dimethylated product is not released from the enzyme. In contrast, in a distributive mechanism, demethylation of trimethylated peptide is followed by a release of dimethylated intermediate prior to the dimethylated intermediate rebinding and conversion to the monomethyl species.

To test these two possibilities, we carried out pulse-chase experiments in which demethylation of biotinylated substrate peptide (ARK(Me$_3$)STGGK-biotin) with a limiting amount of the enzyme was challenged by the addition of an excess of unlabeled trimethylated peptide (ARK(Me$_3$)STGGK) chase. Following 5 min of ARK(Me$_3$)STGGK-biotin preincubation, the reaction was equally divided and chase was added (20-fold excess of ARK(Me$_3$)STGGK chase in water or an equivalent volume of water alone). The peptide product distributions were monitored by mass spectrometry over time.

In the presence of chase, the amount of ARK(Me$_1$)STGGK-biotin is substantially less than in the no chase control (Figure 2-3), suggesting that the chase peptide competes with the biotinylated peptide consistent with a distributive mechanism. This distributive mechanism of cJMJD2A is further supported by the multiple turnover time course experiment (Figure 2-2C) where

56

ARK(Me$_2$)STGGK accumulated to amounts greater than the enzyme concentration.

Demethylation of nucleosomes

To assess the ability of cJMJD2A to demethylate nucleosomes, we prepared homogeneous, site-specifically modified nucleosomes using methyllysine analogs (MLAs) (Simon et al., 2007). In this method, a methyl lysine mimic is incorporated into histone H3 via alkylation of a mutant cysteine residue substituting lysine 9 in histone H3, and the modified histone is subsequently incorporated into recombinant nucleosomes (Figure 2-4A). To quantitatively compare demethylation kinetics between analog-modified and native substrates, we first determined cJMJD2A activity on a trimethyllysine analog peptide ARK9C(Me$_3$)STGGK (Figure 2-4B). We observed an approximate four-fold decrease in k_{cat} (0.48 min^{-1}) and five-fold increase in K_M (330 μM) as compared to endogenous trimethylated peptide (Figure 2-2A).

Demethylation of nucleosomes by cJMJD2A was carried out under single-turnover conditions with excess enzyme, a method that better enables the measurement of rates of the catalytic step (Johnson, 1992). To allow for sufficient assay sensitivity, demethylation was monitored by quantitative western blotting using antibodies specific for H3K9(Me$_3$) and H4 (for normalization). To ensure protein quantification accuracy, the amounts of nucleosomes used in these experiments were within the linear detection range of H3K9(Me$_3$) and H4 antibodies (Figure 2-5A). Importantly, under these conditions, no cross-reactivity

was observed between H3K9(Me$_3$)-specific antibody and mono- and dimethyl recombinant MLA nucleosomes (Figure 2-5B). By using H3K9(Me$_3$)-specific antibody to monitor disappearance of starting material and an antibody against H4 as a loading control, we were able to monitor the loss of the trimethylated nucleosome substrate as a function of enzyme concentration. In these experiments, nucleosome concentration was kept constant at 300 nM, while the concentration of cJMJD2A was varied between 50 - 400 μM. For each enzyme concentration, the ratio of H3K9C(Me$_3$) to H4 signal was monitored as a function of time, which is used to determine the first-order rate constant for starting material consumption (k_{obs}) (Figure 2-4C). A catalytic step rate (k_{max}) of 0.16 min^{-1} and an apparent K_M (K'_M) of 240 μM were determined by nonlinear regression analysis of observed first-order rate constants as a function of enzyme concentration (Figure 2-4D).

DISCUSSION

Histone methylation, a post-translational modification critical to the regulation of transcription, is controlled by the opposing actions of histone methyltransferases and demethylases. Tight control of the site and extent (mono-, di-, or tri-) of methylation is crucial for proper cellular function. Jumonji histone demethylases are critical regulators of nucleosomal methylation, and their misregulation is associated with cancer and neurological disorders (Kooistra and Helin, 2012). By antagonizing repressive H3K9 di- and trimethylation, enzymes belonging to JMJD2 family of demethylases have a crucial impact on transcription, an effect well studied in the context of nuclear hormone receptor mediated transcription (Wissmann et al., 2007). Herein, we report our findings on the processivity and kinetic analysis of nucleosome demethylation by cJMJD2A. Determining the intrinsic behavior of the catalytic domain of JMJD2A provides a better understanding of how this demethylase may be regulated.

The ability of cJMJD2A to catalyze demethylation was first analyzed on methylated histone tail peptides. The kinetic parameters obtained show high turnover for this family of enzymes (k_{cat}(ARK(Me$_3$)STGGK) = 1.8 min^{-1}; k_{cat}(ARK(Me$_2$)STGGK) = 1.0 min^{-1}) (Figure 2-2), indicating that enzyme obtained in this manner is well behaved and comparable to the most active preparations published (Krishnan et al., 2012). Our findings also indicate that the trimethylated peptide is a better substrate than the dimethylated variant for cJMJD2A, predominantly due to differences in K_M (K_M(ARK(Me$_3$)STGGK) = 67 μM; K_M(ARK(Me$_2$)STGGK) = 410 μM). The preference for trimethylated substrate is

consistent with previous reports using His-tagged catalytic constructs of JMJD2A (Couture et al., 2007; Hillringhaus et al., 2011). Additionally, mass spectrometric monitoring of demethylation of the trimethylated peptide over time showed the rapid disappearance of trimethylated species and the accumulation of the intermediate dimethylated peptide, which slowly decays to a monomethyl product (Figure 2-2C). These findings are consistent with our kinetic measurements indicating strong preference for trimethylated peptide.

Mechanistically, multiple methyl marks can be demethylated either distributively or processively, depending on whether peptide substrates dissociate or remain enzyme-bound between consecutive demethylations. Our findings indicate that the catalytic domain of JMJD2A by itself is distributive in its action. The release of the dimethyl intermediate may have a significant impact on the regulation of transcription. For example, HP1 is recruited to heterochromatic loci by specific association with H3K9($Me_{2/3}$), while sites containing H3K9($Me_{1/0}$) generally lack HP1 and remain euchromatic (Bannister et al., 2001; Canzio et al., 2011; Fischle et al., 2008; Grewal and Jia, 2007; Lachner et al., 2001). Thus in one possible scenario, the release of the dimethyl peptide may serve as an additional check-point before full commitment to the functional output signaled by the monomethylated state. Moreover, the observation that the dimethylated peptide is a ten-fold poorer substrate than the trimethylated peptide raises the possibility that demethylation of dimethylated substrates may, in some instances, be carried out by other demethylases. For example, in the context of androgen receptor-mediated transcription, JMJD2C associates with a flavoprotein

60

demethylase LSD1, and in this complex, LSD1 acts on mono- and dimethyl H3K9 marks (Metzger et al., 2005; Wissmann et al., 2007). Like JMJD2C, JMJD2A is also known to associate with LSD1 in an androgen receptor-dependent fashion (Kauffman et al., 2011).

Our data further imply that cJMJD2A does not significantly discriminate between histone tail peptide and nucleosomal substrates. The k_{cat}/K_M values for these two substrates are within 2.5-fold of one another (k_{cat}/K_M (ARK9C(Me$_3$)STGGK) = 1.5 x 10^{-3} μM^{-1}min^{-1} and k_{max}/K'_M (H3K9C(Me$_3$) Nuc) = 0.67 x 10^{-3} μM^{-1}min^{-1}). This result implies that the catalytic domain of JMJD2A predominantly recognizes residues immediately surrounding the H3K9 residue, and does not recognize additional features on the nucleosome. Recognition of other chromatin features or other modifications by the double Tudor or PHD domains of the full-length demethylase may result in tighter association and an increase in demethylase activity. Such additional interactions may also increase the processivity of the catalytic domain. By analogy, protein interacting partners may also contribute to the regulation of activity and processivity. *In vivo*, it is plausible that in the presence of the relevant chromatin marks and/or protein partners, full-length JMJD2A may demethylate in a processive manner yielding monomethylated product. Such regulation of processivity would have significant implications for controlling the specific output of JMJD2A proteins in a context dependent manner (Bua et al., 2009; Collins et al., 2008; Iwase et al., 2007; Kim et al., 2006; Rottach et al., 2010).

Overall, our ability to quantitatively assess the removal of methyl marks from site-specifically methylated nucleosomes by a demethylase is the necessary first step in further detailed investigations of chromatin modification by demethylases and demethylase-containing protein complexes. These studies will also address the importance of the cross-talk between chromatin marks in the regulation of histone methylation.

METHODS

Demethylation of nucleosomes

Demethylations of nucleosomes were performed by incubation of nucleosomes containing H3K9C(Me3) (300 nM) with α-ketoglutarate (1 mM), ascorbate (1 mM), varying concentrations of JMJD2A (50 – 400 μM), and Fe(NH$_4$)$_2$(SO$_4$)$_2$ (twice the concentration of JMJD2A) in 50 mM Hepes (pH 7.5) at room temperature. Reactions were initiated by addition of methylated nucleosomes. Time points were quenched using 3:1 mixture of 6X SDS sample loading buffer and 0.5 M EDTA pH 8.0 and boiled at 100 °C for 2 min. Samples were run on 15% Criterion gels at 200 V for 40 min and transferred onto Immunblot PVDF membranes (Bio-Rad) at 4 °C for 2 hr at 600 mAmp. Membranes were blocked at room temperature in 10 mL Odyssey Blocking Buffer (LI-COR Biosciences) for 75 min, and then incubated overnight with H3K9C(Me3) antibody (Upstate 07-442, Lot: 2017310) and H4 antibody (Active Motif 39269, Lot: 11908001) at 1:800 and 1:1000 dilutions, respectively in 1:1 mixture of 1X PBS and Odyssey Blocking Buffer containing 0.02% Tween-20 at 4 °C. Membranes were subsequently washed with 1X TBS and 0.05% Tween-20 (4 times, 4 min each), and then incubated with IRDye 680LT Goat Anti-Rabbit secondary antibody (LI-COR 926-68021, Lot: C10628-01) at 1:20,000 dilutions in 1:1 mixture of 1X PBS and Odyssey Blocking Buffer containing 0.02% Tween-20 for 40 min at room temperature. Following this, membranes were washed as described above and analyzed using Odyssey Application Software (LI-COR Biosciences).

Data were analyzed by dividing fluorescent antibody signal of H3K9C(Me3) by that of H4. These ratios were normalized to the H3K9C(Me3)/H4 ratio at time zero, graphed as a function of time, and fitted to the equation $[\text{H3K9C(Me3)}] = [\text{H3K9C(Me3)}]_{t=0}e^{-k_{obs}t}$. Obtained k_{obs} values were then graphed against cJMJD2A concentrations and fit to $k_{obs} = (k_{max}X)/(X+K'_M)$ with nonlinear regression to determine k_{max} and K'_M parameters, where X is the concentration of cJMJD2A.

Analysis of the processivity of peptide demethylation

To a reaction mixture containing cJMJD2A (5 μM), α-ketoglutarate (1 mM), ascorbate (1 mM), and $Fe(NH_4)_2(SO_4)_2$ (50 μM) in 50 mM Hepes (pH 7.5), ARK(Me3)STGGK-biotin (150 μM) (Genscript) was added and reaction mixture incubated at room temperature for 5 min. Subsequently, ARK(Me3)STGGK (3 mM, 10 μL) (Genscript) chase or water (10 μL) was added and reactions were allowed to proceed at room temperature. Time points were taken and quenched with equal volume of 0.5 M EDTA pH 8.0 and desalted through C_{18} ZipTips (Millipore). The extent of demethylation of biotinylated peptide was analyzed by MALDI-TOF MS.

Protein cloning, expression, and purification

The catalytic domain of human JMJD2A (1-350 aa) was cloned into pBH4 plasmid containing TEV cleavable N-terminal hexahistidine tag (gift from Wendell Lim Laboratory) using *NotI* and *BamHI* sites. Transfected Rosetta2(DE3)pLysS

(Novagen) cells were grown at 37 °C to OD_{600} 0.6 and induced with a final concentration of 0.4 mM isopropyl β-D-thiogalactoside at 18 °C for 12 hr. Cells were lysed in 50 mM Hepes (pH 7.5), 500 mM NaCl, 20 mM imidazole, 0.5 mM TCEP, 1 mM $MgCl_2$, 1 mM $CaCl_2$, and 0.1 mg/mL DNaseI (Sigma). Cell debris was removed by centrifugation and the supernatant was incubated with Ni-NTA beads (Qiagen) at 4 °C for 1 hr. Beads were washed with 50 mM Hepes (pH 7.5), 500 mM NaCl, 40 mM imidazole and 0.5 mM TCEP, and the protein eluted with 50 mM Hepes (pH 7.5), 500 mM NaCl, 250 mM imidazole, and 0.5 mM TCEP. Eluted JMJD2A fractions were pooled and incubated with recombinantly expressed His-tagged TEV protease (1:10 by weight) at 4 °C for 3 hr while dialyzing in 50 mM Hepes (pH 7.5), 500 mM NaCl, 20 mM imidazole, and 0.5 mM TCEP. To separate TEV protease and the cleaved His tag, the sample was incubated with Ni-NTA beads (Qiagen) for 30 min at 4 °C. The flow-through was collected, concentrated, and purified on HiLoad 26/60 Superdex75 (GE Healthcare) in 50 mM Hepes (pH 7.5) and 500 mM NaCl at 4 °C.

Nucleosome preparation

H2A, H2B, H3K9C, and H4 were prepared as described (Luger et al., 1999; Simon et al., 2007). H3K9C was alkylated as described (Simon et al., 2007). Octamers were prepared as previously described (Luger et al., 1999). For each assembly, octamer to DNA ratio was adjusted to allow for a complete assembly of nucleosomes (Luger et al., 1999). For these experiments, 601 sequence of DNA was used and assemblies performed. Hepes-based buffers

containing 2 mM DTT were used, otherwise identical to those previously used (Luger et al., 1999; Simon et al., 2007). Nucleosomes were purified by Superdex 200 10/300 GL (GE Healthcare) in 50 mM Hepes (pH 7.5) and 2 mM DTT buffer at 4 °C and stored at ~ 20 μM concentrations. Concentrations of nucleosomes were determined based on 260 nm absorbance of the DNA.

Demethylation of peptides

Kinetic parameters for demethylation of peptides were determined by an enzyme-coupled assay that monitors the production of formaldehyde (Couture et al., 2007). In these experiments, cJMJD2A (1 μM), NAD$^+$ (2 mM), formaldehyde dehydrogenase (FDH, 0.05 U, Sigma), α-ketoglutarate (1 mM), ascorbate (1 mM), and $Fe(NH_4)_2(SO_4)_2$ (50 μM) were incubated with varying concentrations of ARK(Me3)STGGK (Genscript), ARK(Me2)STGGK (Genscript), or ARK9C(Me3)STGGK in 50 mM Hepes (pH 7.5). Reactions were started by addition of substrate and followed at 15 sec intervals at room temperature on a SpectraMax M5e (Molecular Devices) using 350 nm excitation and 460 nm emission wavelengths. An NADH standard curve was used to convert fluorescence to concentration of product formed. The initial 2.5 min were used to calculate initial velocities, which were graphed against substrate concentration. Michaelis-Menten parameters were determined by non-linear least squares fitting using Kaleidagraph.

In vitro analysis of demethylation of ARK(Me3)STGGK over time by LC-MSMS

Reactions were performed by incubating cJMJD2A (1 μM) with α-ketoglutarate (1 mM), ascorbate (1 mM), Fe(NH$_4$)$_2$(SO$_4$)$_2$ (50 μM) and ARK(Me3)STGGK (200 μM, Genscript) in 50 mM Hepes (pH 7.5) at room temperature. 20 μL time points were quenched with 5 μL of 0.5 M EDTA (pH 8.0). After quenching with EDTA, samples were spun and 5 μL from each time point was diluted with 45 μL of internal standard solution (1 μM ARTKQTARK(Me3)STG in 0.1% formic acid). Samples were quantitated using a QTRAP 5500 triple quadrupole mass spectrometer (AB-Sciex, Foster City, CA) with online separation performed by a nanoAcquity UPLC system (Waters, Milford, MA) equipped with a 100 μm x 10 cm BEH130 1.7 μm analytical C$_{18}$ column and a 180 μm x 2 cm Symmetry 5 μm C$_{18}$ trap column (Waters). 5 μL of sample was loaded onto the trap column for 4 min at flow rate of 5 μL/min with 1% mobile phase B (0.1% formic acid in ACN) and 99% mobile phase A (0.1% formic acid in H$_2$O). The flow was then switched to the analytical column and the peptides were eluted with a linear gradient from 1-8% mobile phase B in 10 minutes at a flow rate of 600 nL/min. The column was then washed with 80% mobile phase B for 3 minutes and re-equilibrated at 1% mobile phase B for 7 minutes before starting the next analysis. Tri-, di-, and mono-methyl variants of the ARK(Mex)STGGK peptide were analyzed by multiple reaction monitoring (MRM) in the positive ion mode with a 25 msec dwell time. Three transitions were used for each peptide and the sum of their areas compared to the sum of

three transitions from the internal standard (see below). Calibration curves were generated from serial dilutions of reference solutions. Peaks were integrated using Analyst software (version 1.5.1; AB Sciex).

Peptide	Q1 (m/z)	Q3 (m/z)	CE (V)	annotation
ARK(Me)STGGK	409.75	211.1	34	b_2 - NH_3
ARK(Me)STGGK	409.75	345.7	35	b_7 + H_2O (2+)
ARK(Me)STGGK	409.75	644.4	35	a_7
ARK(Me2)STGGK	416.75	211.1	35	b_2 - NH_3
ARK(Me2)STGGK	416.75	352.7	36	b_7 + H_2O (2+)
ARK(Me2)STGGK	416.75	658.4	36	a_7
ARK(Me3)STGGK	423.76	211.1	36	b_2 - NH_3
ARK(Me3)STGGK	423.76	359.7	37	b_7 + H_2O (2+)
ARK(Me3)STGGK	423.76	655.4	37	a_7 - NH_3
ARTKQTARK(Me3)STG	449.60	560.4	33	y_{10} (2+)
ARTKQTARK(Me3)STG	449.60	644.4	33	y_6 - NH_3
ARTKQTARK(Me3)STG	449.60	745.4	33	y_7 - NH_3
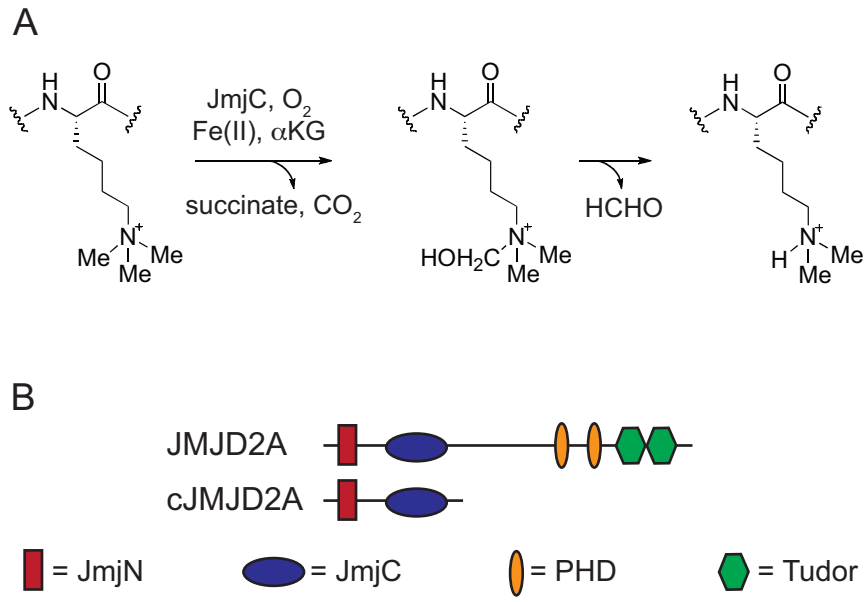
Figure 2-1. Catalysis and domain architecture of JMJD2A. (A) The abbreviated catalytic mechanism of Jumonji histone demethylases showing the hemiaminal intermediate. (B) Domain organization in JMJD2A.
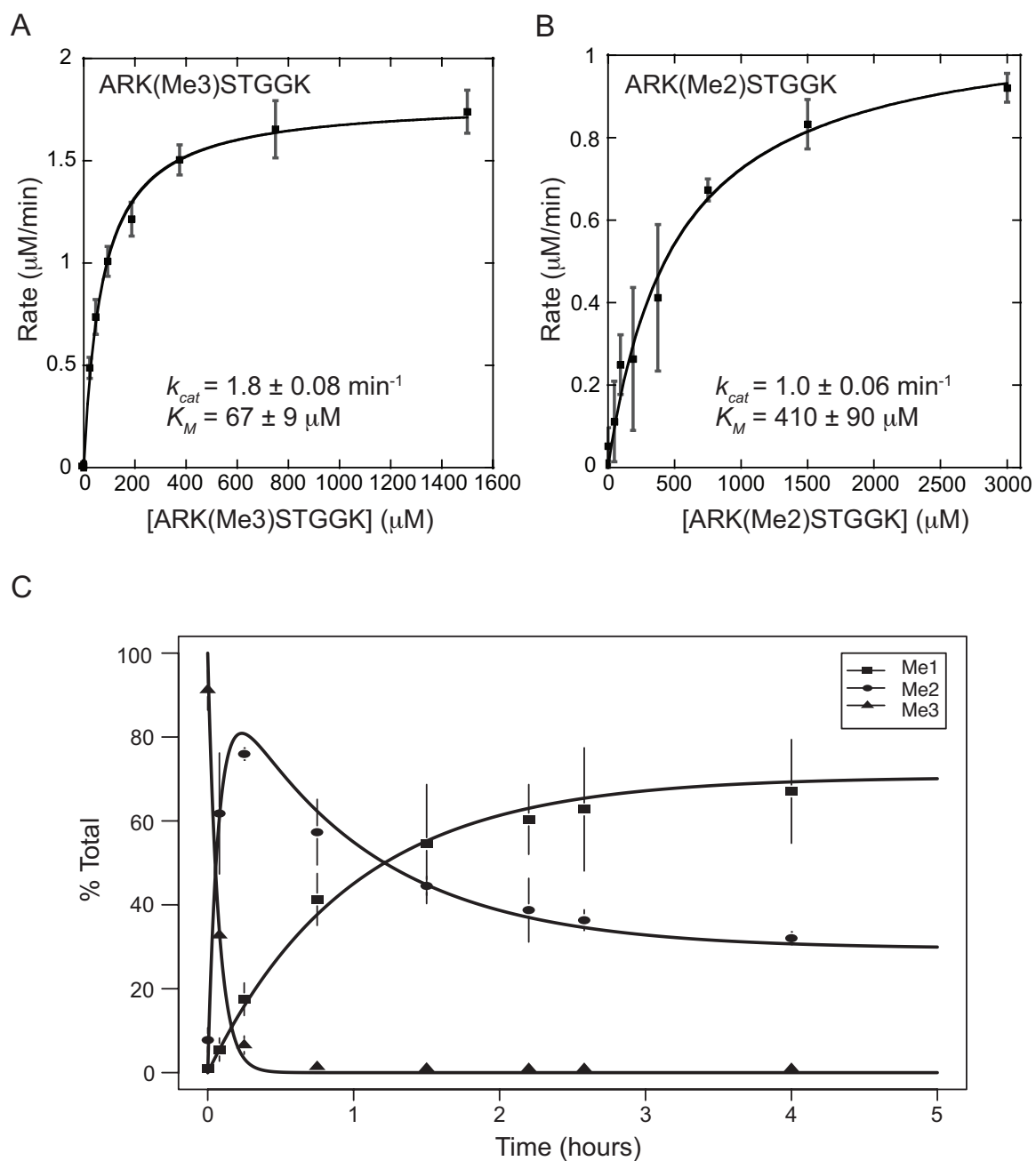
Figure 2-2. Kinetic analysis of cJMJD2A-mediated demethylation of peptides. (A-B) Michaelis-Menten plots of initial velocity as a function of the concentration of ARK(Me3)STGGK (A) and ARK(Me2)STGGK (B). Experiments were done in

triplicate and are represented as mean ± SEM. For experimental conditions and procedure, see Supporting Information. (C) Demethylation of ARK(Me3)STGGK monitored over time using LC-MSMS. Lines connecting data points are introduced to facilitate visualization and do not represent kinetic fits.
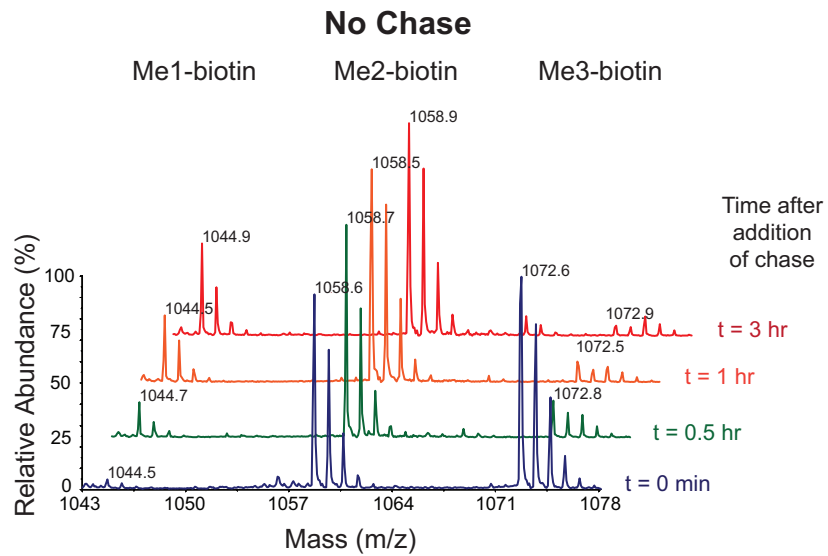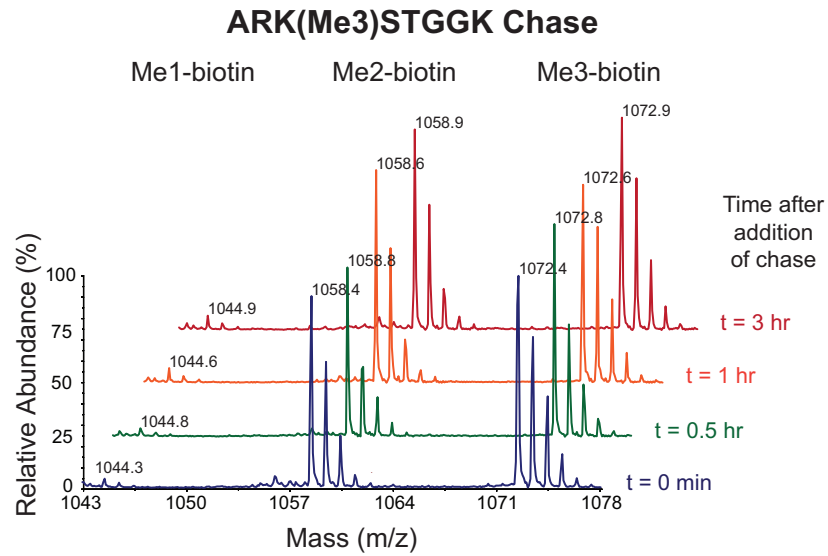
Figure 2-3. Analysis of processivity in cJMJD2A-catalyzed demethylation. Labeled peaks correspond to mono-, di- or trimethylated biotinylated peptides detected in the presence (top) or absence (bottom) of the chase.
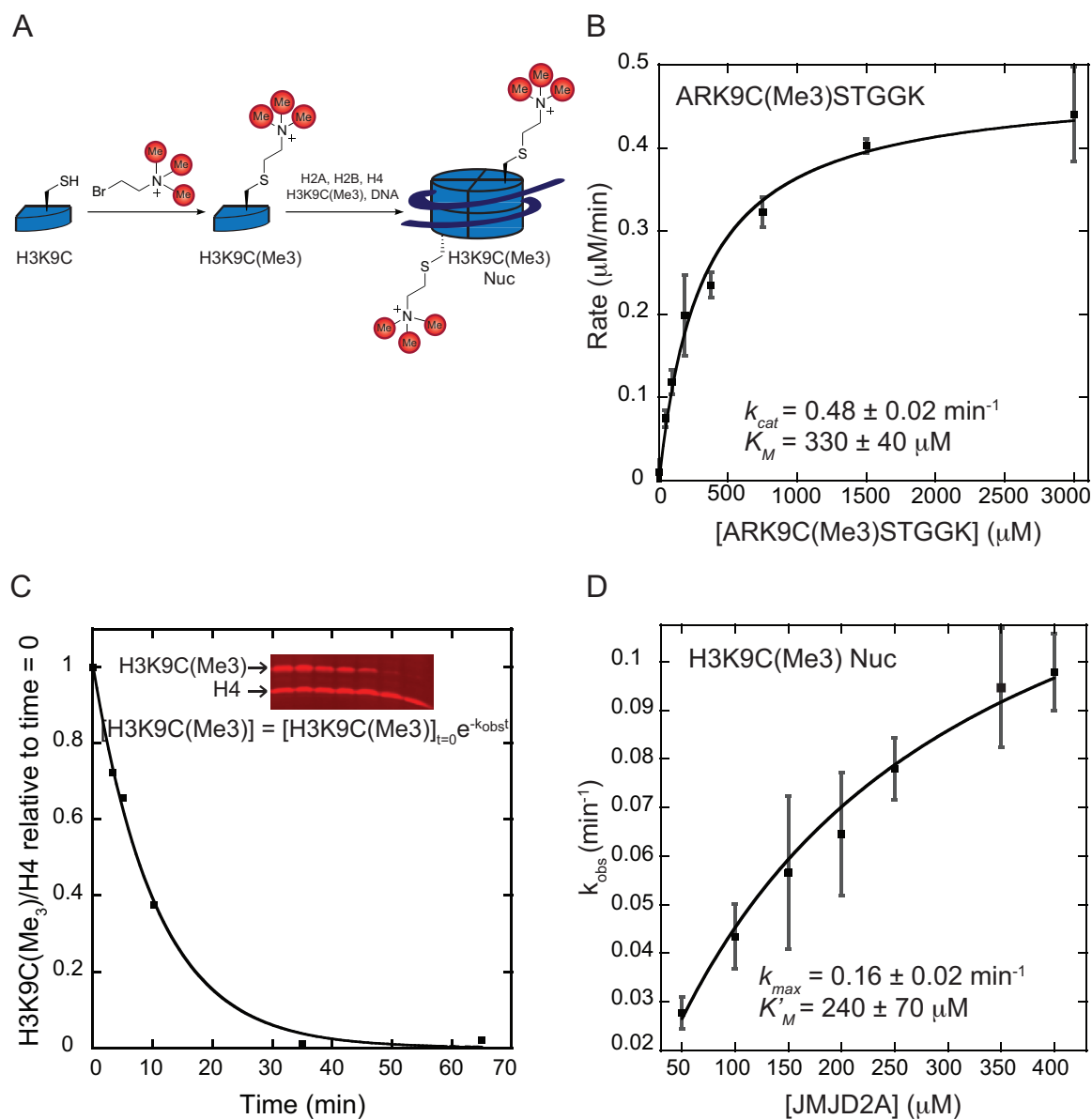
Figure 2-4. Kinetic analysis of cJMJD2A-mediated demethylation of methyllysine analog (MLA)-containing peptides and nucleosomes. (A) Preparation of recombinant homogeneous H3K9(Me3) nucleosomes. Recombinant histone H3K9C was alkylated with (2-bromoethyl)trimethylammonium bromide to form H3K9C(Me3) histones. Subsequent assembly with histone H2A, H2B, H4, and

601 sequence DNA provided homogeneous H3K9C(Me3) nucleosomes. (B) Michaelis-Menten plot for demethylation of MLA-containing peptide. (C) Western blot analysis of an experiment performed at 350 μM cJMJD2A. Data analysis and extrapolation of k_{obs} is described in experimental procedures. (D) Kinetics of demethylation of MLA-containing nucleosomes. Data were obtained from three independent experiments and represented as mean ± SEM. See also Figure 2-S1.
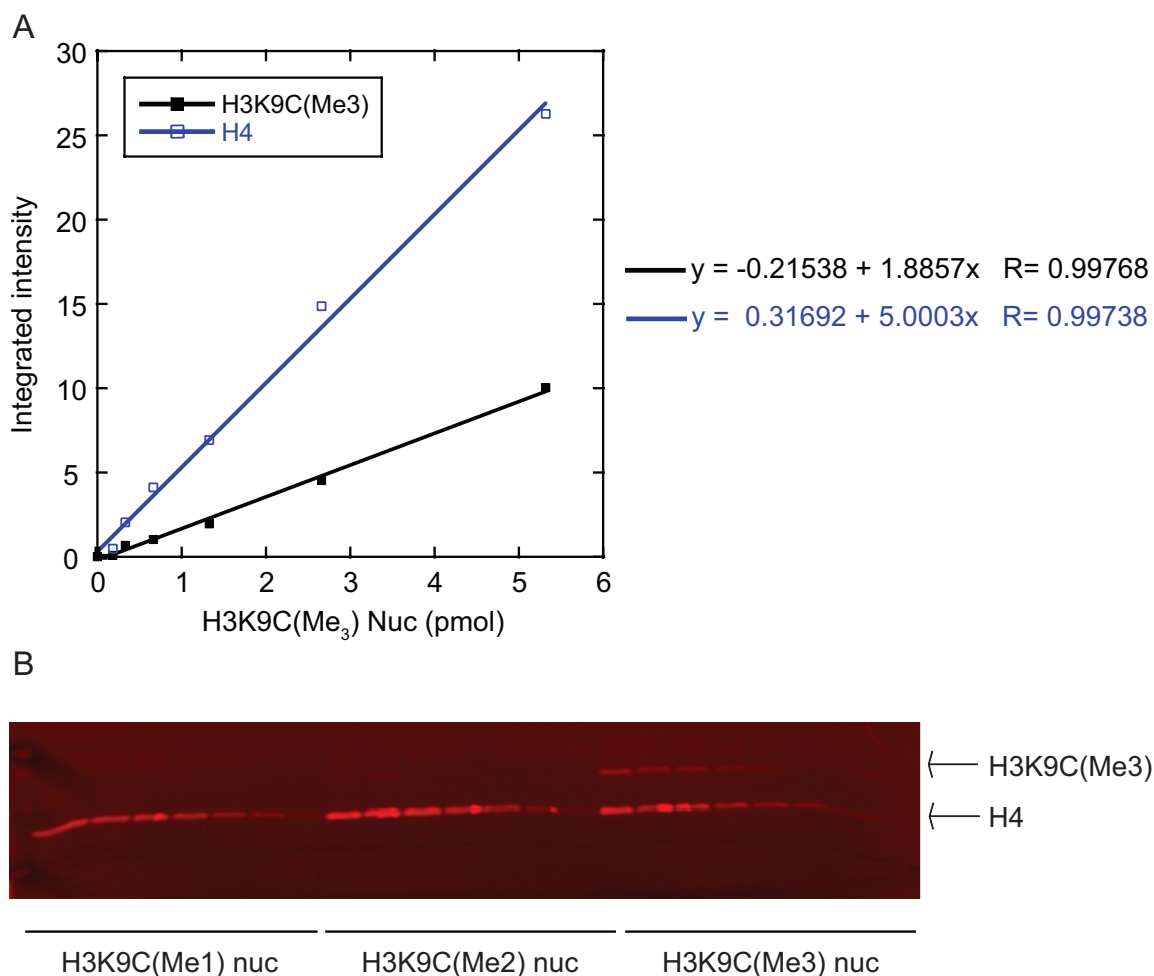
Figure 2-5. Linear detection range and specificity of H3K9C(Me3) and H4 antibodies. (A) Linear range of detection for H3K9(Me3) and H4 antibodies. Antibody detection is linear within tested conditions (0 – 5.25 pmol). Nucleosome demethylation reactions contained 3.6 pmol of H3K9C(Me3) nucleosomes. (B) Specificity of H3K9(Me3) antibody. Detection of H3K9C(Me1), H3K9C(Me2), and H3K9C(Me3) MLA recombinant nucleosomes (containing 5.25 pmol, 4.5 pmol, 3.75 pmol, 3 pmol, 2.25 pmol, 1.5 pmol, and 0.75 pmol) by H3K9C(Me3) antibody (Upstate 07-442). Nucleosome demethylation experiments contained 3.6 pmol nucleosomes.

ACKNOWLEDGMENTS

REFERENCES

Bannister, A.J., Zegerman, P., Partridge, J.F., Miska, E.A., Thomas, J.O., Allshire, R.C., and Kouzarides, T. (2001). Selective recognition of methylated lysine 9 on histone H3 by the HP1 chromo domain. Nature *410*, 120-124.

Berry, W.L., Shin, S., Lightfoot, S.A., and Janknecht, R. (2012). Oncogenic features of the JMJD2A histone demethylase in breast cancer. Int J Oncol *41*, 1701-1706.

Bua, D.J., Kuo, A.J., Cheung, P., Liu, C.L., Migliori, V., Espejo, A., Casadio, F., Bassi, C., Amati, B., Bedford, M.T.*, et al.* (2009). Epigenome microarray platform for proteome-wide dissection of chromatin-signaling networks. PLoS ONE *4*, e6789.

Canzio, D., Chang, E.Y., Shankar, S., Kuchenbecker, K.M., Simon, M.D., Madhani, H.D., Narlikar, G.J., and Al-Sady, B. (2011). Chromodomain-Mediated Oligomerization of HP1 Suggests a Nucleosome-Bridging Mechanism for Heterochromatin Assembly. Mol Cell *41*, 67-81.

Cloos, P.A.C., Christensen, J., Agger, K., Maiolica, A., Rappsilber, J., Antal, T., Hansen, K.H., and Helin, K. (2006). The putative oncogene GASC1 demethylates tri- and dimethylated lysine 9 on histone H3. Nature *442*, 307-311.

Collins, R.E., Northrop, J.P., Horton, J.R., Lee, D.Y., Zhang, X., Stallcup, M.R., and Cheng, X. (2008). The ankyrin repeats of G9a and GLP histone methyltransferases are mono- and dimethyllysine binding modules. Nat Struct Mol Biol *15*, 245-250.

Couture, J.-F., Collazo, E., Ortiz-Tello, P.A., Brunzelle, J.S., and Trievel, R.C. (2007). Specificity and mechanism of JMJD2A, a trimethyllysine-specific histone demethylase. Nat Struct Mol Biol *14*, 689-695.

Fischle, W., Franz, H., Jacobs, S.A., Allis, C.D., and Khorasanizadeh, S. (2008). Specificity of the chromodomain Y chromosome family of chromodomains for lysine-methylated ARK(S/T) motifs. J Biol Chem *283*, 19626-19635.

Fodor, B.D., Kubicek, S., Yonezawa, M., O'Sullivan, R.J., Sengupta, R., Perez-Burgos, L., Opravil, S., Mechtler, K., Schotta, G., and Jenuwein, T. (2006). Jmjd2b antagonizes H3K9 trimethylation at pericentric heterochromatin in mammalian cells. Genes Dev *20*, 1557-1562.

Grewal, S.I., and Jia, S. (2007). Heterochromatin revisited. Nat Rev Genet *8*, 35-46.

Hillringhaus, L., Yue, W.W., Rose, N.R., Ng, S.S., Gileadi, C., Loenarz, C., Bello, S.H., Bray, J.E., Schofield, C.J., and Oppermann, U. (2011). Structural and evolutionary basis for the dual substrate selectivity of human KDM4 histone demethylase family. J Biol Chem *286*, 41616-41625.

Hopkinson, R.J., Hamed, R.B., Rose, N.R., Claridge, T.D., and Schofield, C.J. (2010). Monitoring the activity of 2-oxoglutarate dependent histone demethylases by NMR spectroscopy: direct observation of formaldehyde. Chembiochem *11*, 506-510.

Iwase, S., Lan, F., Bayliss, P., de la Torre-Ubieta, L., Huarte, M., Qi, H.H., Whetstine, J.R., Bonni, A., Roberts, T.M., and Shi, Y. (2007). The X-linked

mental retardation gene SMCX/JARID1C defines a family of histone H3 lysine 4 demethylases. Cell *128*, 1077-1088.

Johnson, K.A. (1992). Transient-State Kinetic Analysis of Enzyme Reaction Pathways. The Enzymes *20*, 1-61.

Karytinos, A., Forneris, F., Profumo, A., Ciossani, G., Battaglioli, E., Binda, C., and Mattevi, A. (2009). A novel mammalian flavin-dependent histone demethylase. J Biol Chem *284*, 17775-17782.

Kauffman, E.C., Robinson, B.D., Downes, M.J., Powell, L.G., Lee, M.M., Scherr, D.S., Gudas, L.J., and Mongan, N.P. (2011). Role of androgen receptor and associated lysine-demethylase coregulators, LSD1 and JMJD2A, in localized and advanced human bladder cancer. Molecular carcinogenesis.

Kawazu, M., Saso, K., Tong, K.I., McQuire, T., Goto, K., Son, D.O., Wakeham, A., Miyagishi, M., Mak, T.W., and Okada, H. (2011). Histone demethylase JMJD2B functions as a co-factor of estrogen receptor in breast cancer proliferation and mammary gland development. PLoS ONE *6*, e17830.

Kim, J., Daniel, J., Espejo, A., Lake, A., Krishna, M., Xia, L., Zhang, Y., and Bedford, M.T. (2006). Tudor, MBT and chromo domains gauge the degree of lysine methylation. EMBO Rep *7*, 397-403.

Klose, R.J., Kallin, E.M., and Zhang, Y. (2006a). JmjC-domain-containing proteins and histone demethylation. Nat Rev Genet *7*, 715-727.

Klose, R.J., Yamane, K., Bae, Y., Zhang, D., Erdjument-Bromage, H., Tempst, P., Wong, J., and Zhang, Y. (2006b). The transcriptional repressor JHDM3A demethylates trimethyl histone H3 lysine 9 and lysine 36. Nature *442*, 312-316.

Kondo, Y., Shen, L., Yan, P.S., Huang, T.H., and Issa, J.P. (2004). Chromatin immunoprecipitation microarrays for identification of genes silenced by histone H3 lysine 9 methylation. Proc Natl Acad Sci U S A *101*, 7398-7403.

Kooistra, S.M., and Helin, K. (2012). Molecular mechanisms and potential functions of histone demethylases. Nat Rev Mol Cell Biol *13*, 297-311.

Krishnan, S., Collazo, E., Ortiz-Tello, P.A., and Trievel, R.C. (2012). Purification and assay protocols for obtaining highly active Jumonji C demethylases. Anal Biochem *420*, 48-53.

Lachner, M., O'Carroll, D., Rea, S., Mechtler, K., and Jenuwein, T. (2001). Methylation of histone H3 lysine 9 creates a binding site for HP1 proteins. Nature *410*, 116-120.

Lee, J., Thompson, J.R., Botuyan, M.V., and Mer, G. (2008). Distinct binding modes specify the recognition of methylated histones H3K4 and H4K20 by JMJD2A-tudor. Nat Struct Mol Biol *15*, 109-111.

Metzger, E., Wissmann, M., Yin, N., Müller, J.M., Schneider, R., Peters, A.H.F.M., Günther, T., Buettner, R., and Schüle, R. (2005). LSD1 demethylates repressive histone marks to promote androgen-receptor-dependent transcription. Nature *437*, 436-439.

Ng, S.S., Kavanagh, K.L., McDonough, M.A., Butler, D., Pilka, E.S., Lienard, B.M.R., Bray, J.E., Savitsky, P., Gileadi, O., von Delft, F*., et al.* (2007). Crystal structures of histone demethylase JMJD2A reveal basis for substrate specificity. Nature *448*, 87-91.

Rottach, A., Frauer, C., Pichler, G., Bonapace, I.M., Spada, F., and Leonhardt, H. (2010). The multi-domain protein Np95 connects DNA methylation and histone modification. Nucleic Acids Res *38*, 1796-1804.

Rui, L., Emre, N.C.T., Kruhlak, M.J., Chung, H.-J., Steidl, C., Slack, G., Wright, G.W., Lenz, G., Ngo, V.N., Shaffer, A.L*., et al.* (2010). Cooperative epigenetic modulation by cancer amplicon genes. Cancer Cell *18*, 590-605.

Shi, Y., Lan, F., Matson, C., Mulligan, P., Whetstine, J.R., Cole, P.A., Casero, R.A., and Shi, Y. (2004). Histone demethylation mediated by the nuclear amine oxidase homolog LSD1. Cell *119*, 941-953.

Simon, M.D., Chu, F., Racki, L.R., De La Cruz, C.C., Burlingame, A.L., Panning, B., Narlikar, G.J., and Shokat, K.M. (2007). The Site-Specific Installation of Methyl-Lysine Analogs into Recombinant Histones. Cell *128*, 1003-1012.

Whetstine, J.R., Nottke, A., Lan, F., Huarte, M., Smolikov, S., Chen, Z., Spooner, E., Li, E., Zhang, G., Colaiacovo, M*., et al.* (2006). Reversal of histone lysine trimethylation by the JMJD2 family of histone demethylases. Cell *125*, 467-481.

Wissmann, M., Yin, N., Müller, J.M., Greschik, H., Fodor, B.D., Jenuwein, T., Vogler, C., Schneider, R., Günther, T., Buettner, R*., et al.* (2007). Cooperative demethylation by JMJD2C and LSD1 promotes androgen receptor-dependent gene expression. Nat Cell Biol *9*, 347-353.

Chapter 3: Possible JMJD2A oligomerization

INTRODUCTION

As of date, characterization of demethylation has been limited to peptides until our work on nucleosomes that was described in Chapter 2. Our initial pursuit of demethylase kinetics of the nucleosome substrate was done using a histidine-tagged catalytic domain construct (His-cJMJD2A). This construct contained the JmjN and JmjC domains and spanned amino acids 1-350. Interestingly, our preliminary study on nucleosome demethylation by His-cJMJD2A suggested cooperativity.

Cooperativity is supported by a previous report (Shin and Janknecht, 2007). Shin et al. mapped oligomerization of JMJD2A to the N-terminal region of the protein through pull-down analysis with various constructs as deletion of the first 300 amino acids resulted in a lack of complex detection. Additionally, heteromers of JMJD2A and JMJD2C was observed (Shin and Janknecht, 2007).

RESULTS AND DISCUSSION

Kinetic analysis of His-cJMJD2A demethylation of methyl lysine analog (MLA) peptide and nucleosome

We first tested His-cJMJD2A demethylation of MLA peptide that contained amino acids 7-14 of the N-terminus of histone H3 (ARK9C(Me3)STGGK) (Figure 3-1). Obtained kinetic parameters of K_M = 340 μM and k_{cat} = 0.97 min^{-1} are similar to those from a recent report (K_M = 390 μM and k_{cat} = 0.78 min^{-1}) (Krishnan, et al., 2012).

Due to the low yield and difficulty in concentrating nucleosomes to high concentrations, we characterized demethylation using single-turnover kinetics, where substrate is limiting and the enzyme is in excess. Given the need for a more sensitive assay than the fluorescence assay used for the peptides, we used the quantitative western blot.

Preliminary data of His-cJMJD2A demethylation of nucleosomes indicate that His-cJMJD2A demethylates homogeneous recombinant H3K9C(Me3) nucleosomes with a single-turnover affinity constant (K'_M) of 30 μM and a catalytic rate (k_{max}) of 1.22 min^{-1} (Figure 3-2). The tighter affinity of His-cJMJD2A to nucleosomes indicates that the nucleosome scaffold (outside of amino acids 7-14) provides additional contacts.

Interestingly, a Hill coefficient of 2.9 was seen in the data indicating oligomerization of His-cJMJD2A. Since peptide kinetics did not exhibit cooperativity, we hypothesize that oligomerization occurs only in the presence of nucleosomes. This may explain why this has not been observed by others.

His-cJMJD2A dimer interface generation

By using PyMol and generating symmetry mates of JMJD2A (PDB: 2OQ6), we found a particularly promising homodimer interface (Figure 3). Proximal to the interface site is the Cys_3-His Zn finger motif. The Zn finger binding site is adjacent to the iron active site, and the activity of JMJD2A is dependent on an intact Zn finger motif. Molecules that displace Zn have been found to disrupt demethylation activity (Sekirnik, et al., 2009). Taken together, intact and properly folded Zn finger motif is important for activity and possibly also dimerization.

The two monomers interface in an interdigitated fashion across a solvent excluded surface area of 299 $Å^2$ (surface defined by residues with Van der Waals overlap greater than or equal to -0.4 Å and less than 6 Å, from which solvent excluded surface area was calculated using Chimera's default parameters). No steric clashes were found using default Chimera settings of Van der Waals overlap greater than or equal to 6 Å. As shown by Figure (3-3B), the interface is lined with hydrophobic residues Leu74, Tyr85, Ile87, and Phe127, residues that have been found to have high propensities for homodimerization (Jones and Thornton, 1996).

Given the placement of the substrate histone H3 tail (Figure 3-4A and Figure 3-4B) and the obtained Hill coefficient, the hypothesized model involves the interaction of four molecules of JMJD2A per nucleosome (Figure 3-5). As depicted, each nucleosome may interact with a set of JMJD2A dimer on each tail.

Preparation of a putative dimer disrupter His-cJMJD2A L74R mutant

To further test this model, we cloned, expressed, and purified a proposed dimer disruption mutant His-cJMJD2A L74R. Activity of His-cJMJD2A L74R mutant was similar to WT His-cJMJD2A (K_M (His-cJMJD2A L74R) = 33 μM, K_M (His-cJMJD2A) = 54 μM, k_{cat} (His-cJMJD2A L74R) = 2.2 min^{-1} and k_{cat} (His-cJMJD2A) = 2.5 min^{-1}; for His-cJMJD2A L74R and WT data, see Figure 3-6 and Figure 1-14, respectively). Comparable kinetics suggests that the L74R mutation does not disrupt the active site and the mutant is properly folded, presenting L74R as an ideal mutant to test.

Additionally, the L74R mutant of the catalytic construct where the histadine-tag was removed (cJMJD2A L74R) was cloned, expressed, and purified. Similar to His-cJMJD2A L74R, cJMJD2A L74R demethylated peptides with a similar rate as its WT counterpart (K_M (cJMJD2A L74R) = 71 μM, K_M (cJMJD2A) = 67 μM, k_{cat} (cJMJD2A L74R) = 2.2 min^{-1} and k_{cat} (cJMJD2A) = 1.8 min^{-1}; for cJMJD2A L74R and WT data, see Figure 3-7 and Figure 1-18A, respectively). This demonstrated that like the histadine-tagged construct, cJMJD2A L74R is properly folded and the L74R mutation does not disrupt the enzyme's ability to demethylate.

Detection of His-cJMJD2A oligomer using gel filtration

Our initial tests for the presence of the His-cJMJD2A oligomer were done using gel filtration (Figure 3-8). Using Superdex 200 10/300 GL (GE Healthcare),

we observed a slight shift in His-cJMJD2A's retention time between His-cJMJD2A only (16.624 mL), His-cJMJD2A in the presence of cofactors α-ketoglutarate and the iron mimic nickel (16.254 mL), and His-cJMJD2A in the presence of the cofactors previously described and nucleosomes (16.06 mL). The His-cJMJD2A in the presence of cofactors and nucleosomes sample showed an additional peak at ~19 mL, which is likely from histones. For experimental conditions, please see Methods.

Detection of JMJD2A oligomer using analytical ultracentrifugation (collaboration with Daniele Canzio)

Analytical ultracentrifugation (AUC) applies centrifugal force on samples, and samples are optically monitored in real-time. Two types of experiments are performed using AUC, sedimentation equilibrium and sedimentation velocity. In sedimentation equilibrium experiments, the final steady state is used for analysis where diffusion and sedimentation forces have equilibrated. These experiments are preferred for molecular weight determination. On the other hand, sedimentation velocity experiments are performed under the conditions where diffusion and sedimentation forces are not in equilibrium. Sedimentation velocity studies provide information on the molecular weight and hydrodynamic shape of proteins and protein complexes. This method is particularly useful for determining oligomeric states and stoichiometry of heterogenous complexes (Lebowitz, et al., 2002; Schuck, 2003).

Using sedimentation velocity, His-cJMJD2A, His-cJMJD2A L74R, and cJMJD2A samples were tested in the presence and absence of nickel and α-ketoglutarate. Precipitation was seen with His-cJMJD2A and His-cJMJD2A L74R samples in the process of 4 °C dialysis. As a result, analysis of high concentrations of His-cJMJD2A and His-cJMJD2A L74R were not possible. Preliminary results from His-cJMJD2A in the presence and absence of nickel show a slight difference in sedimentation coefficient (Sw) (Figure 3-9). Though the obtained data were from different concentrations of demethylase, this data may indicate a difference in molecular weight and macromolecule shape as a result of the presence of nickel. Data from His-cJMJD2A and His-cJMJD2A L74R also suggest a difference in hydrodynamic shape of the protein between WT and L74R mutant (Figure 3-10).

Following this, conditions for overnight dialysis were tested to determine the optimal conditions that would provide the least amount of precipitation. Nickel sulfate and nickel chloride resulted in comparable amounts of precipitation for His-cJMJD2A samples. Under the tested conditions, cobalt resulted in less precipitation. Minimal to no precipitation was seen in the Strep-cJMJD2A samples, suggesting that the nickel cofactor is causing aggregation of the His-tagged cJMJD2A through His-tag coordination.

In attempt to ameliorate the precipitation issue and to ensure that any oligomerization seen is not a result of the histadine tag (Amor-Mahjoub, et al., 2006; Perron-Savard, et al., 2005; Wu and Filutowicz, 1999), AUC experiments were performed on untagged cJMJD2A (Table 3-1). Though some precipitation

was observed, preliminary data from higher cJMJD2A concentrations were obtained. Interestingly, in the presence of 0.2 mM nickel sulfate, 1 mM α-ketoglutarate, and 62 mM NaCl in 50 mM Hepes (pH 7.5), the sedimentation coefficient of 14 μM cJMJD2A is much higher than the rest. This suggests the possibility that oligomerization occurs at a certain concentration and deteriorates at higher concentrations. More experiments need to be done to confirm and further test this.

METHODS

Demethylation of peptide

Kinetic parameters for demethylation of peptides were determined by an enzyme-coupled assay that monitors the production of formaldehyde (Couture, et al., 2007). In these experiments, His-cJMJD2A or His-cJMJD2A L74R (1 μM), NAD+ (2 mM), formaldehyde dehydrogenase (FDH, 0.05 U, Sigma), α-ketoglutarate (1 mM), ascorbate (1 mM), and $Fe(NH_4)_2(SO_4)_2$ (50 μM) were incubated with varying concentrations of ARK(Me3)STGGK or ARK(Me2)STGGK (Genscript) in 50 mM Hepes (pH 7.5). Reactions were started by addition of substrate and followed at 15 sec intervals at room temperature on a SpectraMax M5e (Molecular Devices) using 350 nm excitation and 460 nm emission wavelengths. An NADH standard curve was used to convert fluorescence into concentration of product formed. The initial 2.5 min were used to calculate initial velocities, which were graphed against substrate concentration. Michaelis-Menten values were determined by non-linear least squares fitting using Kaleidagraph.

Demethylation of nucleosomes

Same protocol as previously described in Chapter 2 was used with the exception of using His-cJMJD2A.

Gel filtration analysis of oligomerization

For His-cJMJD2A only sample, His-cJMJD2A was incubated at room temperature for 30 min. For His-cJMJD2A, cofactors, and nucleosome sample, His-cJMJD2A (100 μM), nickel sulfate (0.2 mM), α-ketoglutarate (1 mM), and H3K9C(Me3) nucleosomes (300 nM) were incubated in 50 mM Hepes (pH 7.5) and NaCl (62 mM) at room temperature for 5 min. For His-cJMJD2A and cofactors sample, His-cJMJD2A (100 μM), nickel sulfate (4 mM), and α-ketoglutarate (1 mM) were incubated for 30 minutes at room temperature. All samples were ran on elution buffer pre-equilibriated Superdex 200 GL 10/300 column (GE Healthcare). His-cJMJD2A only was eluted with 50 mM Hepes (pH 7.5) and NaCl (62 mM). The His-cJMJD2A, cofactors and nucleosomes sample was eluted with 50 mM Hepes (pH 7.5) containing 62 mM NaCl, nickel sulfate (0.2 mM), and α-ketoglutarate (1 mM). The His-cJMJD2A and cofactors sample was eluted with 50 mM Hepes (pH 7.5) containing 62 mM NaCl, nickel sulfate (4 mM), and α-ketoglutarate (1 mM).

Preparation of AUC samples

Samples containing JMJD2A (0 – 100 μM) were dialyzed using 6 – 8 kDa molecular weight cutoff dialysis tubes (SpectrumLabs) overnight at 4 °C in nickel sulfate (200 μM), α-ketoglutarate (1 mM), NaCl (62 mM), and 20 mM Hepes (pH 7.5) for His-cJMJD2A samples or 50 mM Hepes (pH 7.5) for cJMJD2A samples. Samples were spun at 21 x 10^3 g for 10 min to remove precipitation.

$k_{cat} = 0.97 \pm 0.04 \text{ min}^{-1}$
$K_M = 340 \pm 50 \text{ μM}$
$k_{cat}/K_M = (2.9 \pm 0.4) \times 10^{-3} \text{ min}^{-1} \text{ μM}^{-1}$
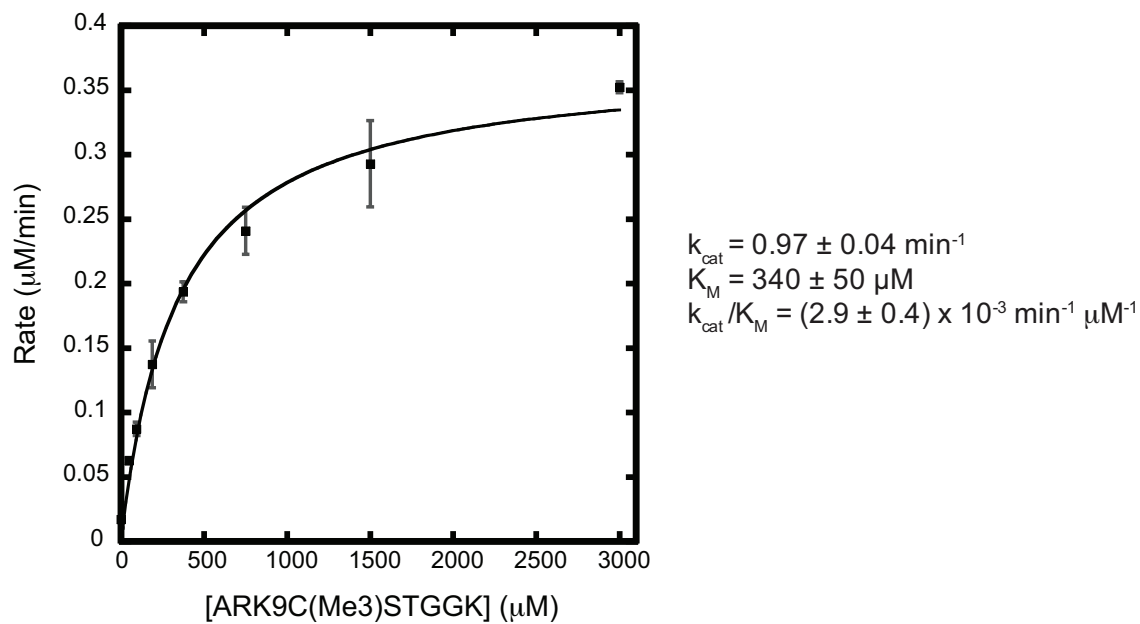
Figure 3-1. Kinetic parameters of His-cJMJD2A demethylation of ARK9C(Me3)STGGK peptide (work from Alen Bozicevic and Idelisse Ortiz Torres).

$k_{max} = 1.2 \pm 0.03$ min^{-1}
$K'_M = 30 \pm 1.5$ μM
$k_{max}/K'_M = (4.1 \pm 0.2) \times 10^{-2}$ min^{-1} μM^{-1}
Hill coefficient = 2.9 ± 0.4
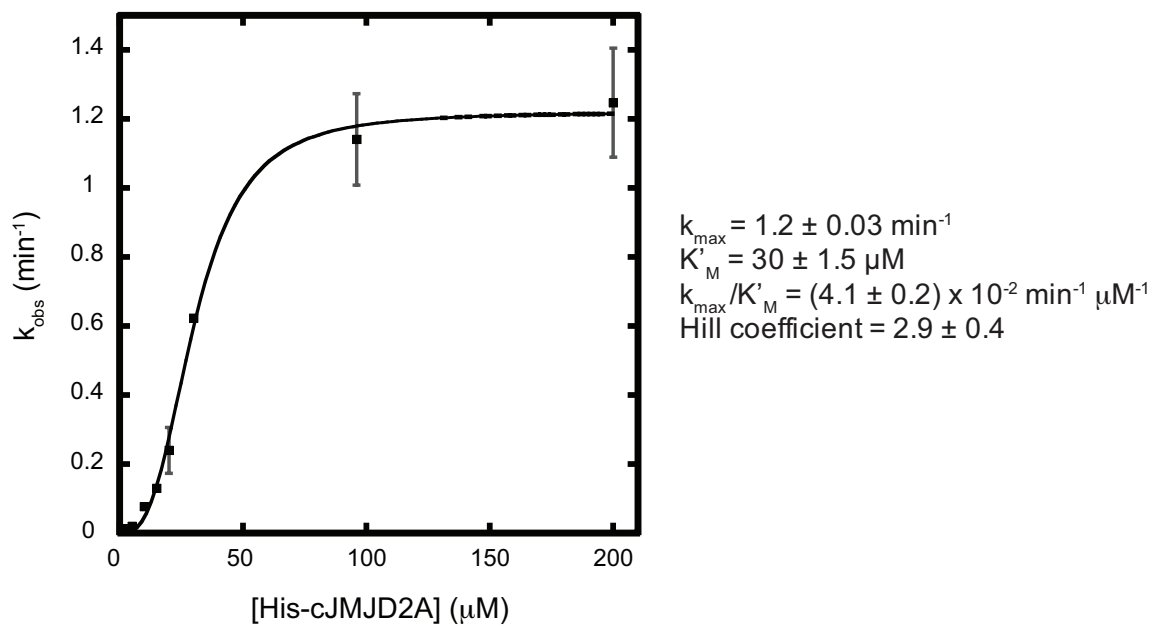
Figure 3-2. Demethylation of nucleosomes by His-cJMJD2A (preliminary results).
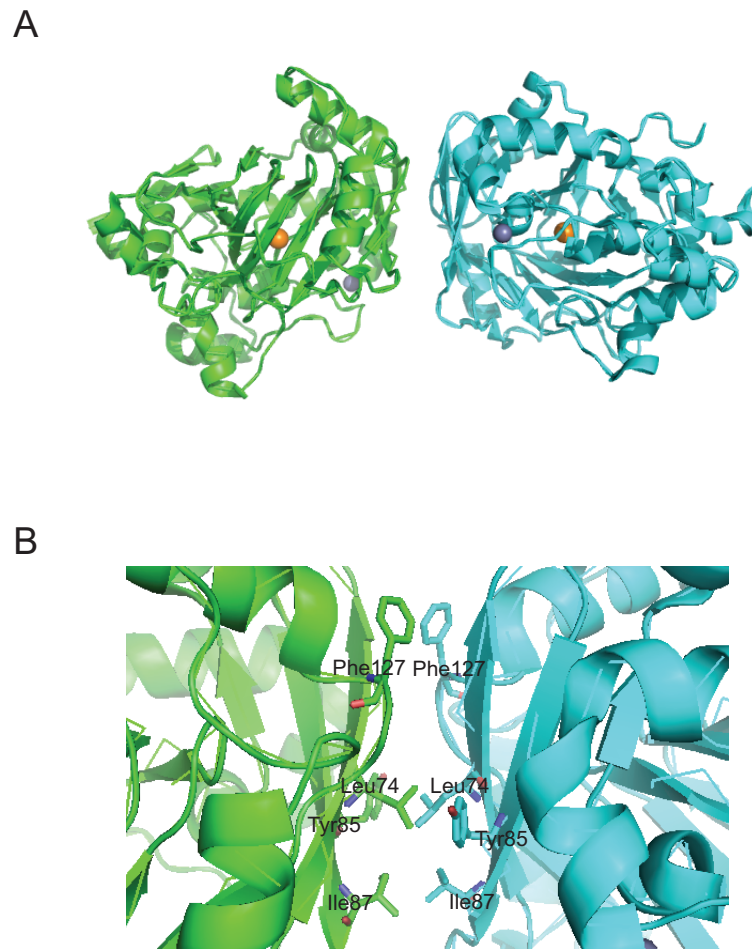
Figure 3-3. Possible JMJD2A homodimer interface. (A) Ribbon model of the two JMJD2A monomers that form the possible dimer. Active-site Fe is depicted in orange and Zn (II) is depicted in gray. (B) Detailed view of the interface. The interface contains several high homodimer propensity residues (Leu74, Tyr85, Ile87, and Phe127). PDB ID: 2OQ6.
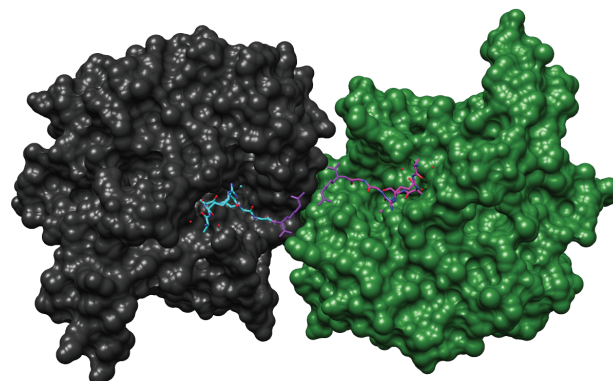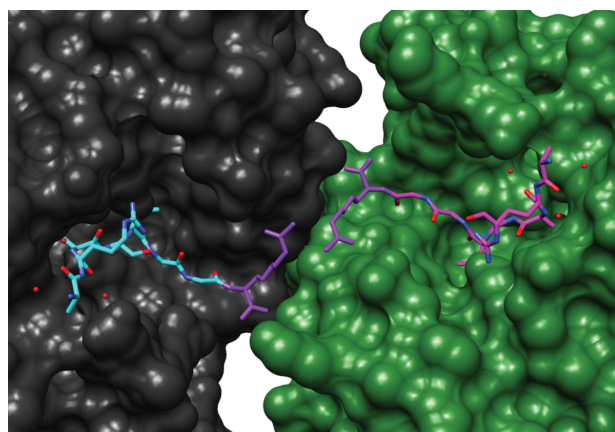
Figure 3-4. Possible JMJD2A homodimer interface with N-terminal histone H3 peptide substrate. (A) Space-filling model of two JMJD2A monomers and ARK(Me3)STGGK (histone H3 amino acids 7-14). (B) Detailed space-filling model of JMJD2A dimer interface with ARK(Me3)STGGK substrate peptides. The C-terminal end of the peptide is colored purple. PDB ID: 2OQ6.
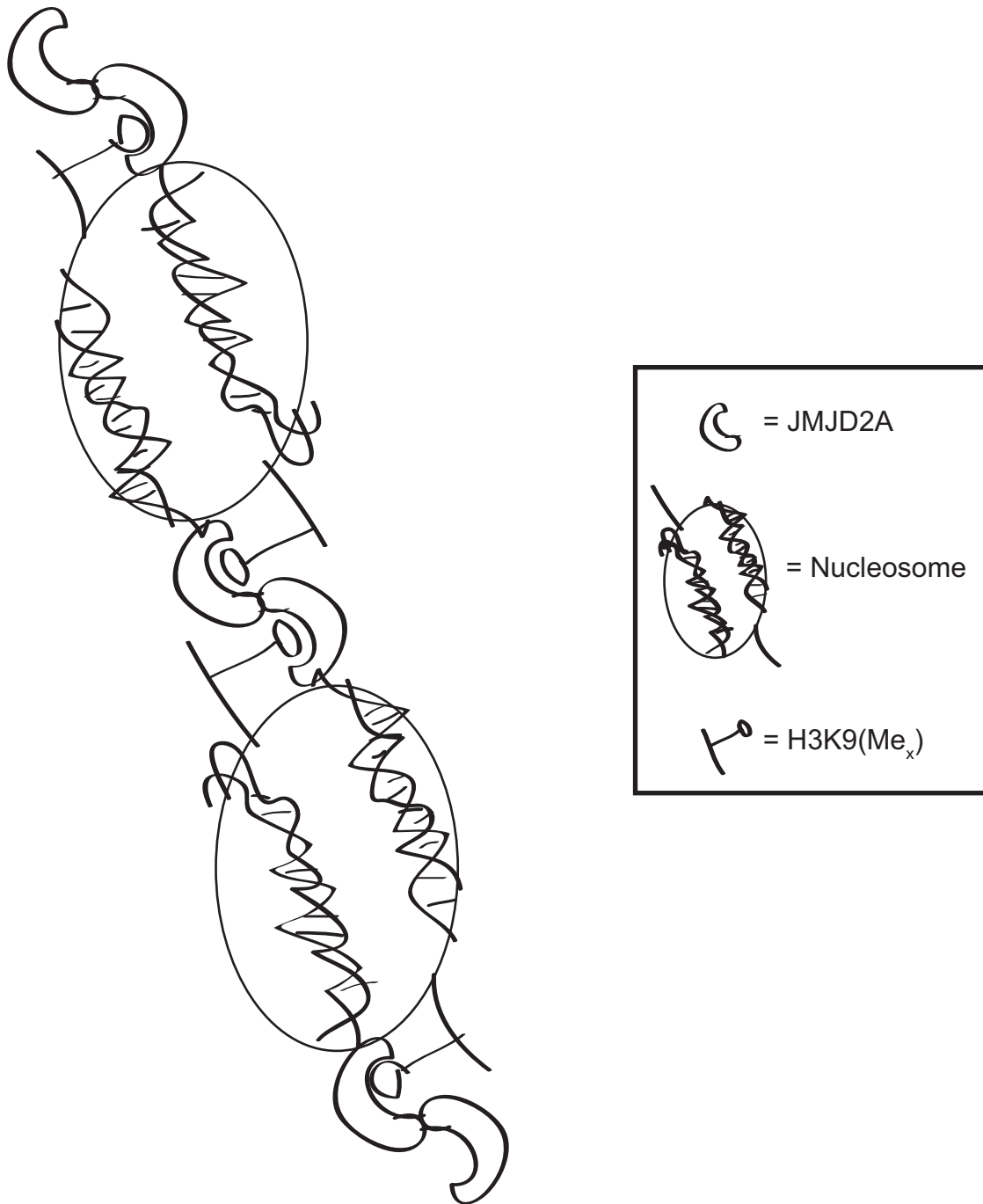
Figure 3-5. Proposed model for JMJD2A oligomerization. A dimer of JMJD2A binds each histone tail of a nucleosome, resulting in four molecules of JMJD2A per nucleosome.

$k_{cat} = 2.2 \pm 0.08 \text{ min}^{-1}$
$K_M = 33 \pm 6 \text{ μM}$
$k_{cat}/K_M = (6.7 \pm 1) \times 10^{-2} \text{ min}^{-1} \text{ μM}^{-1}$
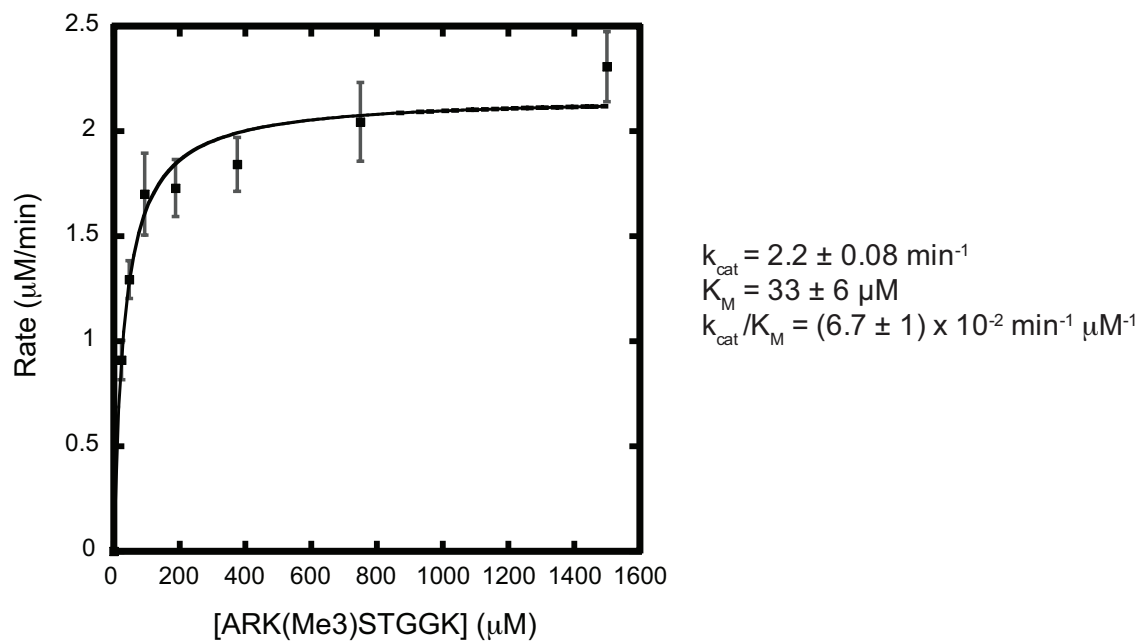
Figure 3-6. Kinetic parameters of His-cJMJD2A L74R demethylation of ARK(Me3)STGGK peptide. Experiments were done in triplicate.
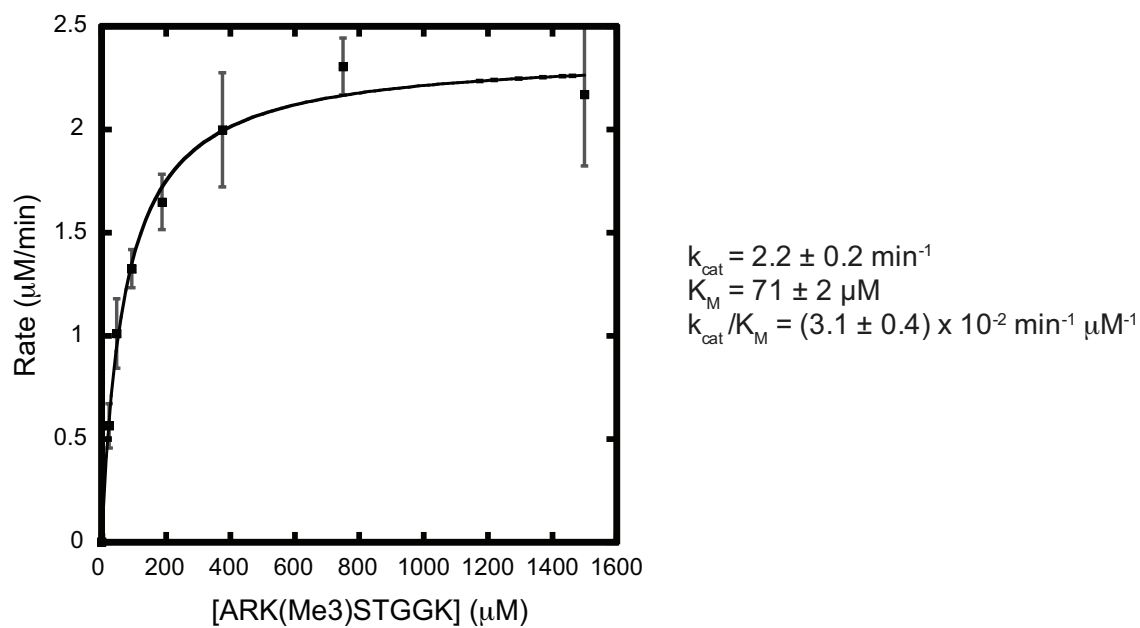
Figure 3-7. Kinetic parameters of cJMJD2A L74R demethylation of ARK(Me3)STGGK peptide. Experiments were done in triplicate.

The figure contains the following kinetic parameters:

$k_{cat} = 2.2 \pm 0.2 \text{ min}^{-1}$

$K_M = 71 \pm 2 \text{ } \mu M$

$k_{cat}/K_M = (3.1 \pm 0.4) \times 10^{-2} \text{ min}^{-1} \text{ } \mu M^{-1}$
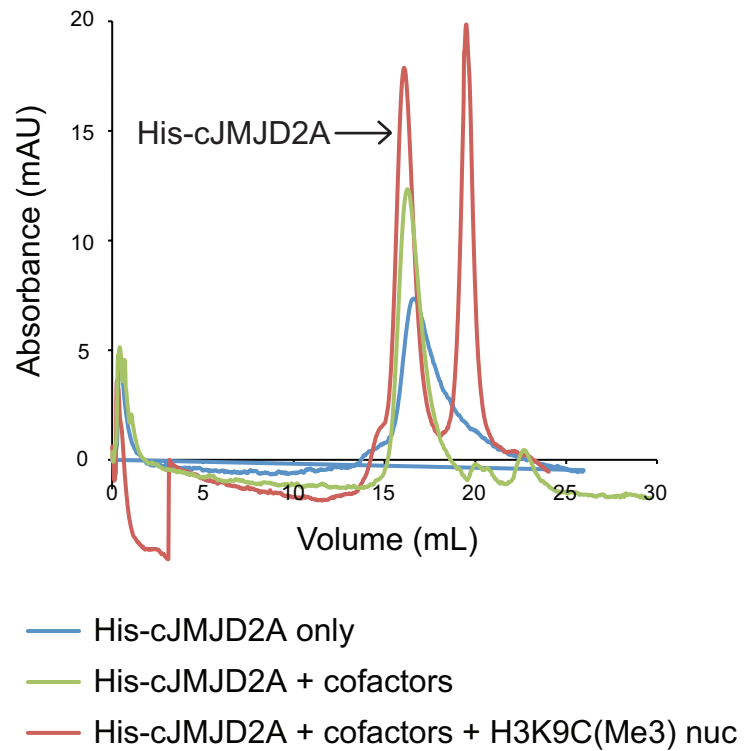
Figure 3-8. Gel filtration analysis of His-cJMJD2A only (blue), His-JMJD2A and cofactors α-ketoglutarate and the iron mimic nickel (green), and His-JMJD2A with cofactors α-ketoglutarate and nickel and H3K9C(Me3) nucleosome (red).
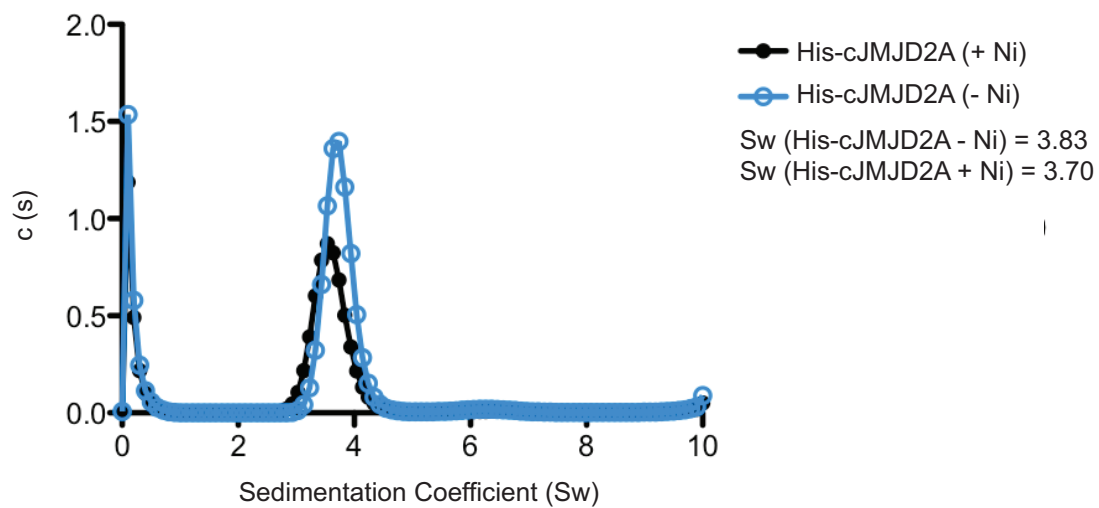
Figure 3-9. AUC data of His-cJMJD2A in the presence and absence of nickel, a mimic of cofactor iron. His-cJMJD2A (+ Ni) and His-cJMJD2A (-Ni) samples contained 7 μM and 23 μM of His-cJMJD2A respectively.
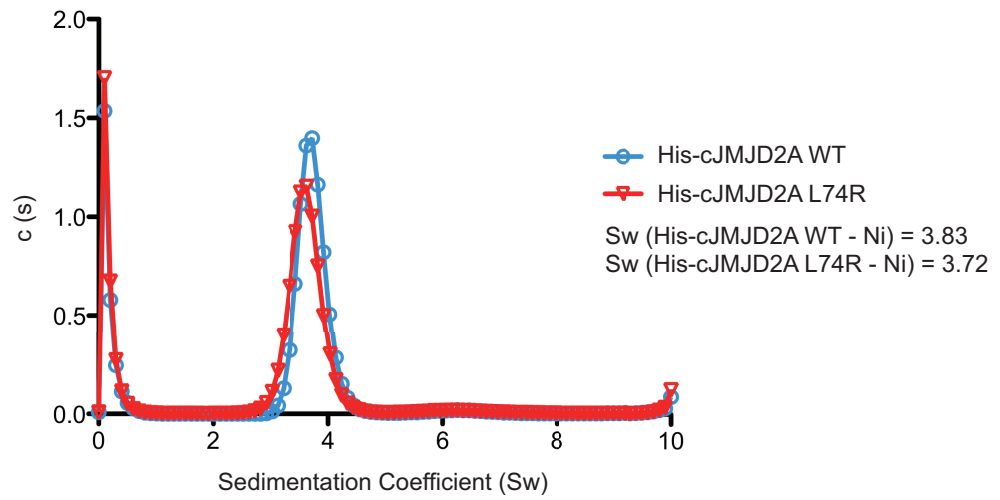
Figure 3-10. AUC data of His-cJMJD2A WT and His-cJMJD2A L74R in the absence of nickel. His-cJMJD2A WT and His-cJMJD2A L74R samples contained 23 μM and 21 μM of demethylase respectively.

[JMJD2A], μM	Sedimentation Coefficient
90	3.822
31	3.85
14.14	4.32
7.43	3.6
3.42	3.7
1.74	3.528

Table 3-1. Preliminary data of sedimentation coefficients of cJMJD2A in the presence of 0.2 mM nickel sulfate and 1 mM α-ketoglutarate in 50 mM Hepes (pH 7.5) and 62 mM NaCl.

REFERENCES

Amor-Mahjoub, M., Suppini, J.-P., Gomez-Vrielyunck, N., and Ladjimi, M. (2006). The effect of the hexahistidine-tag in the oligomerization of HSC70 constructs. J Chromatogr B Analyt Technol Biomed Life Sci 844, 328-334.

Couture, J.-F., Collazo, E., Ortiz-Tello, P.A., Brunzelle, J.S., and Trievel, R.C. (2007). Specificity and mechanism of JMJD2A, a trimethyllysine-specific histone demethylase. Nat Struct Mol Biol 14, 689-695.

Jones, S., and Thornton, J.M. (1996). Principles of protein-protein interactions. Proc Natl Acad Sci U S A 93, 13-20.

Krishnan, S., Collazo, E., Ortiz-Tello, P.A., and Trievel, R.C. (2012). Purification and assay protocols for obtaining highly active Jumonji C demethylases. Anal Biochem 420, 48-53.

Lebowitz, J., Lewis, M.S., and Schuck, P. (2002). Modern analytical ultracentrifugation in protein science: a tutorial review. Protein Sci 11, 2067-2079.

Perron-Savard, P., De Crescenzo, G., and Le Moual, H. (2005). Dimerization and DNA binding of the Salmonella enterica PhoP response regulator are phosphorylation independent. Microbiology (Reading, Engl) 151, 3979-3987.

Schuck, P. (2003). On the analysis of protein self-association by sedimentation velocity analytical ultracentrifugation. Anal Biochem 320, 104-124.

Sekirnik, R., Rose, N.R., Thalhammer, A., Seden, P.T., Mecinović, J., and Schofield, C.J. (2009). Inhibition of the histone lysine demethylase JMJD2A by ejection of structural Zn(II). Chem Commun (Camb), 6376-6378.

Shin, S., and Janknecht, R. (2007). Diversity within the JMJD2 histone demethylase family. Biochem Biophys Res Commun 353, 973-977.

Wu, J., and Filutowicz, M. (1999). Hexahistidine (His6)-tag dependent protein dimerization: a cautionary tale. Acta Biochim Pol 46, 591-599.

Chapter 4: Synthesis and evaluation of candidate mechanism-based inhibitors

INTRODUCTION

Current methods for determining the biological functions of Jumonji histone demethylase (JHDM) utilize genomic means such as quantitative PCR with reverse transcription (Mersman et al., 2009), knockouts (Tateishi et al., 2009), RNA-interference gene silencing (Cloos et al., 2006), and immunocytochemistry (Whetstine et al., 2006). These approaches depend on gene transcription and expression profiling and manipulation to ascertain function and thus cannot distinguish between non-active and active Jumonji demethylases. Appealingly, activity-based probes will allow for the vital detection and profiling of active demethylases. By exploiting the reactivity of the conserved iron-oxo intermediate that these demethylases use to perform catalysis, we proposed to design activity-based probes that target active JHDMs. Successful activity-based probes will enable unprecedented comparison of JHDM activities from different biological contexts. Additionally, through identification of site-specific protein complex partners, it would advance understanding of the regulation of demethylases and transcription. Results from these experiments may lead to identification of enzymes with altered activities in disease states and aid understanding of roles of demethylases in cancer as well as serve as a starting point for diagnostic tool development.

A successful activity-based probe that specifically targets one site will provide the ability to distinctly study the regulation of the demethylation activity of one site. This would aid in enhancing the understanding of the regulation of the demethylase to demethylate particular H3K9 or H3K36 sites. We focused on

H3K9 because it is a better model to use in the initial testing of our approach as it is the better substrate for JMJD2A (Couture et al., 2007; Hillringhaus et al., 2011).

With the goal of establishing an activity-based approach that will specifically target JMJD2A at the H3K9 site, our strategy was based on mechanism-based enzyme inactivation. By definition, a mechanism based probe is a latent group-containing substrate analog that is unreactive. Upon reaction with enzyme, it becomes highly reactive while it is still in the active site of the enzyme and spontaneously forms a covalent linkage with the enzyme or its cofactor. The enzyme is thus rendered permanently inactive. Using this strategy, the probe was designed to be an endogenous substrate mimic with a latent inhibitor moiety head. Upon activation by the characteristic $Fe^{IV}=O$ intermediate of JHDM, a reactive intermediate is expected to form and subsequently covalently inactivate the enzyme (Figure 4-1). As the probe is latent until activation by the $Fe^{IV}=O$ intermediate, it was anticipated to be unreactive towards the remainder of the proteome.

Two types of probes were designed. The first type consisted of three components: a histone H3 tail base, a latent inhibitor moiety head, and a handle. The histone tail base consisted of various lengths of peptide that mimicked the histone H3 tail (eg. 7-ARK*STGGK-14, where K* = methylated Lys; a known substrate for JMJD2A). The second type of probe consisted of the inhibitor moiety head and the full recombinant histone H3 as the base. The H3K9 site of a recombinant histone H3 C110A mutant was mutated to a cysteine for ease of

inhibitor moiety incorporation. The cysteine residue was selected due to its scarcity in histones and unique reactivity, which allowed for its chemoselective modification (Simon et al., 2007). By mutagenizing lysine to cysteine and subsequently alkylating the cysteine, Simon *et al.* demonstrated successful production of methylated lysine analogues (MLA) of both histone H3 peptides and recombinant histones. As a result, the difference between endogenous methyllysine and MLA was the replacement of the γ-methylene with a thioether. Simon *et al.* have shown MLAs to bind methyl-specific antibodies and to successfully partake in ATP-dependent chromatin remodeling by hACF complex. Since then, others have utilized MLA for various studies on chromatin modifiers, such as influence of H3K4(Me3) on HB01 histone acetyltransferase complex activity (Hung et al., 2009), recruitment of Rpd3S histone deacetylase complex by H3K36(Me3/2) (Li et al., 2009), heterochromatin spreading of HP1 (Canzio et al., 2011), and substrate specificity determination of demethylase KDM4A (Lin et al., 2008). These studies demonstrate MLA to be functionally equivalent to their endogenous counterpart. Additionally, the ability for demethylases to demethylate MLA suggests that the thioether linkage substitution does not preclude its binding to the demethylase. Thus, we applied a similar cysteine alkylation strategy in the synthesis of our probes.

Crystal structures show hydrogen bonds and van der Waals interactions between the backbone of the peptide and JMJD2A as the primary contributors for recognition (Couture et al., 2007; Ng et al., 2007). The carbonyl oxygen of Glu169 hydrogen bonds with the main chain to orient the peptide and deposit the

trimethyllysine into the active site, where the butyl chain is in contact with Asp191, Lys241, and Asn290 and the trimethylammonium cation is positioned in an oxygen filled surrounding with the Fe(II) active site nearby. This oxygen wrap is composed of carbonyl oxygen of Gly170, hydroxyl groups of Tyr177 and Ser288 and carboxylate side chain of Fe(II) chelator Glu190. In close proximity to this active site, several additional nucleophilic and aromatic residues are present including conserved Tyr177 and Thr/Lys189. Importantly, extensive hydrogen bonding between the substrate peptide and JMJD2A suggests that the replacement of H3K9(Me3) functionality with the probe will not alter the binding of the activity-based probe with the demethylase.

Successful covalent inactivation of similar systems using alkynes present this functional group as a worthy latent head functionality to explore. Ortiz de Montellano group has shown cytochrome P450b, a heme iron center-containing monooxygenase that also utilizes an iron-oxo intermediate to catalyze oxidation, to be covalently inactivated by phenylacetylene. It is postulated that the reaction proceeds through a phenylketene intermediate (Komives and Ortiz de Montellano, 1987). Additionally, 5-ethynyluracil has been found to covalently inactivate thymine hydroxylase, a member of the Fe(II) and α-ketoglutarate-dependent dioxygenase superfamily, through cyclopropanation of a phenylalanine residue. This finding suggests a reactive ketene intermediate (Lai et al., 1995). Furthermore, a more recent work by Hotopp *et al.* showed covalent inactivation of TfdA, another member of the Fe(II) and α-ketoglutarate-dependent dioxygenase superfamily, using phenylpropiolic acid (Hotopp and Hausinger,

2002). This suggests that the inactivator is not confined to terminal alkynes and that additional moieties can be present.

Based on these studies, we also postulated that our alkyne probes, upon activation by JMJD2A-derived iron-oxo species, would form either reactive ketene or carbene intermediates (Figure 4-1). Following the intermediate formation, we expected ketenes to react with nucleophilic residues in the active site of Jumonji demethylase. As for carbenes, we expected covalent adduct formation with aromatic amino acids that line the demethylase active site and thus covalently inhibit the enzyme. Sequence alignment and crystal structure analysis showed a number of nucleophilic and aromatic residues in the vicinity of JMJD2A active site including the previously mentioned conserved Tyr177 and Thr/Lys189.

RESULTS AND DISCUSSION

Using the cysteine alkylation strategy to incorporate the inhibitor moiety of interest, candidate inhibitor probes were made with various alkynyl moieties and non-alkynyl moieties (Figure 4-2A) on various histone H3 scaffolds ranging from peptides to histones (Figure 4-2B). To test a subset of the candidate probes, western blotting, gel shift, enzyme-coupled fluorescence, and mass spectrometry assays were used (Table 4-1). The candidate inhibitors are designated by two bolded numbers. The first number indicates the chemical moiety and the second number indicates the scaffold (Figure 4-2C). In these assays, probes were incubated with the enzyme along with iron and α-ketoglutarate cofactors, and the reaction mixture analyzed by one or more analytical method listed above.

Detection of covalent inhibition of peptide candidate inhibitors through a western blot assay

For the western blot, the reactions were run on SDS-PAGE gels under reducing conditions. Subsequent transfer followed by the detection of biotinylated inhibitor candidate through HRP-conjugated Streptavidin indicated whether covalent inhibition occurred. In the presence of covalent inhibition, a band at the molecular weight of the His-cJMJD2A and probe adduct (~43 kDa) was expected. In the absence of covalent inhibition, a band at the molecular weight of the inhibitor was expected (~1 kDa).

Using this assay, we observed apparent candidate and demethylase binding in the control samples. An example of this can be seen in Figure 4-3

where bands at the molecular weight of the His-cJMJD2A and peptide probe adduct appeared in the catalytic mutant His-cJMJD2A H188A lanes, indicating a binding of the biotinylated peptide probe with the demethylase in a demethylase activity independent manner. Additionally, band detection of the adduct molecular weight in experiments that lack cofactors suggests that side reactions of the cofactors were not responsible for the non-specific binding. To test non-specific binding and to attempt to dissociate the binding, we added detergent Triton-X (0.01% and 0.1%) at different points of the porotocol. Additionally, different boiling protocols, where samples were not boiled with SDS loading dye prior to the loading and running of the SDS PAGE gels were tried. Even in the presence of Triton-X with various boiling protocols, the non-specific binding remained. To see if this was a non-specific binding that was specific for the demethylase or if it was a promiscuous non-specific binder, we tested BSA with **1-3** (moiety number – scaffold number) in the presence and absence of cofactors (Figure 4-4). We observed detection of BSA in all lanes, which indicates non-specific binding of the probe with BSA. This detection was not abrogated by the addition of Triton-X. A possible reason for this non-specific binding could be the sheer abundance of probe used in the experiments. Because of the high K_M of MLA peptide, the amount of inhibitor candidate used for testing was large (250 μM – 2 mM). The high concentration of the probe may induce non-specific interactions with proteins.

Additionally, we tested various demethylation conditions. We tested the incubation of inhibitor candidates with demethylase over various periods of time

(30 min – overnight), in closed or open systems, mixed constantly or occasionally (shaked or occasionally tapped), at different temperatures (room temperature and 37 °C), and under strict aerobic conditions (enzyme preparation under anaerobic conditions followed by introduction of oxygen at the start of the reaction). Testing these different conditions yielded similar results.

Detection of covalent inhibition of protein candidate inhibitors through a gel shift assay

It is possible that the motif present on the histone that is recognized by the demethylase extends beyond the histone peptide and into other histone residues or structural features. To address this possibility, we developed the histone probe candidates, comprised of the full histone H3 protein and one of various inhibitor moieties (**X–4** compounds, where X = moiety number, see Figure 4-2A for moieties, Figure 4-2B for scaffolds, and Table 4-1 for tested compounds). These probes were tested using a gel shift assay. In this assay, reactions were ran on SDS-PAGE gels under reducing conditions and stained by Coomassie. If the covalent inhibition by the probe were to occur, a band at a higher molecular weight equal to the combined molecular weight of the histone H3 and His-cJMJD2A adduct (~57 kDa) was expected. In samples that lack covalent inhibition, a band at the molecular weight of His-cJMJD2A (~ 42 kDa) was expected.

Figure 4-5 illustrates one such example. Here, His-cJMJD2A and catalytic mutant His-cJMJD2A H188A were tested with candidate inhibitor **3-4** in the

presence and absence of demethylation cofactors. No band at ~ 57 kDa was detected, suggesting that no covalent inhibition had occurred. Similar to the western blot assay, we tested various demethylation conditions. No successful inhibitors have been identified yet.

Detection of covalent inhibition of candidate inhibitors through a fluorescence assay

For quantitative analysis, the enzyme-coupled fluorescent assay was used. As mechanism-based inhibition is a form of covalent inhibition, it is expected to undergo time-dependent inactivation. Longer incubation times were expected to result in more inhibition. Following activity over various incubation times and various inhibitor concentrations would allow for extraction of the inactivation value K_i (Figure 4-6).

For the fluorescence assay assessment of histone compounds, we observed inhibition by the first incubation time point (2.5 min) of His-cJMJD2A with **2-4** using trimethylated histone H3K9 peptides (7-14 aa) as the substrate (Figure 4-7A). This suggests that the additional histone contacts (outside of 7-14 aa) contribute to tighter binding than the peptide, and thus the histone probe outcompetes the peptide substrate in binding to the demethylase and prevents demethylation of the peptide. Further testing of His-cJMJD2A with histone H3 WT also shows inhibition at the earliest incubation time point (1 min) (Figure 4-7B), suggesting that the histone alone inhibits Jumonji demethylase by outcompeting the peptide substrate and that the inhibitor moiety is not necessary for the

inhibition. Taking this finding together with **2-4** not demonstrating clear covalent inhibition through gel shift and western blot assays, suggest that **2-4** and histone H3 WT are competitive non-covalent inhibitors of His-cJMJD2A.

Detection of covalent inhibition of candidate inhibitors through a mass spectrometry assay

For the mass spectrometry assays, LC-MS was used to investigate the presence of the demethylase adduct and LC-MSMS was used to assess the candidate inhibitor modification. In the presence of a successful probe, a mass equal to the sum of the enzyme and candidate inhibitor was expected. On the other hand, for the control reactions where no inhibitor was present, a mass equal to the molecular weight of the enzyme was expected. Out of the candidates tested (Table 4-1), no clear adduct has been found yet. An example trace is shown in Figure 4-8.

LC-MSMS experiments, done in collaboration with Michael Trnka from the Burlingame lab, showed better binding of biotinylated histone H3 8-mer peptide (7-14 aa) than non-biotinylated 8-mer peptide on the QSTAR Pulsar column, demonstrating biotinylated scaffolds as a better scaffold for testing compounds through this protocol. In the analysis of the compounds, we consistently found oxidation of biotin. We also observed demethylation of **10-2** by both His-cJMJD2A and His-cJMJD2D. There was indication of depropargylation and demethylation of **6-2** for His-cJMJD2A reactions. We saw more of the depropargylated and demethylated products in demethylation reactions than in

no enzyme controls. This result suggests the importance of the presence of the positively charged ammonium.

Future directions

Along with synthesizing and testing positively charged ammonium group containing moieties, future work on this project may entail synthesis of more native-like inhibitor candidates (ie. those that do not contain the thioether linkage present in MLA) as they may enable better binding and positioning of the inhibitor moiety, and thus a better chance for inhibition. Furthermore, using a combination of full-length demethylases (that have the auxiliary domains that have been found to increase catalytic efficiency of peptides with dual marks for PHF8, another H3K9 JHDM (Horton et al., 2010)) and inhibitors containing the methylated mark that conveys better binding and the inhibitor moiety at the H3K9 site may increase the odds of finding a H3K9 mechanism-based inhibitor through tighter binding between the enzyme and inhibitor candidate.

METHODS

Synthesis of peptide inhibitor candidates

Peptides (5-10 mg) were dissolved in 8 M GnHCl (200 μL), 1 M Hepes pH 7.5 (1.76 mL), and 1 M DTT (40 μL). Peptides were reduced at 37 °C for 1 hour. Alkynyl moiety containing alkylating agent was added in 20-fold excess of the peptide. Reaction was stirred in the dark at 50 °C and reactions were quenched with 14.2 M β-mercaptoethanol (50 μL) and purified on the HPLC. Samples were loaded onto a Luna preparatory C18 column (10 μm, 21.2 mm × 250 mm) (Phenomenex, Torrance, CA), in a solvent system consisting of water and 0.1% TFA (A) and acetonitrile and 0.1% TFA (B). All peptides were eluted at a flow rate of 15 mL/min. For **1-1** and **3-1**, a gradient of 0-20% B over 30 min was used, and **1-1** eluted at 19.7 min and **3-1** eluted at 23 min. **1-3** was ran on a gradient of 0-60%B over 25 min and eluted at 14.1 min. **1-5**, **4-3**, and **7-3** were ran on a gradient of 0-30%B over 25 min and eluted at 20.5 min, 19 min, and 21.5 min respectively. For **1-6**, a gradient of 0-60%B over 25 min was used and the product eluted at 14 min. **2-3** was ran on a gradient of 0-30%B over 40 min eluted at 28 min. **3-3** was ran on 5-35% B over 45 min and eluted at 23.9 min. **5-1**, **8-1**, and **10-2** were ran on a gradient of 0-25% B over 40 min and eluted at 24 min, 27 min, and 28 min respectively. **6-1** was run on a gradient of 0-20% B over 25 min and eluted at 13 min. **6-2** was run on a 0-25% B gradient over 25 min and eluted at 20.5 min. **10-1** was ran on a gradient of 0-25% B over 30 min and eluted at 13 min. HPLC peaks were analyzed by MALDI-TOF and the fractions containing the product were collected and lyophilized.

Synthesis of histone inhibitor candidates

Histone H3K9C (1-2 mg) was dissolved in 1 M Hepes pH 7.8, 4 M GnHCl, 10 mM D/L methionine (196 μL) and 1M DTT (4 μL). Samples were reduced at 37 °C for 1 hour. Alkylating agents were added in 20-fold excess of the histone concentration and the reactions were allowed to proceed at room temperature or 50 °C. Reactions were followed by LC-MS and for the reactions that lasted longer than 2 hours, DTT (2 μL) was added and the reaction was allowed to proceed. Reactions were quenched with 14.2 M β-mercaptoethanol (10 μL) at full completion. Samples were desalted using 2 mM β-mercaptoethanol preequilibriated PD-10 desalting column (GE Healthcare) and eluted with 2 mM betamercaptoethanol. Fractions containing protein were collected and lyophilized. The reaction of **2-4** reached completion in 5 min at room temperature. **4-4** reached completion in 15 min at room temperature. The reaction of **1-4** was quenched after stirring at 50 °C for 5 hours. The reaction of **3-4** was quenched after stirring at 50 °C for 2 hours.

Probe screening assays

Jumonji demethylase (0.6 μM – 30 μM) was incubated with α-ketoglutarate (0.5 – 1 mM), ascorbate (0.5 – 1 mM), $Fe(NH_4)_2(SO_4)_2$ (50 – 100 μM), and probe candidate (0.25 – 2 mM) in 10 mM Hepes (pH 7.9) and 50 mM NaCl at room temperature or 37 °C for various amounts of time (0 hours – overnight). For gel shift assays, experiments were quenched with SDS loading

dye, boiled at 100 °C for 2 min, ran on SDS PAGE gels (12% Tris-HCl) under reducing conditions and stained with Coommassie. For the mass spectrometry assays, reactions were analyzed using electrospray mass spectrometry on a LCT Premier Mass Spectrometer (Waters). For fluorescence assays, reactions contained additional components NAD$^+$ (2 mM), formaldehyde dehydrogenase (FDH; Sigma) and H3 tail peptide substrate ARK(Me3)STGGK (0 – 1.5 mM). Reactions were started by addition of substrate and followed at room temperature or 37 °C on a SpectraMax M5e (Molecular Devices) using 350 nm excitation and 460 nm emission wavelengths. For Western blots, samples were quenched with SDS loading dye, boiled at 100 °C for 2 min, and ran on SDS PAGE gels (12% Tris-HCl), transferred onto an Immun-blot PVDF membrane (Bio-Rad) on ice for 1 hour at 100 V. The membrane was blocked at room temperature in 1X TTBS and 5% milk for various times (1 hour – overnight) and washed three times with 1X TTBS for 5 min each. Subsequently, the membrane was incubated with NeutrAvidin Horseradish Peroxidase Conjugated (Thermo Scientific #31001) at 1:100,000 dilution in 1X PBS and 10 mg/mL BSA for one hour at room temperature. After this, the membrane was washed three times with 1X TTBS for 15 min each and visualized using Supersignal West Pico (Thermo Scientific # 34080).
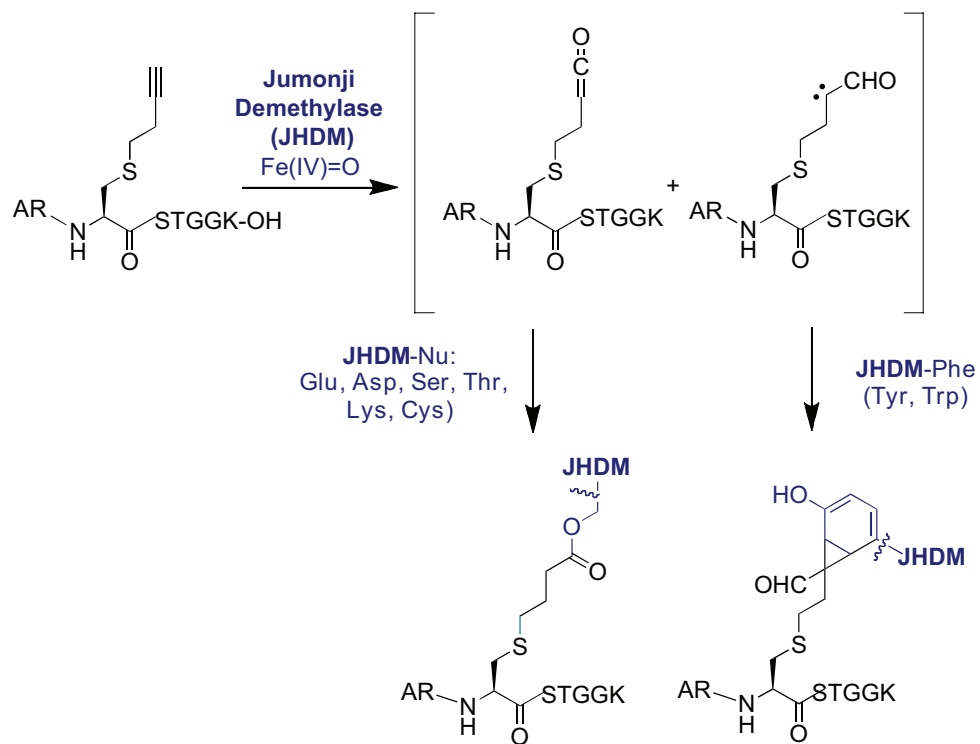
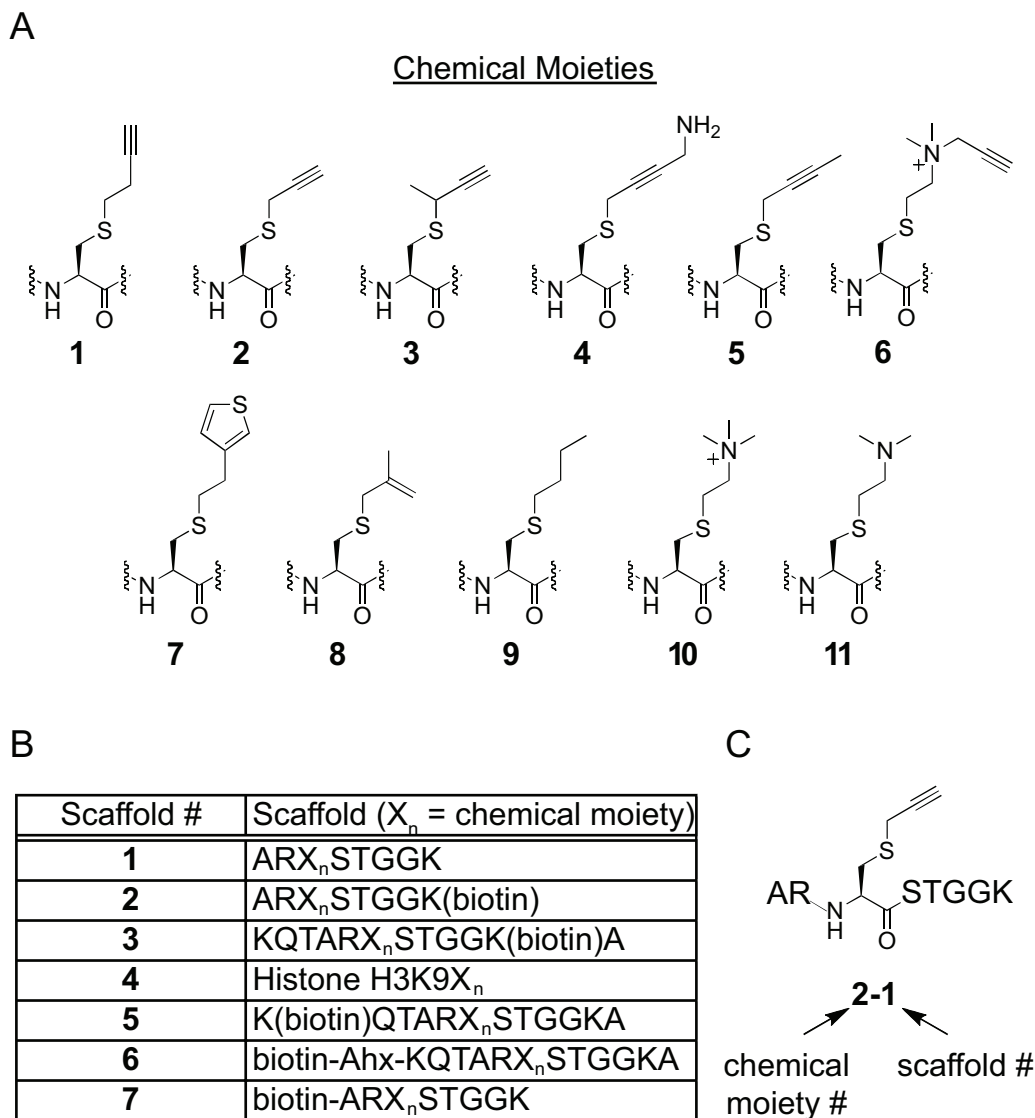**Figure 4-1.** Proposed molecular mechanism of inactivation.

Figure 4-2. Panel of chemical moieties and scaffolds utilized for the probes. (A) Panel of chemical moieties used as inhibitors and controls. (B) Table of scaffolds used as inhibitors. (C) Inhibitor nomenclature. In the body of the text, candidate inhibitors are designated by two bold numbers. The first indicates the chemical moiety number and the second indicates the scaffold number.

Chemical Moiety	Scaffold	Demethylase	Tested Assay
1	1	JMJD2A	F, MS
	3		MS
	4		GS
	5		WB
	6		WB
	1	JMJD2D	F
	3		WB, MS
	4		GS
	3	JMJD1B	WB
2	1	JMJD2A	F
	3		WB
	4		WB, GS, F
	4	JMJD2D	WB
	3	JMJD1B	WB
	4		GS
3	3	JMJD2A	WB, MS
	4		GS
	3	JMJD2D	WB, MS
	4		GS
4	3	JMJD2A	WB
	4		GS
	3	JMJD2D	MS
	4	JMJD1B	GS
5	1	JMJD2A	F
6	1	JMJD2A	MS
	2		WB, MS
	2	JMJD2D	MS
7	3	JMJD2A	WB, F
8	1	JMJD2A	F
9	3	JMJD2D	MS
10	1	JMJD2A	MS, F
	2		MS
	1	JMJD2D	MS, F
	2		MS

F = fluorescence assay, MS = mass spectrometry, GS = gel shift, WB = western blot

Table 4-1. Table of tested inhibitor constructs. Each row contains the chemical moiety, inhibitor scaffold, enzymes against which it was tested, and assays used for testing. Chemical moiety structures and scaffold descriptions are shown in Figure 4-2.
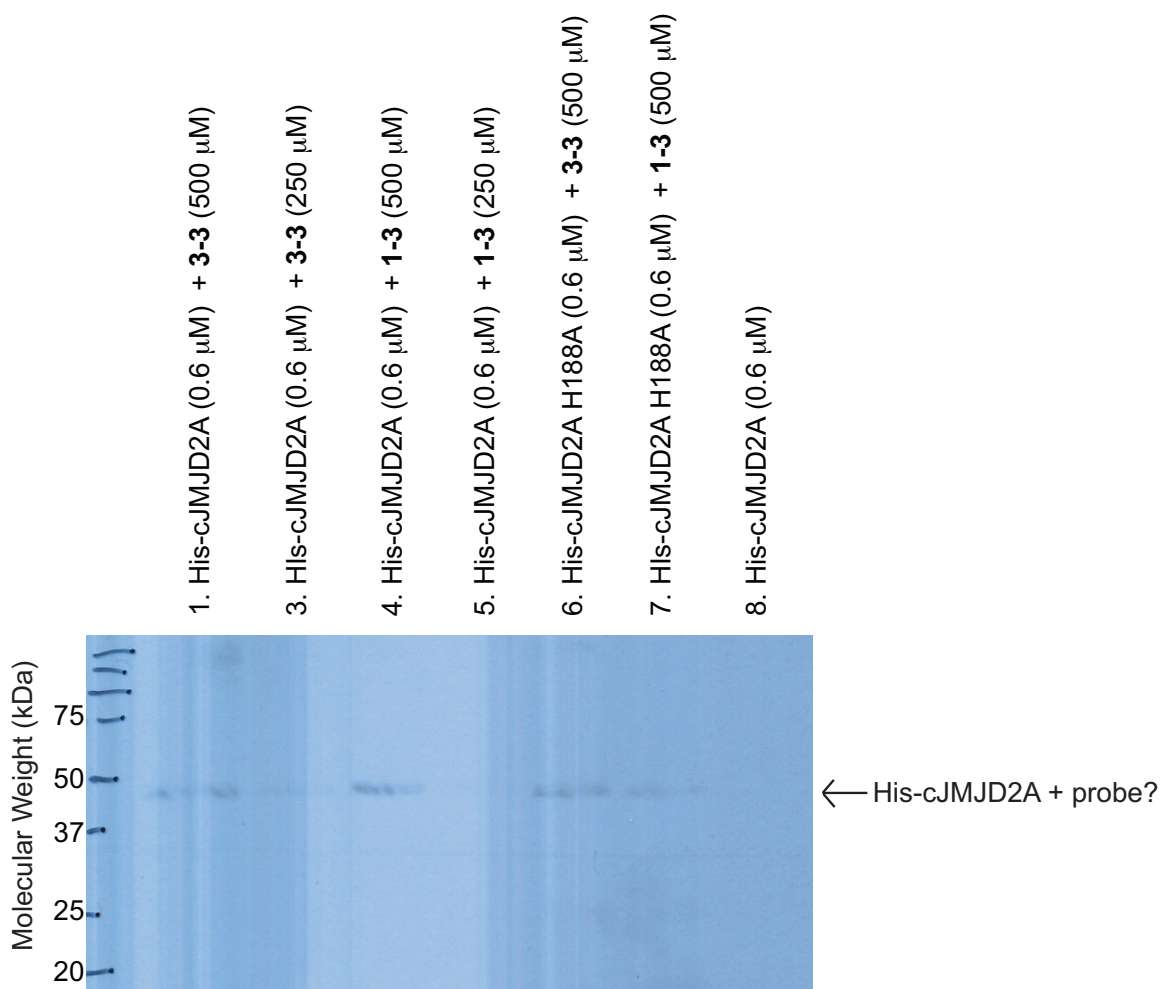
Figure 4-3. Western blot assessment of **1-3** and **3-3** with His-cJMJD2A and catalytic mutant His-cJMJD2A H188A. His-cJMJD2A or His-cJMJD2A H188A (0.6 μM) was incubated with **3-3** or **1-3** (500 μM or 250 μM), α-ketoglutarate (500 μM), ascorbate (500 μM), and Fe(NH$_4$)$_2$(SO$_4$)$_2$ (50 μM) in 10 mM Hepes (pH 7.9) and 50 mM NaCl at room temperature overnight. Samples were quenched with SDS loading dye, boiled at 100 °C for 2 min, and ran on 12% Tris-HCl SDS PAGE gel, transferred onto a Immun-blot PVDF membrane (Bio-Rad) on ice for 1 hour at 100 V. The membrane was blocked at room temperature for 1 hour in 1X

TTBS and 5% milk and washed three times with 1X TTBS for 5 min each. Following which, the membrane was incubated with NeutrAvidin Horseradish Peroxidase Conjugated (Thermo Scientific #31001) at 1:100,000 dilution in 1X PBS and 10 mg/mL BSA for one hour at room temperature. After this, the membrane was washed three times with 1X TTBS for 15 min each and visualized using Supersignal West Pico (Thermo Scientific # 34080).
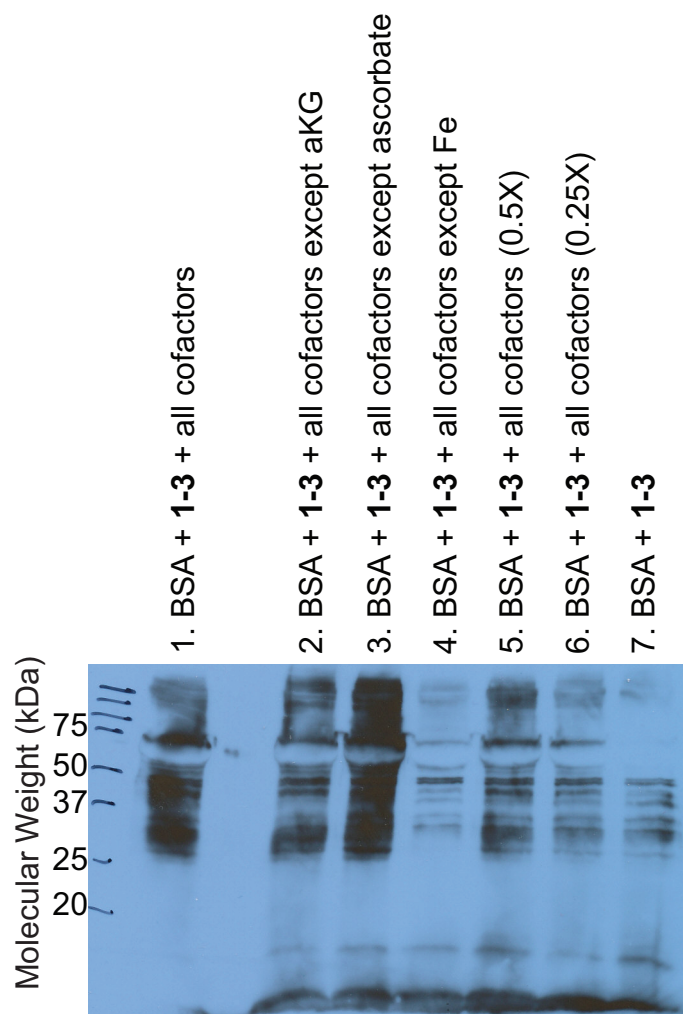
Figure 4-4. Western blot assessment of BSA with **1-3**. BSA (10 μM) was incubated with α-ketoglutarate (1 mM), ascorbate (1 mM), $Fe(NH_4)_2(SO_4)_2$ (100 μM), 0.1% Triton-X, and **1-3** (2 mM) in 10 mM Hepes (pH 7.9) and 50 mM NaCl at 37 °C for 45 min for sample 1. For samples 2 – 4, the same conditions as sample 1 were used with the exception of omission of the indicated cofactor. For sample 5, BSA (10 μM) was incubated with with α-ketoglutarate (0.5 mM), ascorbate (0.5 mM), $Fe(NH_4)_2(SO_4)_2$ (50 μM), 0.1% Triton-X, and **1-3** (2 mM) at 37 °C for 45 min. For sample 6, BSA (10 μM) was incubated with with α-

ketoglutarate (0.25 mM), ascorbate (0.25 mM), $Fe(NH_4)_2(SO_4)_2$ (25 μM), 0.1% Triton-X, and **1-3** (2 mM) at 37 °C for 45 min. For sample 7, BSA (10 μM) was incubated with **1-3** (2 mM) and 0.1% Triton-X at 37 °C for 45 min. Samples were boiled at 100 °C for 10 min and ran on a 12% Tris-HCl SDS PAGE gel, transferred onto a Immun-blot PVDF membrane (Bio-Rad) on ice for 1 hour at 100 V. The membrane was blocked at room temperature for 1 hour in 1X TTBS and 5% milk and washed three times with 1X TTBS for 5 min each. Following which, the membrane was incubated with NeutrAvidin Horseradish Peroxidase Conjugated (Thermo Scientific #31001) at 1:100,000 dilution in 1X PBS and 10 mg/ml BSA for one hour at room temperature. After this, the membrane was washed three times with 1X TTBS for 15 min each and visualized using Supersignal West Pico (Thermo Scientific # 34080).
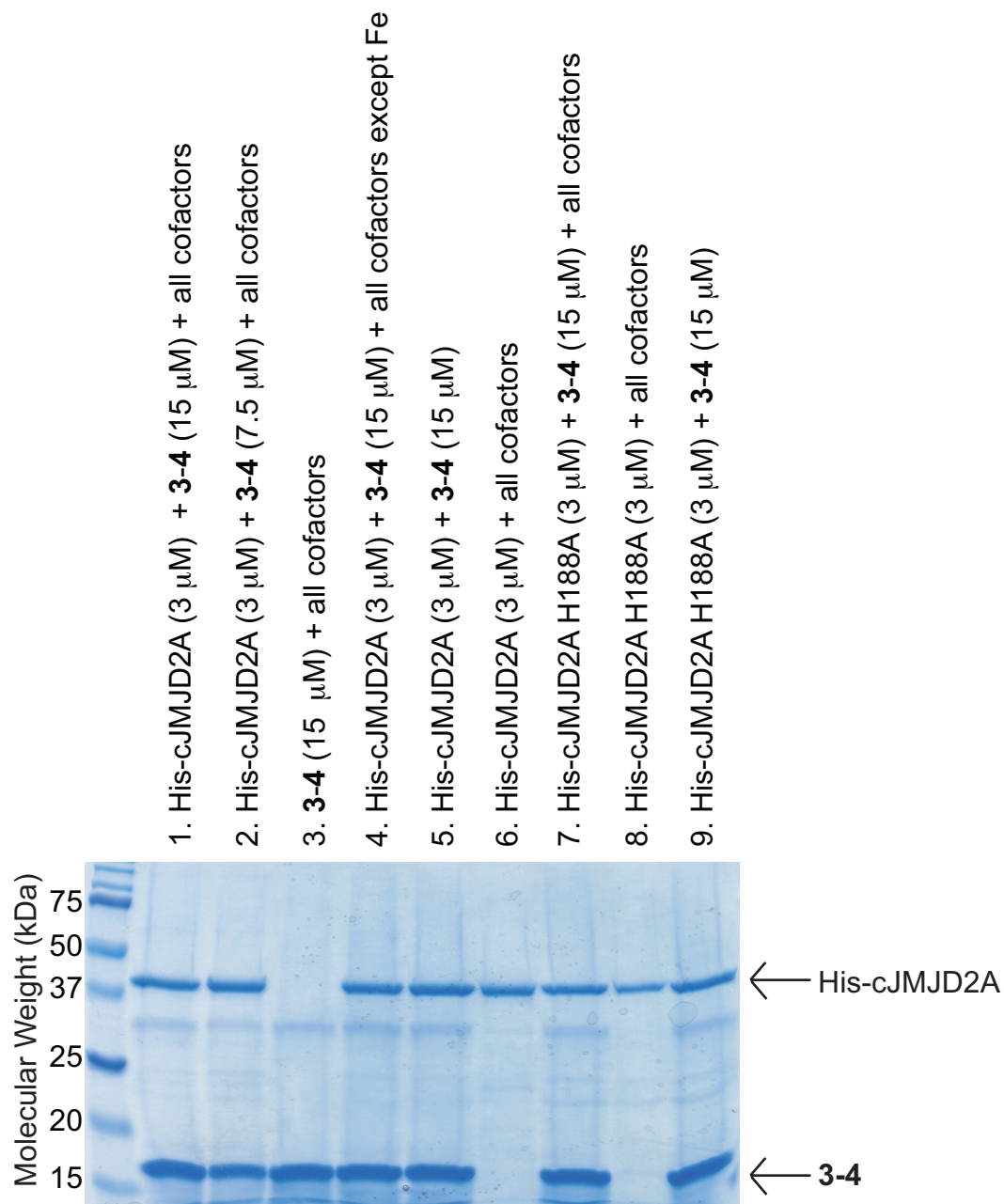
Figure 4-5. Gel shift assay analysis of His-cJMJD2A with **3-4**. His-cJMJD2A (3 μM) was incubated with **3-4** (15 μM or 7.5 μM), α-ketoglutarate (500 μM), ascorbate (500 μM), and $Fe(NH_4)_2(SO_4)_2$ (50 μM) in 10 mM Hepes (pH 7.9) and 50 mM NaCl at room temperature for 3 hours. Samples were quenched with SDS

loading dye, boiled at 100 °C for 2 min, and ran on a 12% Tris-HCl SDS PAGE

gel. The gel was subsequently Coomassie stained.
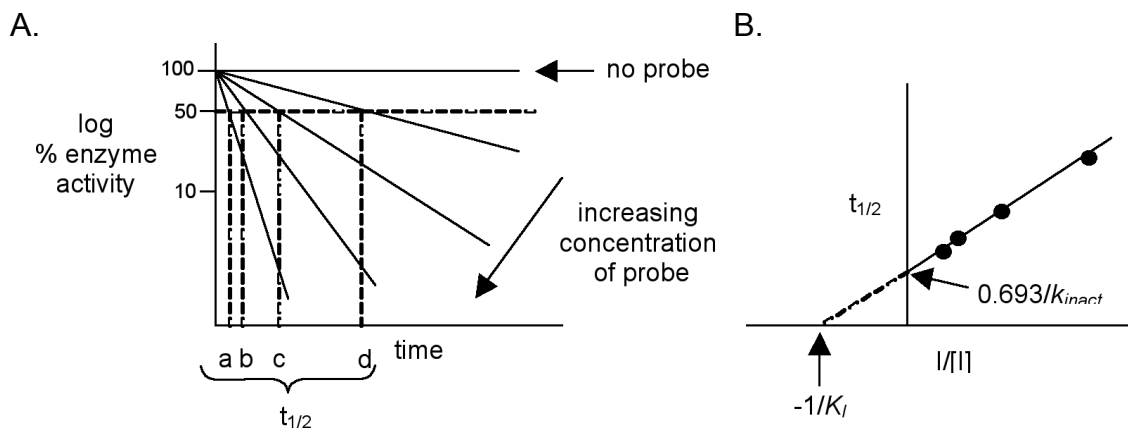
Figure 4-6. Mechanism-based inactivation. (A) Expected time and concentration dependent inactivation data where a, b, c and d are $t_{1/2}$ values for the various probe concentrations, (B) Kitz and Wilson plot of data.
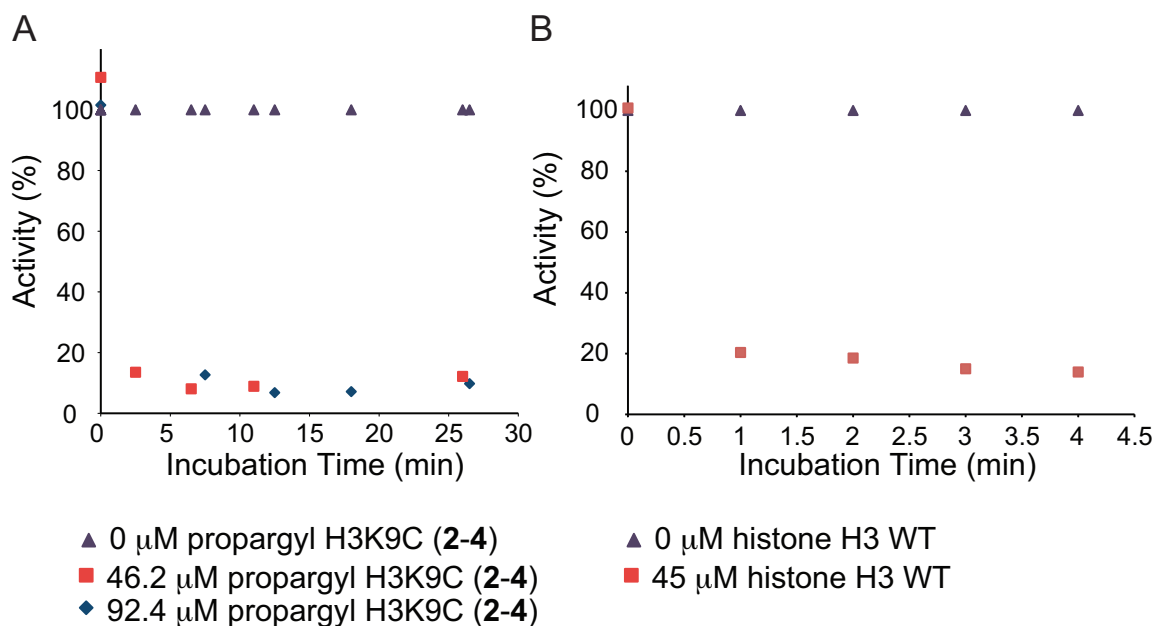
Figure 4-7. Fluorescence inactivation assessment of **2-4** and histone H3 WT with His-cJMJD2A. (A) His-cJMJD2A (30 μM) was incubated with **2-4** (92.4 μM, 46.2 μM, or 0 μM), α-ketoglutarate (1 mM), ascorbate (1 mM), and Fe(NH$_4$)$_2$(SO$_4$)$_2$ (100 μM) in 10 mM Hepes 50 mM NaCl pH 7.9 at 37 °C. Time points (3.68 μL) were diluted with assay buffer (3.68 μL) and read on the fluorimeter at 350 nm excitation and 460 nm emission upon addition to a mixture containing NAD$^+$ (2 mM), FDH (0.1 U), α-ketoglutarate (0.5 mM), ascorbate (0.5 mM), ARK(Me3)STGGK (1.5 mM) and Fe(NH$_4$)$_2$(SO$_4$)$_2$ (50 μM) (47.5 μL). The initial two minutes was used to determine the rate (the slope). The rate was normalized to the rate for 0 μM **2-4** control at each corresponding time point. (B) His-cJMJD2A was incubated with histone H3 WT and the same procedure as that described in (A) was followed.
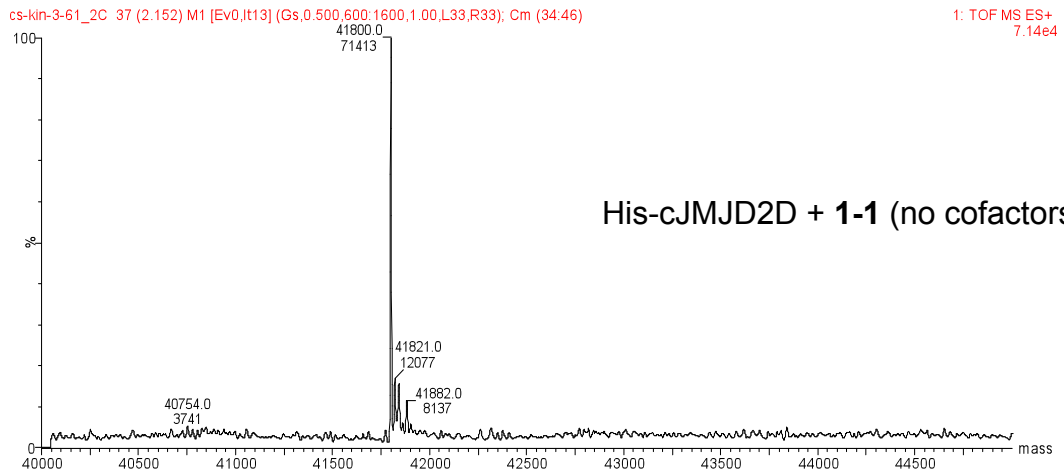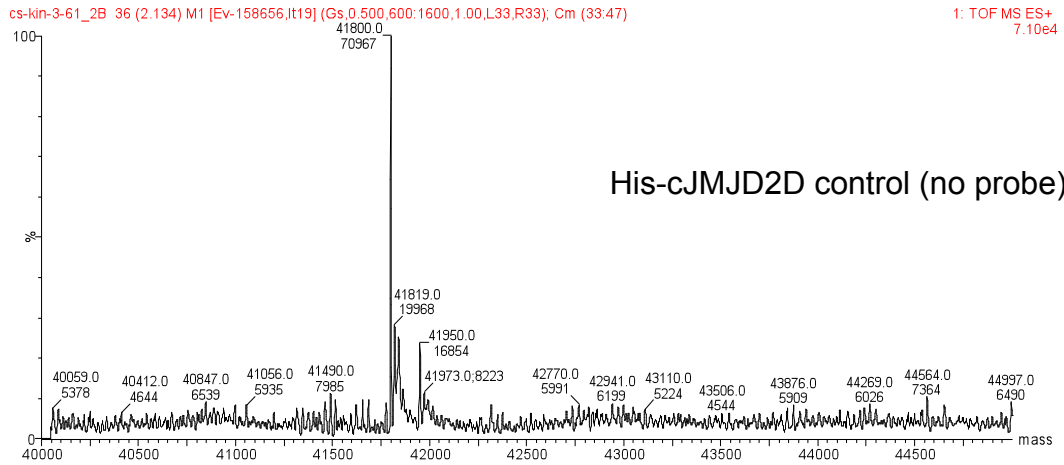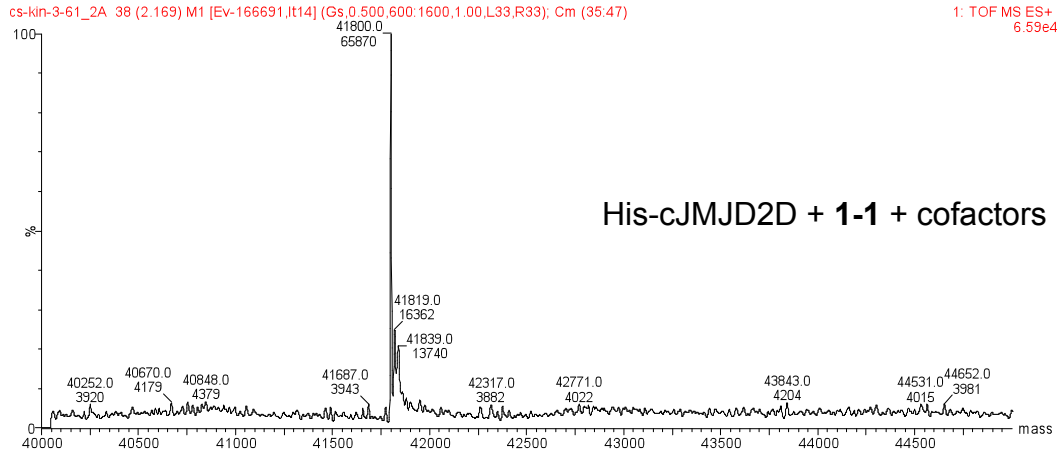
Figure 4-8. LC-MS assessment of inhibition of His-cJMJD2D by **1-1**.

His-cJMJD2D (29 μM) was incubated with α-ketoglutarate (625 μM), ascorbate (625 μM), Fe(NH$_4$)$_2$(SO$_4$)$_2$ (62.5 μM), and **1-1** (1 mM) in 10 mM Hepes (pH 7.9) and 50 mM NaCl at room temperature for 1 hr and 15 min for the experimental sample. For the control samples, the cofactors or probe were omitted. Samples were analyzed by LC-MS.

REFERENCES

Borun, T.W., Pearson, D., and Paik, W.K. (1972). Studies of histone methylation during the HeLa S-3 cell cycle. J Biol Chem *247*, 4288-4298.

Byvoet, P., Shepherd, G.R., Hardin, J.M., and Noland, B.J. (1972). The distribution and turnover of labeled methyl groups in histone fractions of cultured mammalian cells. Arch Biochem Biophys *148*, 558-567.

Canzio, D., Chang, E.Y., Shankar, S., Kuchenbecker, K.M., Simon, M.D., Madhani, H.D., Narlikar, G.J., and Al-Sady, B. (2011). Chromodomain-Mediated Oligomerization of HP1 Suggests a Nucleosome-Bridging Mechanism for Heterochromatin Assembly. Mol Cell *41*, 67-81.

Chen, Z., Zang, J., Whetstine, J., Hong, X., Davrazou, F., Kutateladze, T.G., Simpson, M., Mao, Q., Pan, C.-H., Dai, S.*, et al.* (2006). Structural insights into histone demethylation by JMJD2 family members. Cell *125*, 691-702.

Cloos, P.A.C., Christensen, J., Agger, K., Maiolica, A., Rappsilber, J., Antal, T., Hansen, K.H., and Helin, K. (2006). The putative oncogene GASC1 demethylates tri- and dimethylated lysine 9 on histone H3. Nature *442*, 307-311.

Couture, J.-F., Collazo, E., Ortiz-Tello, P.A., Brunzelle, J.S., and Trievel, R.C. (2007). Specificity and mechanism of JMJD2A, a trimethyllysine-specific histone demethylase. Nat Struct Mol Biol *14*, 689-695.

Culhane, J.C., and Cole, P.A. (2007). LSD1 and the chemistry of histone demethylation. Curr Opin Chem Biol *11*, 561-568.

Hillringhaus, L., Yue, W.W., Rose, N.R., Ng, S.S., Gileadi, C., Loenarz, C., Bello, S.H., Bray, J.E., Schofield, C.J., and Oppermann, U. (2011). Structural and evolutionary basis for the dual substrate selectivity of human KDM4 histone demethylase family. J Biol Chem *286*, 41616-41625.

Horton, J.R., Upadhyay, A.K., Qi, H.H., Zhang, X., Shi, Y., and Cheng, X. (2010). Enzymatic and structural insights for substrate specificity of a family of jumonji histone lysine demethylases. Nat Struct Mol Biol *17*, 38-43.

Hotopp, J.C.D., and Hausinger, R.P. (2002). Probing the 2,4-dichlorophenoxyacetate/alpha-ketoglutarate dioxygenase substrate-binding site by site-directed mutagenesis and mechanism-based inactivation. Biochemistry *41*, 9787-9794.

Hu, Z., Gomes, I., Horrigan, S.K., Kravarusic, J., Mar, B., Arbieva, Z., Chyna, B., Fulton, N., Edassery, S., Raza, A.*, et al.* (2001). A novel nuclear protein, 5qNCA (LOC51780) is a candidate for the myeloid leukemia tumor suppressor gene on chromosome 5 band q31. Oncogene *20*, 6946-6954.

Hung, T., Binda, O., Champagne, K.S., Kuo, A.J., Johnson, K., Chang, H.Y., Simon, M.D., Kutateladze, T.G., and Gozani, O. (2009). ING4 mediates crosstalk between histone H3 K4 trimethylation and H3 acetylation to attenuate cellular transformation. Mol Cell *33*, 248-256.

Karytinos, A., Forneris, F., Profumo, A., Ciossani, G., Battaglioli, E., Binda, C., and Mattevi, A. (2009). A novel mammalian flavin-dependent histone demethylase. J Biol Chem *284*, 17775-17782.

Komives, E.A., and Ortiz de Montellano, P.R. (1987). Mechanism of oxidation of pi bonds by cytochrome P-450. Electronic requirements of the transition state in the turnover of phenylacetylenes. J Biol Chem *262*, 9793-9802.

Krishnan, S., Collazo, E., Ortiz-Tello, P.A., and Trievel, R.C. (2012). Purification and assay protocols for obtaining highly active Jumonji C demethylases. Anal Biochem *420*, 48-53.

Lachner, M., O'Carroll, D., Rea, S., Mechtler, K., and Jenuwein, T. (2001). Methylation of histone H3 lysine 9 creates a binding site for HP1 proteins. Nature *410*, 116-120.

Lai, M.-t., Wu, W., and Stubbe, J. (1995). Characterization of a Novel, Stable Norcaradiene Adduct Resulting from the Inactivation of Thymine Hydroxylase by 5-Ethynyluracil. J Am Chem Soc *117*, 5023-5030.

Li, B., Jackson, J., Simon, M.D., Fleharty, B., Gogol, M., Seidel, C., Workman, J.L., and Shilatifard, A. (2009). Histone H3 lysine 36 dimethylation (H3K36me2) is sufficient to recruit the Rpd3s histone deacetylase complex and to repress spurious transcription. J Biol Chem *284*, 7970-7976.

Lin, C.-H., Li, B., Swanson, S., Zhang, Y., Florens, L., Washburn, M.P., Abmayr, S.M., and Workman, J.L. (2008). Heterochromatin protein 1a stimulates histone H3 lysine 36 demethylation by the Drosophila KDM4A demethylase. Mol Cell *32*, 696-706.

Loh, Y.-H., Zhang, W., Chen, X., George, J., and Ng, H.-H. (2007). Jmjd1a and Jmjd2c histone H3 Lys 9 demethylases regulate self-renewal in embryonic stem cells. Genes Dev *21*, 2545-2557.

Mersman, D.P., Du, H.-N., Fingerman, I.M., South, P.F., and Briggs, S.D. (2009). Polyubiquitination of the demethylase Jhd2 controls histone methylation and gene expression. Genes Dev *23*, 951-962.

Ng, S.S., Kavanagh, K.L., McDonough, M.A., Butler, D., Pilka, E.S., Lienard, B.M.R., Bray, J.E., Savitsky, P., Gileadi, O., von Delft, F.*, et al.* (2007). Crystal structures of histone demethylase JMJD2A reveal basis for substrate specificity. Nature *448*, 87-91.

Paik, W.K., and Kim, S. (1967). Enzymatic methylation of protein fractions from calf thymus nuclei. Biochem Biophys Res Commun *29*, 14-20.

Rea, S., Eisenhaber, F., O'Carroll, D., Strahl, B.D., Sun, Z.W., Schmid, M., Opravil, S., Mechtler, K., Ponting, C.P., Allis, C.D.*, et al.* (2000). Regulation of chromatin structure by site-specific histone H3 methyltransferases. Nature *406*, 593-599.

Shi, Y., Lan, F., Matson, C., Mulligan, P., Whetstine, J.R., Cole, P.A., Casero, R.A., and Shi, Y. (2004). Histone demethylation mediated by the nuclear amine oxidase homolog LSD1. Cell *119*, 941-953.

Simon, M.D., Chu, F., Racki, L.R., De La Cruz, C.C., Burlingame, A.L., Panning, B., Narlikar, G.J., and Shokat, K.M. (2007). The Site-Specific Installation of Methyl-Lysine Analogs into Recombinant Histones. Cell *128*, 1003-1012.

Tateishi, K., Okada, Y., Kallin, E.M., and Zhang, Y. (2009). Role of Jhdm2a in regulating metabolic gene expression and obesity resistance. Nature *458*, 757-761.

Thomas, G., Lange, H.W., and Hempel, K. (1972). [Relative stability of lysine-bound methyl groups in arginie-rich histones and their subfrations in Ehrlich ascites tumor cells in vitro]. Hoppe Seylers Z Physiol Chem *353*, 1423-1428.

Tsukada, Y.-i., Fang, J., Erdjument-Bromage, H., Warren, M.E., Borchers, C.H., Tempst, P., and Zhang, Y. (2006). Histone demethylation by a family of JmjC domain-containing proteins. Nature *439*, 811-816.

Whetstine, J.R., Nottke, A., Lan, F., Huarte, M., Smolikov, S., Chen, Z., Spooner, E., Li, E., Zhang, G., Colaiacovo, M.*, et al.* (2006). Reversal of histone lysine trimethylation by the JMJD2 family of histone demethylases. Cell *125*, 467-481.

Wissmann, M., Yin, N., Müller, J.M., Greschik, H., Fodor, B.D., Jenuwein, T., Vogler, C., Schneider, R., Günther, T., Buettner, R.*, et al.* (2007). Cooperative demethylation by JMJD2C and LSD1 promotes androgen receptor-dependent gene expression. Nat Cell Biol *9*, 347-353.

Yang, Z.Q., Imoto, I., Fukuda, Y., Pimkhaokham, A., Shimada, Y., Imamura, M., Sugano, S., Nakamura, Y., and Inazawa, J. (2000). Identification of a novel gene, GASC1, within an amplicon at 9p23-24 frequently detected in esophageal cancer cell lines. Cancer Res *60*, 4735-4739.

CONCLUDING REMARKS

Histone lysine methylation within nucleosomes is a reversible process catalyzed by opposing actions of histone methyltransferases and histone demethylases. As precise control of the methylation extent of nucleosomes is required for proper gene expression, nucleosome methylation must be tightly regulated. Jumonji histone demethylases are a class of Fe(II) and α-ketoglutarate-dependent dioxygenases that catalyze methyl removal from a number of methylated lysine residues, and their misregulation is correlated with diseases (Cloos et al., 2008; Kooistra and Helin, 2012).

Protocols for the production of reagent quantities of active enzymes from all three H3K9 Jumonji demethylase families and inhibition assays have been established in this thesis. These advances allow for the screening of the next generation of inhibitor candidates. Additionally, our studies on the possible JMJD2A oligomerization raise interesting questions regarding the impact of the oligomeric state on the enzyme's biological function.

Alongside these studies, by quantitatively analyzing the demethylation activity of a catalytic construct of JMJD2A, a member of the human Jumonji demethylases, we provide insight into the ability of a prototypic member of the family to remove a methyl mark. The results point to two important features of the cJMJD2A: an intrinsic distributive nature and its predominant recognition of the histone tail segment surrounding the methyl lysine residue. Our studies directly raise the possibility that the activity and processivity of the catalytic domain may be regulated in a context-specific manner by reader domains outside the catalytic

134

domain. The method developed here to analyze the kinetic parameters for demethylation of nucleosomes will enable future studies on quantifying the mechanistic roles of the non-catalytic regions as well as interacting proteins.

Overall, the work described in this dissertation is expected to help in advancing our understanding of the intrinsic properties of Jumonji demethylase JMJD2A. This work also introduces a method for future quantitative characterization of the activity of other demethylases on complex chromatin substrates and sets the starting foundation for future work on Jumonji demethylase mechanism-based inhibitor development. Together, developed methods will further advance our understanding of the role of demethylases in epigenetic regulation.

REFERENCES

Cloos, P.A.C., Christensen, J., Agger, K., and Helin, K. (2008). Erasing the methyl mark: histone demethylases at the center of cellular differentiation and disease. Genes Dev *22*, 1115-1140.

Kooistra, S.M., and Helin, K. (2012). Molecular mechanisms and potential functions of histone demethylases. Nat Rev Mol Cell Biol *13*, 297-311.

Publishing Agreement

It is the policy of the University to encourage the distribution of all theses, dissertations, and manuscripts. Copies of all UCSF theses, dissertations, and manuscripts will be routed to the library via the Graduate Division. The library will make all theses, dissertations, and manuscripts accessible to the public and will preserve these to the best of their abilities, in perpetuity.

I hereby grant permission to the Graduate Division of the University of California, San Francisco to release copies of my thesis, dissertation, or manuscript to the Campus Library to provide access and preservation, in whole or in part, in perpetuity.

_____   December 20, 2012
                                                _____
Author Signature Date   Date